Explorations and Applications of Novel Sensing Approaches –Wireless Sensing Systems

by

Weiping Li

A dissertation submitted to the Graduate Faculty of
Auburn University
in partial fulfillment of the
requirements for the Degree of
Doctor of Philosophy

Auburn, Alabama
August 4, 2012

Keywords: Polyaniline, Rechargeable Battery, Magnetostrictive Particle (MSP), Antibody/Antigen, Sensor, Electrogenerated Chemiluminescence (ECL)

Approved by

Curtis Shannon, Chair, Professor of Chemistry and Biochemistry
Zhongyang Cheng, Professor of Materials Engineering
Wei Zhan, Associate Professor of Chemistry and Biochemistry
Christopher Easley, Assistant Professor of Chemistry and Biochemistry

Abstract

The aim of this dissertation is to explore novel sensing approaches and their applications in the detection of alcohol, the investigation on reactions between antibodies and antigens, as well as the studies of visually rechargeable batteries by combining electrochemical, especially bipolar electrochemical, technique with other chemical and analytical chemical techniques.

To detect alcohol, a novel enzyme catalytic alcohol sensor has been fabricated with MWCNT, NAD^+, ADH and PDDA immobilized on one end and $Ru(bpy)_3^{3+}$/Nafion coated on the other end of a platinum bipolar electrode based on the principles of bipolar electrochemistry and electrochemiluminescence. The amount of current flowing through the bipolar electrode is proportional to the concentration of alcohol and can be monitored using electrogenerated chemiluminescence (ECL) from the $Ru(bpy)_3^{3+}$/Nafion coated cathodic pole.

Magnetostrictive particles (MSPs) expand when exposed to a magnetic field, exhibiting the Joule Effect or Magnetostriction. By monitoring the reactions between antibodies and antigens that take place on the surfaces of Au-modified MSPs placed in a magnetic field, the reaction association constant can be achieved. The experimental results indicate the high affinity of antibody-antigen binding reaction.

The surface functionalization of Fe-based materials is a crucial issue because it not only protects Fe-based materials from corrosion but also broadens the application of

Fe-based materials. In this work, alkane phosphonate SAMs formed on Fe and MSPs surfaces are used to build a multifunctional sensor platform, using which, people can detect two different things on one sensor. In other words, the functionality of sensors will be improved greatly.

Polyaniline is a conductive polymer that has different colors which correspond with different oxidation states. In light of this property, polyaniline can be utilized as electrochromic materials. A bipolar electrode with polyaniline modified on one end and Ag on the other end can act as a rechargeable battery. The processes of charge and discharge can be observed visually through the color change. In order to fulfill the miniaturization of experiments, a simple method for making Au microarray electrodes was discussed and the batteries fabricated on a microarray were characterized via photography, linear sweep voltammetry and Raman spectroscopy.

ACKNOWLEDGMENTS

The dissertation couldn't have been made possible without the dedication, time, and effort of not only me, but everyone who helped to give me a push in the right direction; family, friends, professors, advisors, and anyone else that helped whether they know it or not. Words are powerful indeed, but even they cannot fully express the extent of my appreciation for all that everyone's done to help me.

These people have helped me so much that it would be an injustice not to single them out for all of their work on my behalf:

Thanks Dr. Curtis Shannon for introducing me to the cutting edge field of bipolar electrochemistry. His endless enthusiasm, encouragement, and guidance have led me through the graduate studies.

Thanks Dr. Zhongyang Cheng for his guidance and a lot of precious suggestions.

Thanks Dr. Wei Zhan for sharing his expertise in biosensor and numerous valuable suggestions during my entire study in auburn university.

Thanks Dr. Christopher Easley for helping in making microarray electrodes and a number of precious suggestions.

I would like to thank Dr. Minseo Park for being the outside reader for my dissertation.

I would like to thank my colleagues and friends in Dr. Shannon's group; Drs Tsunghsueh Wu, Junxua Xin, Chaokang Gu, Anand Sankarraj, Hongxia Zhang, Sridevi

Ramakrishnan, Rajakumari Ramaswamy, Ms.Yajiao Yu, Mrs. Sanghapi Ndzesse Sanghapi, Mrs. Tanyu Wang for their stimulating discussion and collaborations.

I would like to thank Dr. Kewei zhang for his help and valuable discussion.

I would like to express my thanks to all professors and staff in chemistry department.

I give my special thanks to my parents, my sister and brother for encouragement and support during this study. I also thank my family (my husband, daughter & son) for their unselfish support and consistent encouragement and love during these years.

Table of Contents

List of Tables

List of Figures

List of Pictures

List of Schemes

List of Abbreviations

MWCNTs	Multiwalled carbon nanotubes
MSPs	Magnetostrictive particles
SAMs	Self-assembled monolayers
pAPP	4-aminophenyl phosphate
ECL	Electrochemiluminescence
ADH	Alcohol dehydrogenase
NAD^+	Nicotinamide adenine dinucleotide
PANI	Polyaniline
NHS	Hydroxysuccinimide
EDC	N-(3-Dimethylaminopropyl)-N'-ethylcarbodiimide hydrochloride
SERs	Surface Enhanced Raman Spectroscopy
AP	Alkaline phosphatase
BPE	Bipolar electrode

Chapter 1

INTRODUCTION

1.0 Project Overview

This dissertation deals with four wireless sensing systems and their applications. The first project involves the detection of alcohol in a bipolar electrochemical cell by modifying platinum and gold electrodes using alcohol dehydrogenase and the coenzyme NAD^+(nicotinamide adenine dinucleotide) to implement the catalytic oxidation reaction of alcohol. This is an amperometric sensor with electrogenerated chemiluminescence (ECL) as a detected element (reporter). To the best of our knowledge, cathodic ECL from the surface-confined $Ru(bpy)_3^{2+}$ is firstly reported here.

The second one describes a rechargeable microarray battery based on the electrochromic properties of polyaniline. The chemicals (silver and polyaniline) used as the materials of the positive and negative poles are immobilized on the two ends of a microarray Au electrode using the bipolar electrochemical technique. The conversion of different oxidation states of polyaniline has been studied via spectroelectrochemical measurements by combining the bipolar electrochemical technique and the spectroscopic technique. The charge-discharge processes can be monitored visually.

The third project studies the interactions between antibodies and antigens. By measuring the frequency shift of an antibody modified MSPs sensor derived from mass loading due to the antibody-antigen interactions, the association constant of the binding reaction is acquired.

The last project discusses the formation of the phosphonate SAMs on Fe-based materials and its application as a multifunctional sensor platform.

1.1 Introduction to Sensors

Sensors are the devices which produce measurable responses to the changes in reactions and convert them to some kinds of signals such as electrical, acoustic, optical output signals that can be read by instruments or observers. A sensor is composed of two parts, which includes a sensing material and a transducer. The transducer converts the change in reaction between the analytes and the sensing materials to a readable signal. Figure 1.1 schematically shows the sensing process.

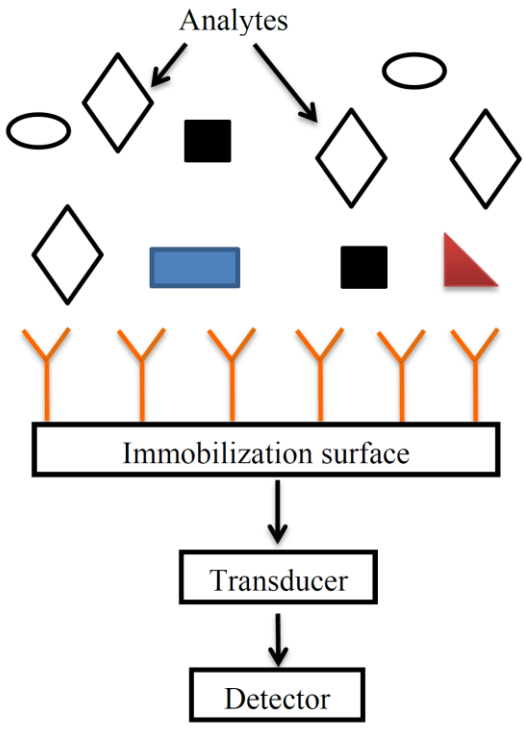

Figure 1.1 Schematic description of the sensing process.

Based on the principal physics and operating mechanisms, sensors can be classified into five groups: chromatography and spectrometry, electrochemical sensors, mass sensors, thermal sensors and optical sensors. Electrochemical sensors operate by the sensing materials modified on the electrodes reacting with analytes and producing an electrical signal proportional to the concentration of the analytes while chromatography and spectrometry rely on the physical and chemical properties to separate and identify the analytes. Mass sensors measure the changes to the mass of the sensors during interaction with analytes. Optical sensors detect the changes in visible light or other electromagnetic waves during sensing materials reacting with analytes. Even though the sensors have been divided into five categories, there is no distinct line between the different categories. The sensors may exhibit characteristics that overlap with other categories.[1] In this chapter, mass and electrochemical sensors will be discussed in detail due to their applications in these projects reported in this dissertation.

1.2 Mass Sensors

1.2.1 Surface Acoustic Wave Sensors

The working principle of this kind of sensors is that the resonance frequency of an acoustic wave will decay exponentially with depth into the substrate when an acoustic wave travels along the surface of a material. A surface acoustic wave device consists of an input transducer, a sensing material, and an output transducer on a piezoelectric substrate (quartz). When an electric field is applied on the input transducer, the input transducer emits an acoustic wave which travels through the sensing material and is

detected by the output transducer.[2] The reactions between the sensing materials and analytes which cause the mass loading on the substrate will affect the velocity and attenuation of wave propagation and result in the shift of the resonance frequency.

1.2.2 Microcantilever Sensors

A microcantilever is a device that can act as a physical, chemical or biological sensor by detecting changes in cantilever deflection or resonance frequency.[3-8] In order to detect the target of the interest, a sensing material is deposited on a microcantilever to absorb the target. The changes of mass derived from the reaction of sensing material and target induce the changes in cantilever bending or resonance frequency.

1.2.3 Introduction to Magnetostrictive Particles (MSPs)

Magnetostrictive particles are a whole class of amorphous metallic glass ribbons called Metglas.[9] Due to the special process of formation,[10] Metglas have unique magnetic properties. Of those ribbons, amorphous iron- and nickel-based alloys ($Fe_{40}Ni_{38}Mo_4B_{18}$ (Metglas brand 2826MB)) have been used to make different sensors such as position sensors,[11] strain sensors,[12] and biological sensors.[13-16] The typical property of magnetostrictive particles is the magnetostriction. When a magnetic field is imposed on the magnetostrictive particles, the small magnetic domains will rotate to make their principal axes of anisotropy align with the magnetic field, and the orientation of these small domains creates a strain field which results in the deformation of magnetostrictive particles.

If the frequency of the alternating current magnetic field matches the mechanical resonance of magnetostrictive particles, the magnetostrictive particles experience a magnetoelastic resonance. For ribbon-shaped MSPs, the resonance frequency of the longitudinal oscillation can be expressed by: [17]

$$f_n = \frac{n}{2L}\sqrt{\frac{E_s}{\rho_s(1-\sigma^2)}} \tag{1.1}$$

where n denotes integers (n=1, 2, 3), L is the length of the ribbon, E_s is Young's modulus, σ is the Poisson's ratio and ρ_s is the density of magnetostrictive particles.

The resonance frequency can also be measured by the following way. Firstly, the mechanical vibration of the magnetostrictive particles is generated by applying alternating current magnetic field, and then, through the inverse magnetoelastic effect, the vibration of MSPs generates a time varying magnetic flux which can be measured. Running a Fast Fourier Transform (FFT) can convert the time-domain signal into the frequency domain. Consequently, the resonance frequency is acquired.[18]

If we change the density of MSPs through coating some materials with mass Δm on the surface, the equation (1.1) will be substituted by [19]

$$f_{load} = \frac{1}{2L}\sqrt{\frac{1}{1+\Delta m/m_s}\frac{Ad}{m_s}\frac{E_s}{\rho_s(1-\sigma^2)}} = f_0\sqrt{\frac{1}{1+\Delta m/m_s}} \tag{1.2}$$

where A is the surface area and d is the thickness of the MSPs.

When the mass of MSPs is much bigger than the coated mass, the resonance frequency shift of the MSPs is depicted approximately as: [17]

$$\Delta f = f - f_0 = - f_0 \Delta m/2m_s \quad (1.3)$$

where f_0 is the resonance frequency of MSPs, f is the resonance frequency of MSPs after coating, m_s is the mass of MSPs before coating.

Based on equation (1.3), the MSPs can be used as a sensor platform to detect the reactions taking place on the surfaces of MSPs. The resonance frequency shift is proportional to the change to the mass of the sensor.

1.2.4 Magnetostrictive Sensors

Comparison to other sensors, MSPs-based sensors can be monitored without the use of electrical connections, namely wireless. This is an advantage of magnetostrictive sensors over other sensors.

To act as a sensor, the surfaces of MSPs need to be modified with the sensing materials. The resonance frequency will shift once the sensing materials react with the analytes. By monitoring the resonance frequency shift, one can obtain the information about the analytes.

1.3 Electrochemical Sensors

1.3.1 Conventional Electrochemical Sensor

Electrochemical sensors include potentiometric sensors, amperometric and conductometric sensors.[20-24] Potentiometric sensors measure the potential difference

between the sensing electrode and reference electrode with near-zero current flowing through them. Amperometric sensors measure the current between the sensing and auxiliary electrode which is induced by a redox reaction at the sensing electrode. Conductometric sensors detect the analytes by converting the sensing reaction into a resistance signal. Normally, an electrochemical sensor consists of a working electrode (sensing electrode), an auxiliary electrode as well as a reference electrode separated by electrolyte. A typical example of potentiometric sensors is a pH sensor. It is widely used in measuring the acidity and alkalinity of solutions in agriculture, biology, medicine, environmental protection and many chemical processes. Many amperometric sensors are used in gas (or volatile organic compound) monitoring in areas such as the food and beverage industry, and in hazardous materials emergency response to detect dangerous (explosive or poisonous) gases.

The oldest electrochemical sensors can be dated back to 1909 with the occurrence of ion-selective electrode.[25] Ever since, tremendous efforts have been made. New concepts and techniques are introduced. Miniaturization, simplification as well as less cost have become a general trend on the design of sensors. Therefore, the wireless electrochemical sensors have been sprouting.

1.3.2 Wireless Electrochemical Sensors

1.3.2.1 Bipolar Electrochemistry and Bipolar Electrode (BPEs)

An electrically isolated substrate which can be any kind of conductive materials such as metals, semiconductors and coated insulators immersed in an electrolyte, can act

as both an anode and a cathode, that is, as a bipolar electrode, if a sufficiently large potential difference is applied across the electrolyte. And hence bipolar electrochemistry occurs.[26] Figure 1.2 schematically shows the setup of a bipolar electrochemical cell.[26] The two driving electrodes are connected to the power supply, and the bipolar electrode floats in the solution. The dotted lines show the current paths generating from electrochemical reactions taking place in the bipolar electrochemical cell.

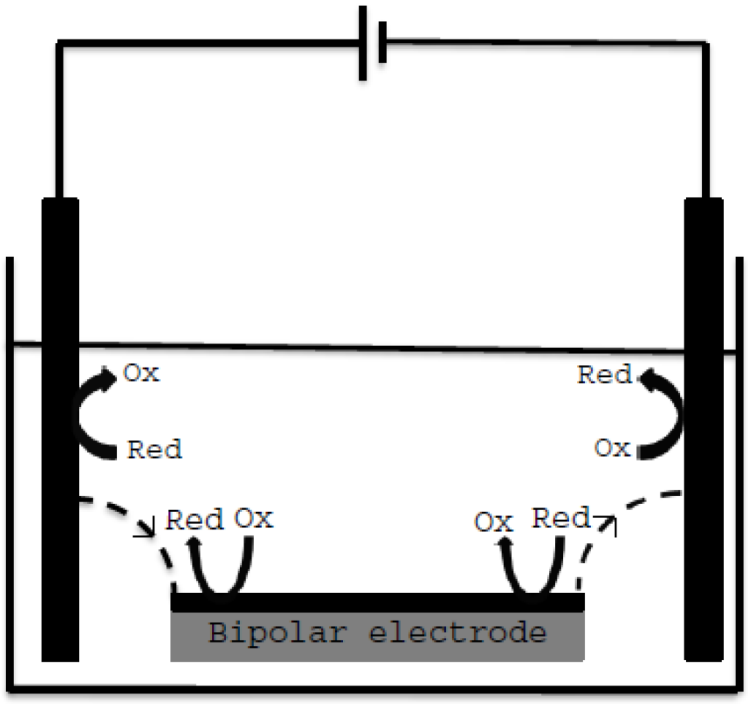

Figure 1.2 Setup of bipolar electrochemical cell.

1.3.2.2 Working Principle of Bipolar Electrode

When a potential is applied between the two driving electrodes, the electric field will induce the polarization of bipolar electrode that results in the formation of anode-cathode pairs on the two ends of bipolar electrode. Because of the resistance of solution, the applied potential will drop and thus form the potential gradient along the bipolar electrode. If the difference (overpotential) between the potential of the solution and the potential of the bipolar electrode is sufficiently high, oxidation and reduction reactions will take place on the two ends of the bipolar electrode, and a current will flow through the bipolar electrode.[28-30] Figure 1.3 shows the origin of driving force (overpotential) for redox reactions occurring on the two ends of bipolar electrode. Based on the charge balance, the faradaic currents for both cathode and anode of bipolar electrode are equal.

Compared to the conventional electrochemistry, bipolar electrochemistry exhibits a simple experimental setup due to no physical connection needed between the bipolar electrode and the power supply as well as the size dependent relationship between the applied potential and onset of bipolar electrochemistry. Manz and coworkers visually demonstrated the relationship of size dependence.[31] Table 1.1 displays the differences between the bipolar electrochemistry and conventional electrochemistry.

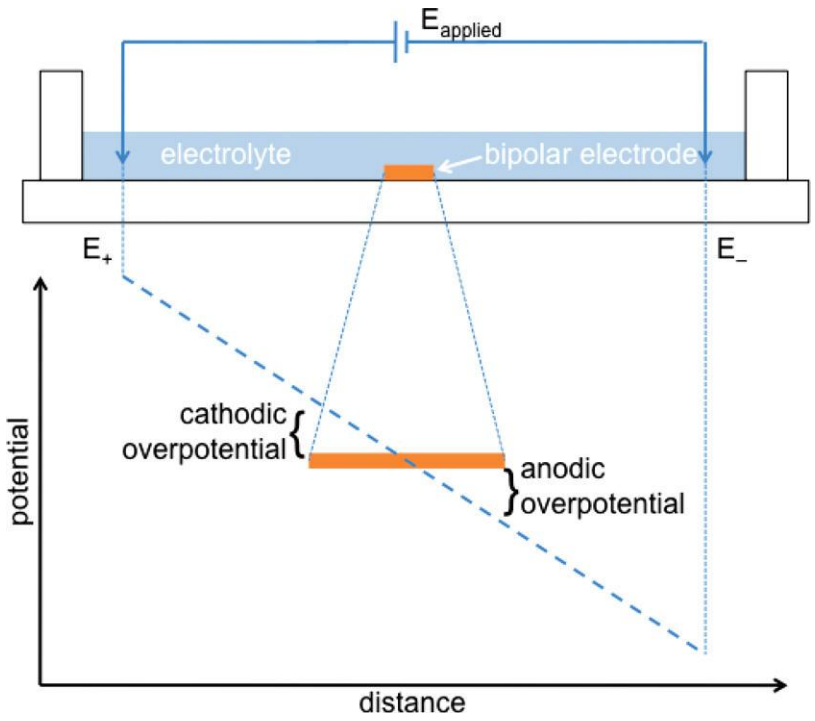

Figure 1.3 Origin of cathodic overpotential and anodic overpotential

Table 1.1 Comparison of bipolar electrochemistry and conventional electrochemistry

Bipolar electrochemistry	Conventional electrochemistry
Wireless	Wire
The anodic process occurs at the negative side of the electric field	The anodic process occurs at the positive side of the electric field
Potential is length dependent and can be controlled by the applied driving potential	Potential is controlled with respect to that of a reference electrode
Electrodeposition is implemented on a relatively big electrode	Electrodeposition can be performed on a relatively small electrode

Recent years, the studies of bipolar electrochemistry are mainly focused on three aspects. One is to use bipolar electrodes as sensing platform to detect organic molecules and biomolecules. In these studies, bipolar electrochemical technique was combined with other experimental techniques such as Electrogenerated chemiluminescence, Photography, Raman spectroscopy, etc. to indicate the sensing reactions.[32-34] Crooks and co-workers reported a wireless electrochemical DNA microarray sensor in which Au microarray electrodes were modified with thiol-functionalized, 25-mer DNA capture probes, and 6-mercaptohexanol, and the target DNA was labeled with 4 nm Pt-NPs. The nanoparticles of platinum catalyzed oxygen reduction on cathodic pole, and ECL was observed simultaneously on the anode of Au bipolar electrodes. The advantages of this work are that the function of the microarray sensor made of three Au electrodes is just

controlled by two driving electrodes and the sensing reaction can be monitored by light emission. The second aspect is to investigate the formation of chemical composition gradient on the bipolar electrodes.[35-36] The last one is the applications of electrodeposition utilizing bipolar electrochemical technique.[36] For example, Bradley et al. deposited palladium onto micrometer-scale particles, carbon nanotubes, and nanofibers by using bipolar electrochemistry.[38]

In contrast to electrodeposition performed by using the conventional electrochemical technique, bipolar electrodeposition allows conductive materials such as metals and some polymers to be deposited onto micrometer-scale, nanometer-scale substrate due to the wireless feature, which offers a new scope and opportunity in chemical synthesis.

1.4 Optical Sensors

Optical sensors use electromagnetic radiation to produce the analytical signal in a transduction element. Based on the various optical principles, such as luminescence, fluorescence, and absorbance etc., the analytes can be detected by measuring the intensity of light, refractive index, scattering, diffraction and polarization. Optical sensors have been used in chemical, food industries, as well as in environmental control. For instance, Optical fiber sensors with doped sol–gel coatings were employed to measure the pH of solution, monitor gas and determine solvents.[39]

1.5 Electrochemiluminescence (ECL)

1.5.1 Features of Electrochemiluminescence

Electrochemiluminescence (electrogenerated chemiluminescence) is a kind of luminescence generated during electrochemical reactions in solutions or on the surface of the electrode. In the electrochemiluminescence, the intermediates produced electrochemically undergo highly energetic electron-transfer reactions to form excited states which can emit light.

Electrochemiluminescence is a form of chemiluminescence (CL). Even if both of ECL and CL involve the light emission, luminescence in CL is initiated by the mixing of chemical reagents and often controlled by the careful manipulation of fluid flow; whereas, luminescence in ECL is initiated and controlled by varying the electrode potentials.

ECL has the advantage of not needing a light source compared with other spectroscopy-based analytical techniques such as fluorescence methods.[40] Thus, background signals are decreased or eliminated, allowing optical detectors to be used at their maximum sensitivity.

1.5.2 ECL Reaction Mechanisms

Even though the earliest ECL observation was reported by Harvey and co-workers in an aqueous alkaline solution from luminol in 1927,[41] the first detailed ECL studies were published by Hercules and Bard et al. in 1964 and 1965.[42-43] Bard and co-workers observed the ECL from $Ru(bpy)_3^{2+}$ in acetonitrile (MeCN) using tetrabutylammonium tetrafluoroborate ($TBABF_4$) as the electrolyte in 1972.[44] Since then, thousands of papers related to ECL have been published each year. Ruthenium complexes, for example,

tris(bipyridine) ruthenium(II): $Ru(bpy)_3^{2+}$ as an excellent luminophore is used in the studies of ECL due to its strong luminescence, solubility in many aqueous and nonaqueous solvents at room temperature and its ability undergoing reversible one electron-transfer reactions at easily attainable potentials.

ECL based on $Ru(bpy)_3^{2+}$ has been extensively studied including fundamentals and applications. Here, the reaction mechanisms of ECL are described as below.

Table 1.2 Typical coreactant ECL systems

Type of coreactant ECL	luminophore	coreactant	main coreactant intermediate	E^0 of intermediate (V, vs. NHE)	refs
oxidative-reduction	$Ru(bpy)_3^{2+}$ $Ru(bpy)_3^{2+}$ $Ru(bpy)_3^{2+}$	oxalate ($C_2O_4^{2-}$) pyruvate/Ce(III) tri-n propylamine (TPrA)	$CO_2^{\bullet-}$ $CH_3CO^{\bullet}$ $TPrA^{\bullet+}$,$TPrA^{\bullet}$	$CO_2/CO_2^{\bullet-}$ -1.9V $TPrA^{\bullet+}/TPrA$ +1.1 V $P1/TPrA^{\bullet}$ -1.5 V	48,49 49 47
reductive-oxidation	$Ru(bpy)_3^{2+}$ $Ru(bpy)_3^{2+}$ Aromatic hydrocarbons $Ru(bpy)_3^{2+}$	Hydrazine(N_2H_4) persulfate ($S_2O_8^{2-}$) benzoyl peroxide hydrogen peroxide	N_2H_2, $N_2H_3^{\bullet}$ $SO_4^{\bullet-}$ $PhCO_2^{\bullet}$ $OH^{\bullet}$	N_2H_2/N_2 < -2.3V $SO_4^{\bullet-}/SO_4^{2-}$ +2.9V $PhCO_2^{\bullet}/PhCO_2$+1.7V $OH^{\bullet}/OH^-$1.77–1.91 V	50-53 54, 55 56-58 59

1.5.2.1 Coreactant ECL

A coreactant is a compound that can form a strong reducing or oxidizing intermediate after being oxidized or reduced. This intermediate can react with an oxidized or reduced luminophore to form excited states capable of emitting light. Table 1.2 shows the typical coreactant ECL systems.

1.5.2.2 ECL of Oxalate as a Co-reactant

Oxalate ion ($C_2O_4^{2-}$) was the first reported coreactant.[48] In an aqueous solution of containing $Ru(bpy)_3^{2+}$ mixed with $C_2O_4^{2-}$, $Ru(bpy)_3^{2+}$ is firstly oxidized on the electrode to form the $Ru(bpy)_3^{3+}$ cation under the condition of anodic potential scanning. In the diffusion layer close to the electrode surface, $C_2O_4^{2-}$ is oxidized by $Ru(bpy)_3^{3+}$ cation to generate an oxalate radical anion ($C_2O_4^{\bullet-}$) that decomposes to form a strong reducing radical anion ($CO_2^{\bullet-}$).The intermediate can either reduce $Ru(bpy)_3^{3+}$ back to $Ru(bpy)_3^{2+}$ or reduce $Ru(bpy)_3^{2+}$ to $Ru(bpy)_3^{+}$. Following, $Ru(bpy)_3^{3+}$ reacts with $Ru(bpy)_3^{+}$ to form the excited state $Ru(bpy)_3^{2+}*$ that emits light (scheme 1.1).[47]

Scheme 1.1 ECL mechanism of oxalate as a coreactant

$$Ru(bpy)_3^{2+} - e^- \rightarrow Ru(bpy)_3^{3+} \quad (1.1)$$

$$Ru(bpy)_3^{3+} + C_2O_4^{2-} \rightarrow Ru(bpy)_3^{2+} + C_2O_4^{\bullet-} \quad (1.2)$$

$$C_2O_4^{\bullet-} \rightarrow CO_2^{\bullet-} + CO_2 \quad (1.3)$$

$$Ru(bpy)_3^{3+} + CO_2^{\bullet-} \rightarrow Ru(bpy)_3^{2+*} + CO_2 \quad (1.4)$$

$$Ru(bpy)_3^{2+} + CO_2^{\bullet-} \rightarrow Ru(bpy)_3^{+} + CO_2 \quad (1.5)$$

$$Ru(bpy)_3^{3+} + Ru(bpy)_3^{+} \rightarrow Ru(bpy)_3^{2+}* + Ru(bpy)_3^{2+} \quad (1.6)$$

$Ru(bpy)_3^{2+*} \rightarrow Ru(bpy)_3^{2+} + h\nu$ (2.1 eV, 610 nm) (1.7)

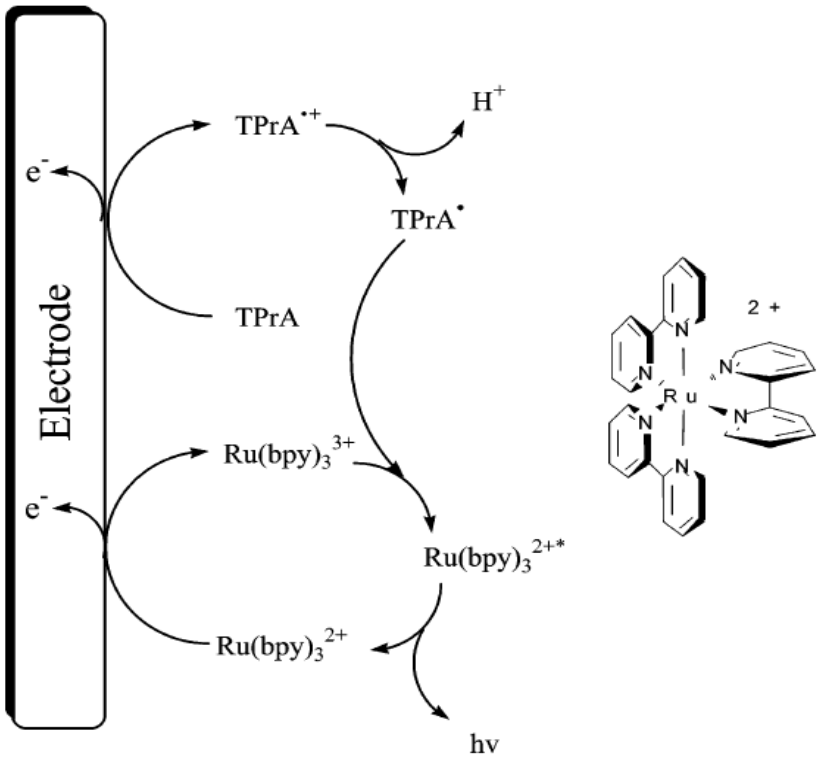

Figure 1.4 Proposed mechanism for $Ru(bpy)_3^{2+}$/TPrA ECL system.

(Copied from Ref 46 with ACS permission)

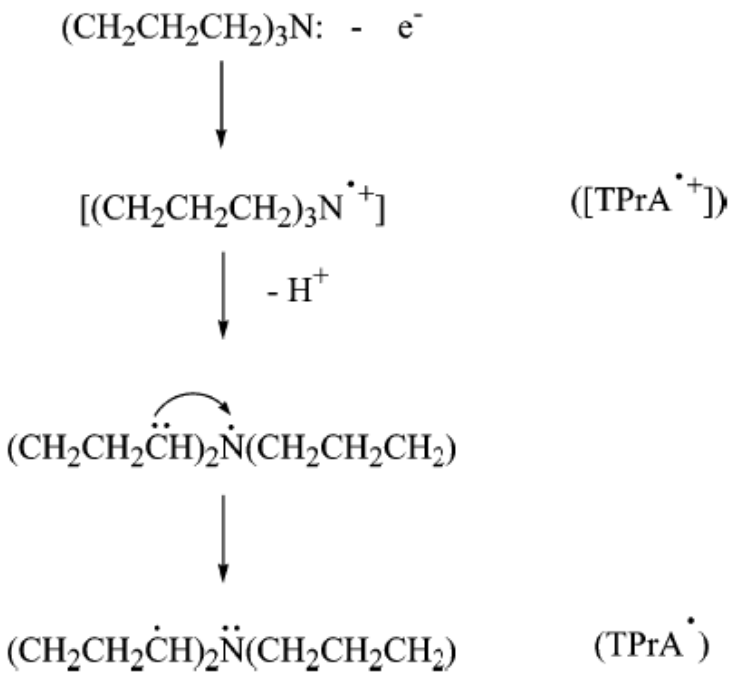

Figure 1.5 Proposed tri-n-propylamine oxidation/reaction sequences with abbreviations in parentheses

(Copied from Ref 46 with ACS permission)

1.5.2.3 ECL of Tri-n-propylamine (TPrA) as a coreactant

In $Ru(bpy)_3^{2+}$/ TPrA ECL system, $Ru(bpy)_3^{2+}$ and TPrA are oxidized concomitantly at the electrode. $Ru(bpy)_3^{3+}$, the products of oxidation, subsequently interacts with radical $TPrA^{\bullet}$ to produce the excited state $Ru(bpy)_3^{2+*}$ and then emits light. Figures 1.4 and 1.5 illustrate the formation of $TPrA^{\bullet}$ free radicals and the emission of the light.

Scheme 1.2 ECL mechanism of Tri-n-propylamine (TPrA) as a coreactant

$$Ru(bpy)_3^{2+} - e^- \rightarrow Ru(bpy)_3^{3+} \quad (1.8)$$

$$TPrA - e^- \rightarrow [TPrA^{\bullet}]^+ \rightarrow TPrA^{\bullet} + H^+ \quad (1.9)$$

$$Ru(bpy)_3^{3+} + TPrA^{\bullet} \rightarrow Ru(bpy)_3^{2+*} + \text{products} \quad (1.10)$$

$$Ru(bpy)_3^{2+*} \rightarrow Ru(bpy)_3^{2+} + h\nu \quad (1.11)$$

1.5.2.4 ECL of Persulfate ($S_2O_8^{2-}$) as a Coreactant

Scheme 1.3 describes the proposed pathways for $Ru(bpy)_3^{2+}/S_2O_8^{2-}$ system to obtain ECL.[47] In this case, $Ru(bpy)_3^{2+}$ is firstly reduced to $Ru(bpy)_3^{+}$ and then reacts with strong oxidant $SO_4^{\bullet-}$ produced by the reduction of $S_2O_8^{2-}$ to generate the excited state $Ru(bpy)_3^{2+*}$. This is the first reported example of "reductive-oxidation" coreactant ECL system. These experiments showed that the ECL intensity was the function of $S_2O_8^{2-}$ concentration and maximum ECL intensity was obtained at the concentration ratio 1mM: 15–20 mM for $Ru(bpy)_3^{2+}$ and $S_2O_8^{2-}$.[54]

Scheme 1.3 ECL mechanism of Persulfate ($S_2O_8^{2-}$) as a Coreactant

$$S_2O_8^{2-} + e^- \rightarrow S_2O_8^{\bullet 3-} \quad (1.12)$$

$$Ru(bpy)_3^{2+} + e^- \rightarrow Ru(bpy)^{3+} \quad (1.13)$$

$$Ru(bpy)_3^{+} + S_2O_8^{2-} \rightarrow Ru(bpy)_3^{2+} + S_2O_8^{\bullet 3-} \quad (1.14)$$

$$S_2O_8^{\bullet 3-} \rightarrow SO_4^{2-} + SO_4^{\bullet -} \quad (1.15)$$

$$Ru(bpy)_3^{+} + SO_4^{\bullet -} \rightarrow Ru(bpy)_3^{2+}* + SO_4^{2-} \quad (1.16)$$

$$Ru(bpy)_3^{2+} + SO_4^{\bullet -} \rightarrow Ru(bpy)_3^{3+} + SO_4^{2-} \quad (1.17)$$

$$Ru(bpy)_3^{3+} + Ru(bpy)_3^{+} \rightarrow Ru(bpy)_3^{2+}* + Ru(bpy)_3^{2+} \quad (1.18)$$

$$Ru(bpy)_3^{\bullet 2+} \rightarrow Ru(bpy)_3^{2+} + h\nu \quad (1.19)$$

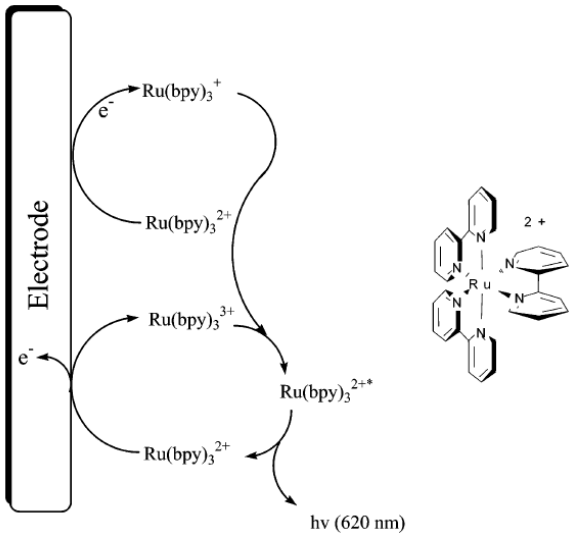

Figure 1.6 Structure of $Ru(bpy)_3^{2+}$ and proposed mechanism for $Ru(bpy)_3^{3+}/Ru(bpy)_3^{+}$ ECL system.

(Copied from ref. 46 with ACS permission)

1.5.2.5 Annihilation ECL

The mechanism of the Annihilation ECL involves the formation of the excited state $Ru(bpy)_3^{2+}$* as a result of annihilation reaction between $Ru(bpy)_3^{3+}$ and $Ru(bpy)_3^{+}$ (Figure 1.6)

Scheme 1.4 Annihilation mechanism of ECL

$$Ru(bpy)_3^{2+} - e^- \rightarrow Ru(bpy)_3^{3+} \qquad (E°_{Ru}{}^{2+/3+} = +1.2 \text{ V vs SCE}) \qquad (1.20)$$

$$Ru(bpy)_3^{2+} + e^- \rightarrow Ru(bpy)_3^{+} \qquad (E°_{Ru}{}^{2+/1+} = -1.4 \text{ V vs SCE}) \qquad (1.21)$$

$$Ru(bpy)_3^{3+} + Ru(bpy)_3^{+} \rightarrow Ru(bpy)_3^{2+*} + Ru(bpy)_3^{2+} \qquad (1.22)$$

$$Ru(bpy)_3^{2+*} \rightarrow Ru(bpy)_3^{2+} + h\nu \qquad (2.1 \text{ eV}, 610 \text{ nm}) \qquad (1.23)$$

Owing to the unique features, ECL has been successfully exploited as a detector in capillary electrophoresis, injection analysis (FIA) and high-performance liquid chromatography (HPLC), and been applied to many areas such as DNA detection, immunoassay, food industry etc.[58]

1.6 Introduction to Polyaniline

Polyaniline as a conductive polymer has attracted a great deal of attention due to its special properties, such as tunable electrical conductivity, controllable electrochromic properties, nanostructured shapes (films, nanowires, nanoparticles), good environmental, thermal stability, and simple low cost synthesis, and thus is a highly studied polymer.

1.6.1 Structure of Polyaniline

The basic repeat unit of polyaniline as shown in Figure 1.7 is four aniline monomer units long with three benzenoid rings and one quinoid ring, where m and n are the number of the reduced and oxidized forms of the repeat unit in polyaniline respectively, x is the degree of polymerization. If the reduced form of the repeat unit in polyaniline structure is substituted by the oxidized form, the pernigraniline thus is formed which contains a half quinoid rings. On the contrary, leucoemeraldine form of polyaniline (m=1, n=0) represents a fully reduced state which is only composed of benzenoid rings. Emeraldine also called emeraldine base contains 3/4 benzenoid rings.[61-63]

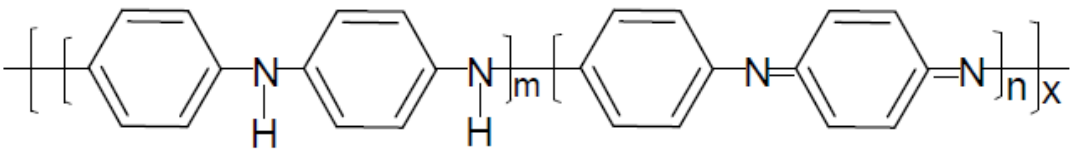

Figure 1.7 Structure of polyaniline

Figure 1.8 displays the three oxidation states of polyaniline and emeraldine salt. From leucoemeraldine form of polyaniline (fully reduced state) to pernigraniline form of polyaniline (fully oxidized state), accompanying with the gradually increase of conjugated chain in the chemical backbone, the color of polyaniline varies from yellow or colorless to blue or violet. The reason is that the band gap energy required by an electron to excite from the highest occupied molecular orbital (HOMO) to the lowest unoccupied molecular orbital (LUMO) reduces with the increase of the double bond in the conjugated

system which results in the system absorbing photons with the low energy (longer wavelength) and therefore, the blue or violet color is presented.

The structure of the imine (–N=) and amine (–NH–) nitrogen possessing the nonbonding pairs of the electrons on the polymer backbone causes the easier protonation of the polyaniline (EB) that responds to the strong change of the polyaniline conductivities. The conductivity of polyaniline reduces from 4.4 to 6.0×10^{-11} S cm^{-1} for the de-protonation of polyaniline.[64] So, except for the protonated polyaniline which is emeraldine salt, all of the three oxidation states of the polyaniline are electrically non-conductive.

Polyaniline can transform from one oxidation state to another one through controlling potential, and thus, polyaniline is a prospective conductive polymer being used in electrochromics.

1.6.2 Synthesis of Polyaniline.

Several approaches are used to synthesize polyaniline including chemical and electrochemical polymerization. Figure 1.9 describes the polymerization of aniline in an acidic aqueous medium and persulfate ($(NH_4)_2S_2O_8$) as the oxidizing reagent.[65] The reaction produces the protonated, partially oxidized form of the polymer, namely, emeraldine salt.[66] By treating with $NH_3\cdot H_2O$, emeraldine salt can be converted to emeraldine base (figure 1.9).[65,67]

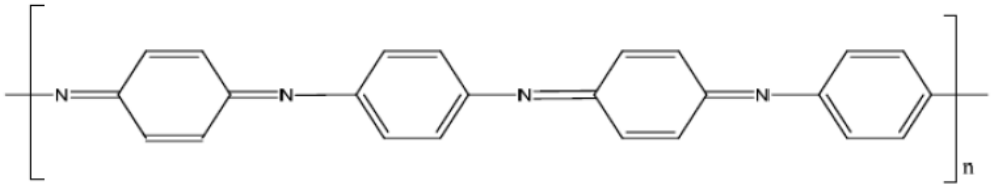

Pernigraniline (PNB)

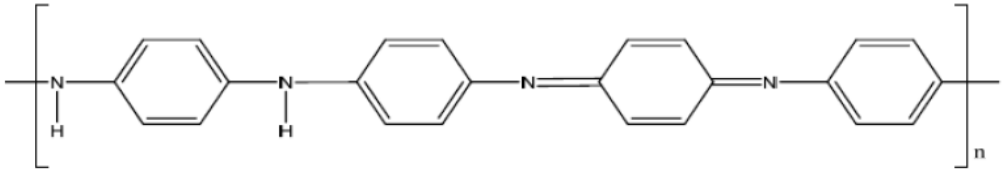

Emeraldine base (EB)

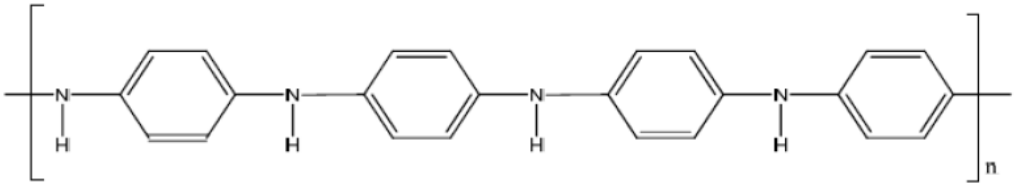

Leucoemeraldine (LEB)

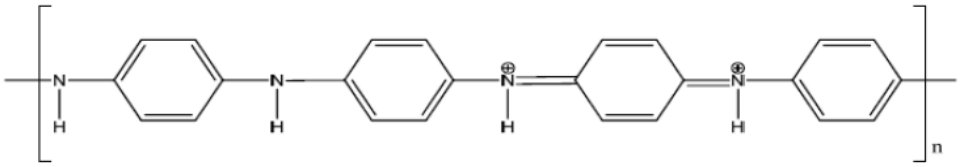

Emeraldine salt.

Figure 1.8 Structures of different oxidation states of polyaniline

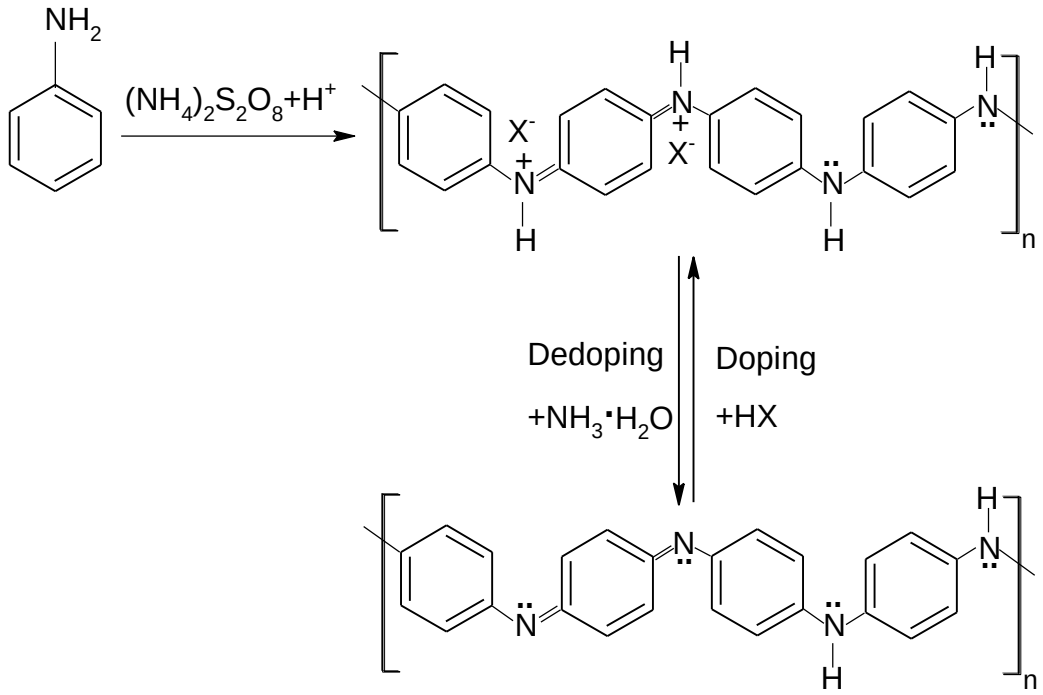

Figure 1.9 Describing the polymerization of aniline in an acidic aqueous medium and persulfate ($(NH_4)_2S_2O_8$) as the oxidizing reagent

(Adapted from Ref. 64)

Many other oxidants such as KIO_3, $KMnO_4$, $FeCl_3$, K_2CrO_4, $KBrO_3$, and $KClO_3$ have been used in oxidative polymerization of aniline as well.[68-71] The disadvantage of using inorganic oxidant such as $(NH_4)_2S_2O_8$ involves the formation of the amount of by-products. The use of hydrogen peroxide and molecular oxygen as oxidants were thus suggested.[72-78] Figure 1.10 depicts the mechanism of aniline polymerization.[79-82]

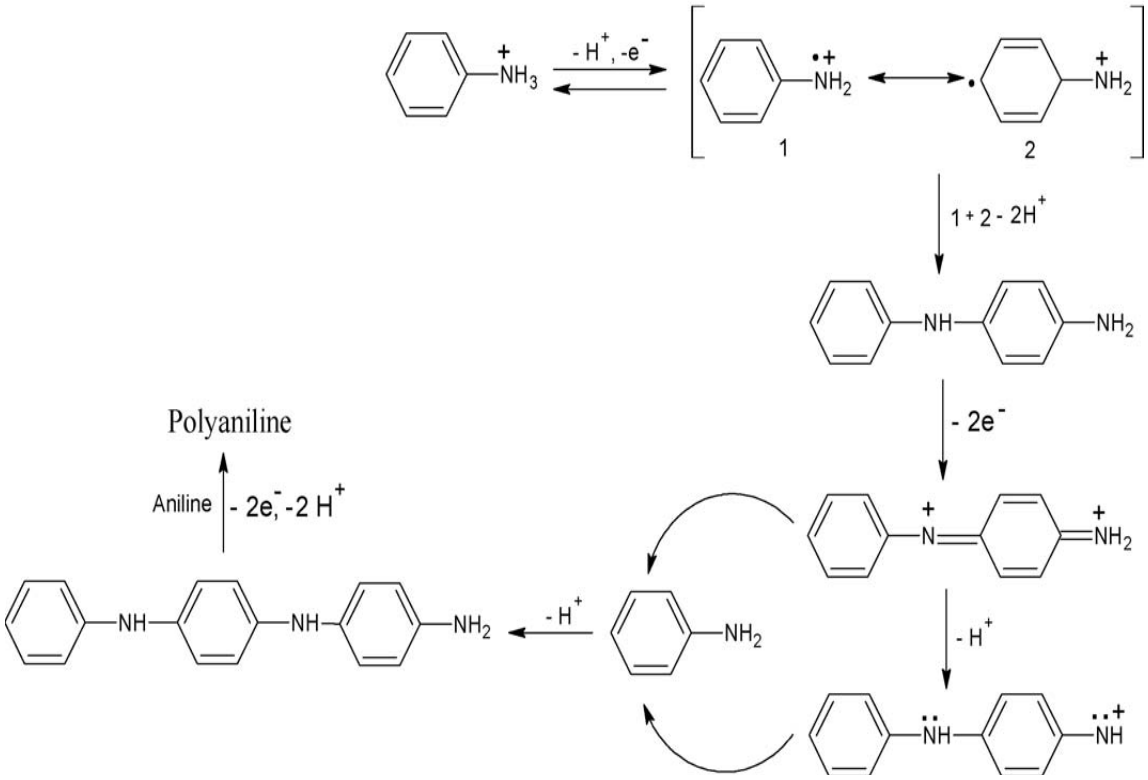

Figure 1.10 Mechanism of the aniline polymerization.

(Copied from Ref 83 with the permission of Elsevier)

Electrochemical polymerization offers the merits over the chemical synthesis, that is, a thickness-controlled uniform film with a precise control of potential and oxidized

state of polymer. Therefore, cyclic voltammetry, potentiostatic, and galvanostatic techniques have been applied on electrochemical polymerization.

For the cyclic voltammetry technique, the electrochemical polymerization of aniline is carried out in an aqueous acidic solution (H_2SO_4, HCl, HNO_3, $HClO_4$, CF_3-COOH and HBF_4) with scan range from -0.2V to 0.8V (vs. SCE) on the electrodes of Au, Pt, stainless steel, carbon etc. The first layer of polyaniline on the electrode is a rather compact globular structure. Subsequently, the porous fibrous structures are formed.[84-86]

1.7 Introduction to Antibodies

An antibody is an immune protein also called immunoglobulin that recognizes and aids the immune response to invaders like viruses and bacteria. Each antibody possesses a Y-shaped structure which is composed of two heavy chains containing four domains and two light chains having two domains joined with each other (Figure 1.11). These domains are divided into two regions, the constant region and the variable region. Relying on the difference in the size and the composition of heavy chains, antibodies are classified as five classes: IgG, IgA, IgD, IgE, and IgM. In the variable region, the different antibodies have the different amino acid sequence which determines the specificity of antibody for binding antigen, whereas the constant region is identical in all antibodies of the same class.

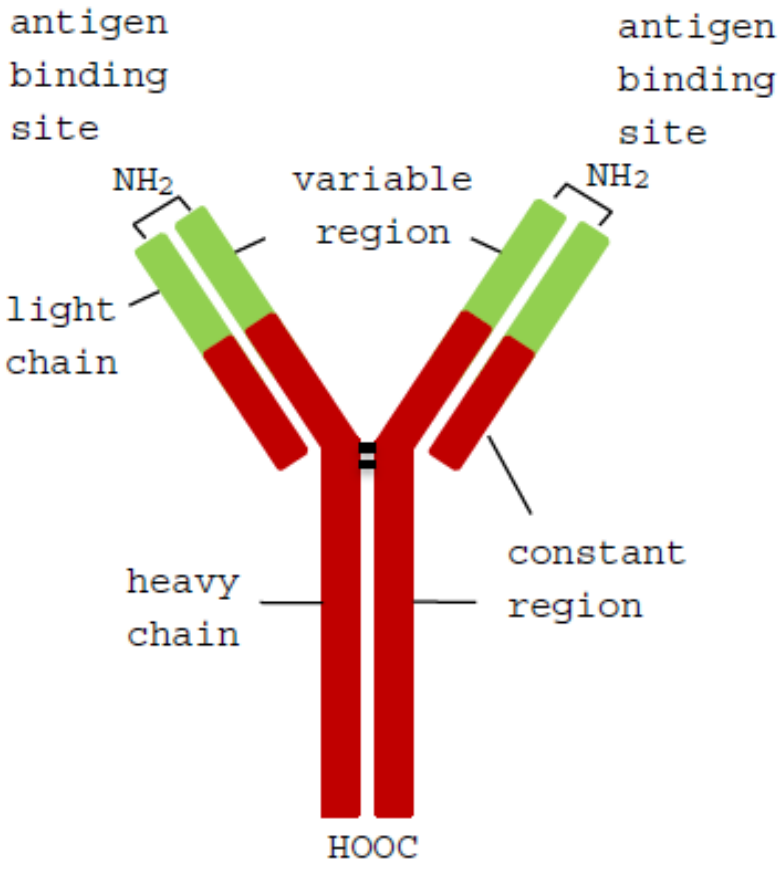

Figure 1.11 Schematic design of a typical antibody (IgG)

1.8 Research Objectives

The objectives of this dissertation are to explore novel sensing approaches and their applications, and the following studies have been implemented:

1. A novel wireless amperometric sensor, which was used to detect alcohol, has been fabricated in which a bipolar electrode was modified to carry out the enzyme catalytic oxidation reaction of alcohol. ECL from the cathode was chosen as an indicator.
2. A rechargeable microarray battery has been developed using bipolar electrochemical technique. The charge-discharge processes can be monitored visually. By changing the pattern of array and the amount of microarray electrodes, the microarray batteries with a wide range of voltages can be constructed.
3. A multifunctional sensing platform based on alkane phosphonate SAMs has been successfully designed to improve the efficiency of the sensors.
4. An antibody-modified MSP sensor has been successfully constructed and been utilized to study antibody-antigen interaction.

References

(1) Yogeswaran, U.; and Chen, S.M. *Sensors* **2008**, *8*, 290-313.

(2) María-Isabel, R.G.; Carmen, M.I.; Angel, M.B.; Antonio, A.V. *Sensors* **2009**, 9 5740-5769.

(3) Zhu, Q. *Sensors & Transducers Journal*, **2011**, 125, 1-21

(4) Vashist, S.K. *Journal of nanotechnology* on line June 18th, **2007**.

(5) Bashir, R.; Hilt, J. Z.; Elibol, O.; Gupta, A.; Peppas, N.A. *Applied Physics Letters* **2002**, 81, 3091-3093**.**

(6) Yan, X.; Xu, X. K. and Ji, H. F. *Analytical Chemistry* **2005**, 77, 6197-6204.

(7) Thundat, T. G.; Chen,G.Y.; Warmack, R. J.; Allison, D. P.; Wachter, E.A. *Anal. Chem.* **1995**, 67, 519-521.

(8) Arntz, Y.; Seelig, J. D.; Lang, H. P.; Zhang, J.; Hunziker, P.; Ramseyer, J.P.; Meyer, E.; Hegner, M; Gerber, C. *Nanotechnology*, **2003**, 14, 86-90.

(9) Grimes, C.A.; Ong, K.G.; Loiselle, K.; Stoyanov, P.G.; Kouzoudis, D.; Liu, Y.; Tong, C. & Tefiku, F. *Smart Matererials and Structures* 1**998**, 8, 639–646.

(10) Lacheisserie, E.T.; Gignoux, D.; Schlenker, M. *Magnetism-Materials and Applications*, Springer, **2004**.

(11) Barandiaran, J. M. and Gutierrez, J. *Sensors Actuators* **1997**, A **59,** 38–42

(12) Mitchell, E. E,; DeMoyer, R. and Vranish, J. *IEEE Trans. Ind. Elec.* **1986**, **33,** 166–70.

(13) Lakshmanan, R.S.; Guntupallia, R.; Hu, J.; Kim, D.J.; Petrenko, V.A.; Barbaree, J.M. and Chin, B.A. *Journal of Microbiological Methods* **2007**, 71, 55-60.

(14) Huang, S.J.; Pang, P.F.; Xiao, X.L.; He, L.W.; Cai, Q.Y. and Grimes, C.A. *Sensors and Actuators* **2008,** B 131, 489–495.

(15) Shen, W.; Lakshmanan, R.S.; Mathison, L.C.; Petrenko, V.A.; Chin, B.A. *Sensors and Actuators* **2009**, B 137, 501–506.

(16) Huang, S.J.; Wang, Y.J; Cai, Q.Y.; Fang, J.D. *Chinese Journal of Analytical Chemistry*, **2008**, 38, 105–10.

(17) Grimes, C.A.; Mungle, C.S.; Zeng, K.F.; Jain, M.K.; Dreschel, W.R.; Paulose, M.; Ong, K.G. *Sensors* **2002**, 2, 294-313.

(18) Loiselle, K. T.; Grimes, C. A. *Rev. Sci. Instrum.* **2000**, *71(3)*, 1441-1446.

(19) Grimes, C. A.; Cai, Q.; Ong, K. G.; Loiselle, K. *Proc. SPIE* **2000**, *4097*, 123-133.

(20) Siegmann-Thoss, C.; Renneberg, R.; Glatz, J. F. C.; Spener, F., *Sens. Actuators B: Chem.* **1996,** 30, 71.

(21) Buck, R. P.; Kinder, E., *Pure Appl. Chem.* **1994**, 2527.

(22) Janata, J. *Chem. Rev.* **1990**, 90, 691-703.

(23) Janata, J. *Anal. Chem.* **1992**, 64(12), 196R-219R.

(24) Wilson, LG., L.G. Everett, and S.J. Cullen (eds.), Handbook of Vadose Zone Characterization & Monitoring, CRC Press, Boca Raton, FL. **1995** *www.intl**sensor**.com/pdf/**electrochemical**.pdf*

(25) Haber, F.; Klemensiewicz, Z. *The Society of Chemistry in Karlsruhe* **1909,** January 28.

(26) Goodridge, F. *Electrochim. Acta.* **1977**, 22, 929-933.

(27) Ulrich, C.; Andersson, O.; Nyholm, L.; Bjorefors, F. *Angew. Chem. Int. Ed.* **2008**, 47, 3034 –3036.

(28) Levich, V. G. *Physicochemical Hydrodynamics*; Prentice-Hall: Englewood Cliffs, NJ, **1962**, 507.

(29) Fleischmann, M.; Ghoroghchian, J.; Pons, S. *J. Phys. Chem.* **1985**, 89, 5530–5536.

(30) Duval, J.; Mieke-Kleijn, J.; van Leeuwen, H. P. *J. Electroanal. Chem.* **2001**, 505, 1–11.

(31) Arora, A.; Eijkel, J. C. T.; Morf, M. E.; Manz, A. A. *Anal. Chem.* **2001**, 73, 3282-3288.

(32) Zhan, W.; Alvarez, J.; Crooks, R. M. *J. Am. Chem. Soc.* **2002**, 124, 13265–13270.

(33) Mavre, F.; Chow, K. F.; Sheridan, E.; Chang, B. Y.; Crooks, J. A. and Crooks, R. M. *Anal. Chem.* **2009**, 81, 6218–6225

(34) Chow, K. F.; Mavre, F.;, and Crooks, R. M. *J. Am. Chem. Soc.* **2008**, 130, 7544–7545

(35) Ulrich, C.; Andersson, O.; Nyholm, L.; Bjorefors, F. *Anal. Chem.* **2009**, 81, 453–459.

(36) Ishiguro, Y.; Inagi, S. and Fuchigami, T. *Langmuir* **2011**, 27, 7158–7162.

(37) Bradley, J.C.; Chen, H.M.; Crawford, J.; Eckert, J.; Ernazarova, K.; Kurzeja, T.; Lin, M.; McGee, M.; Nadler, W.; Stephens, S. G. *Nature* **1997**, 389 (6648), 268–271.

(38) Bradley, J.; Babu, S.; Ndungu, P. Fullerenes, Nanotubes, *Carbon Nanostruct.* **2005**, 13, 227–237.

(39) Jerónimo, P. C.A.; Araújo, A. N.; Conceição, M.; Montenegro, B.S.M. *Talanta* **2007**, 72, 13–27.

(40) Electrogenerated Chemiluminescence; Bard, A. J., Ed.; Dekker: New York, **2004.**

(41) Harvey, N. *J. Phys. Chem.* **1929**, 33, 1456.

(42) Hercules, D. M. *Science* **1964**, 145, 808.

(43) Santhanam, K. S. V.; Bard, A. J. *J. Am. Chem. Soc.* **1965**, 87, 139.

(44) Tokel, N.; Bard, A. J. *J. Am. Chem. Soc.* **1972**, 94, 2862.

(45) Miao, W.J. *Chem. Rev.*, **2008**, 108(7), 2506-2553.

(46) Richter, M. M.; *Chem. Rev.* **2004**, 104(6), 3003-3036.

(47) Miao, W.; Choi, J.-P. *In Electrogenerated Chemiluminescence*; Bard, A. J., Ed.; Dekker: New York, **2004**; Chapter 5, 213.

(48) Chang, M.-M.; Saji, T.; Bard, A. J. *J. Am. Chem. Soc.* **1977**, 99, 5399.

(49) Rubinstein, I.; Bard, A. *J. J. Am. Chem. Soc.* **1981**, 103, 512.

(50) Hercules, D. M. *Acc. Chem. Res*. **1969**, 2, 301.

(51) Li, B.; Zhang, Z.; Zheng, X.; Xu, C. *Chem. Anal.* (Warsaw) **2000**, 45, 709.

(52) Hercules, D. M.; Lytle, F. E. *Photochem. Photobiol*. **1971**, 13, 123.

(53) Martin, J. E.; Hart, E. J.; Adamson, A. W.; Gafney, H.; Halpern, J. *J. Am. Chem. Soc.* **1972**, 94, 9238.

(54) White, H. S.; Bard, A. J. *J. Am. Chem. Soc.* **1982**, 104, 6891.

(55) Bolletta, F.; Ciano, M.; Balzani, V.; Serpone, N. *Inorg. Chim. Acta* **1982**, 62, 207.

(56) Lai, R. Y.; Fleming, J. J.; Merner, B. L.; Vermeij, R. J.; Bodwell, G. J.; Bard, A. J. J. *Phys. Chem.* A **2004**, 108, 376.

(57) Akins, D. L.; Birke, R. L. *Chem. Phys. Lett.* **1974**, 29, 428.

(58) Santa Cruz, T. D.; Akins, D. L.; Birke, R. L. *J. Am. Chem. Soc.* **1976**, 98, 1677.

(59) Choi, J.P.; Bard, A. J. *Anal. Chim. Acta* **2005**, 541, 143.

(60) Yin, X.B.; Dong, S.; Wang, E. *Trends Anal. Chem.* **2004**, 23, 432.

(61) Chiang, J.C.; MacDiarmid, A.G. *Synthetic Metals*, **1986**, 13, 193-205.

(62) MacDiarmid, A.G.; Chiang, J.C.; Richter, A.F.; Epstein, A.J. *Synthetic Metals* **1987**, 18, 285-290.

(63) Huang, W.S.; Humphrey, B. D.; MacDiarmid, A. G. *J. Chem. Soc. Faraday Trans* **1986**, 82, 2385-2400.

(64) Stejskal, J.; Gilbert, R.G. *Pure Appl. Chem.* **2002**, 74, 857.

(65) Skotheim, T.A. Reynolds, J.R. Conjugated polymers: theory, synthesis, properties and characterization, in: Handbook of Conducting Polymers, Third ed., Taylor Francis Group, **2007**, 7.

(66) Somasiri, N. L. D.; MacDiarmid, A. G. *J. Appl. Electrochem.* **1988**, 18, 92

(67) MacDiarmid, A. G.; Chiang, J.-C.; Halpern, M.; Huang, W. S.; Krawczyk, J. R.; Mammone, R. J.; Mu, S. L.; Somasiri, N. L. D.; Wu, W. *Am. Chem. Soc., Div. Polym. Chem*. **1984**, 25, 248.

(68) Mallick, K.; Witcomb, M.J.; Dinsmore, A.; Scurrell, M.S. *Langmuir* **2005**, 21, 7964.

(69) Wang, Y.; Liu, Z.; Han, B.; Sun, Z.; Huang, Y.; Yang, G. *Langmuir* **2005**, 21, 833.

(70) Sun, Z.; Geng, Y.; Li, J.; Wang, X.; Jing, X.; Wang, F. *J. Appl. Polym. Sci.* **1999**, 72, 1077.

(71) Sarma, T.K.; Chowdhury, D.; Paul, A.; Chattopadhyay,A. *Chem. Commun.* **2002**,1048.

(72) Moon, D.K.; Osokada, K.; Maruyama, T.; Yamamoto, T. *Makromol. Chem.* **1992**, 193, 1723.

(73) Chen, Z.; Pina, C. D.; Falletta, E.; Rossi, M. *J. Catal.* **2009**, 267, 93.

(74) Pina, C. D.; Falletta, E.; Faro, M. L.; Pasta, M.; Rossi, M. *Gold Bull.* **2009**, 42, 27.

(75) Chen, Z.; Pina, C. D.; Falletta, E.; Faro, M. L.; Pasta, M.; Rossi, M. ; Santo, N. *J. Catal.* **2008**, 259, 1.

(76) Bicak, N.; Karagoz, B. *J. Polym. Chem.* **2006**, 44, 6025.

(77) Dias, H.V.R.; Rajapakse, R.M.G.; Krishantha, D.M.M.; Fianchini, Wang, M.; X.; Elsenbaumer, R.L. *J. Mater. Chem.* **2007**, 17, 1762.

(78) Dias, H.V.R.; Wang, X.; Rajapakse, R.M.G.; Elsenbaumer, R.L. *Chem. Commun.* **2006**, 976.

(79) Wei, Y.; Jang, G.-W.; Chan, Ch.-Ch.; Hsuen, K.F.; Hariharan, R.; Patel, S.A.; Whitecar, C.K. *J. Phys. Chem.* **1990**, 94, 7716.

(80) Wei, Y.; Tang, X.; Sun, Y.; Focke, W.W. *J. Polym. Sci.* **1989**, 27, 2385.

(81) Wei, Y.; Hariharan, R.; Patel, S.A. *Macromolecules* **1990**, 23, 758.

(82) Wei, Y.; Hsueh, K.F.; Jang, G.W. *Polymer* **1994**, 35, 3572.

(83) Pina, C. D.; Falletta, E.; Rossi, M. *Catalysis Today* **2011**, 160, 11–27

(84) Mailhe-Randolph, C.; Desilvestro, J. *J. Electroanal. Chem.* **1989**, 262, 289.

(85) Desilvestro, J.; Scheifele, W. J. *Mater. Chem.* **1993**, 3, 263.

(86) Rishpon, J.; Redondo, A.; Derouin, C.; Gottesfeld, S. *J. Electroanal. Chem.* **1990**, 294, 73

Chapter 2

FABRICATION AND CHARACTERIZATION OF A RECHARGEABLE MICROARRAY BATTERY

2.1 Introduction

As discussed in the chapter one, polyaniline has been extensively studied for decades because of its special properties such as electrical properties. Polyaniline is a conjugated polymer, also known as an intrinsically conducting polymer due to the existence of delocalized π electron system. The significant conductivity of polyaniline can be achieved when the imine nitrogen in polymer backbone is partly or fully protonated. The conductivity rises from the insulating polyaniline base to the conducting polyaniline salt with the doping from undoped form to fully doped form. A common acid and base, for instance, HCl and $NH_3 \cdot H_2O$ are used as doping and undoping reagents.[1] Figure 2.1 displays the reversible doping mechanism and conversion of different states of polyaniline.[2] The change of the electronic structure of polyaniline which responds to the conversion of the different oxidation states of polyaniline will cause a change in the optical properties of polymer. Therefore, polyaniline can be used in electrochromic displays and as optical sensors. Tamura and co-workers revealed the reversible color changes of polyaniline-coated electrode from yellow, green, dark blue to black, depending on the potential between -0.2 and 1.0 V vs. saturated calomel electrode (SCE).

The other applications include lightweight battery electrodes,[6] electromagnetic shielding devices,[7] and as chemical sensors to detect NO_2, O_3, O_2, NH_3, H_2S etc.[8-9]

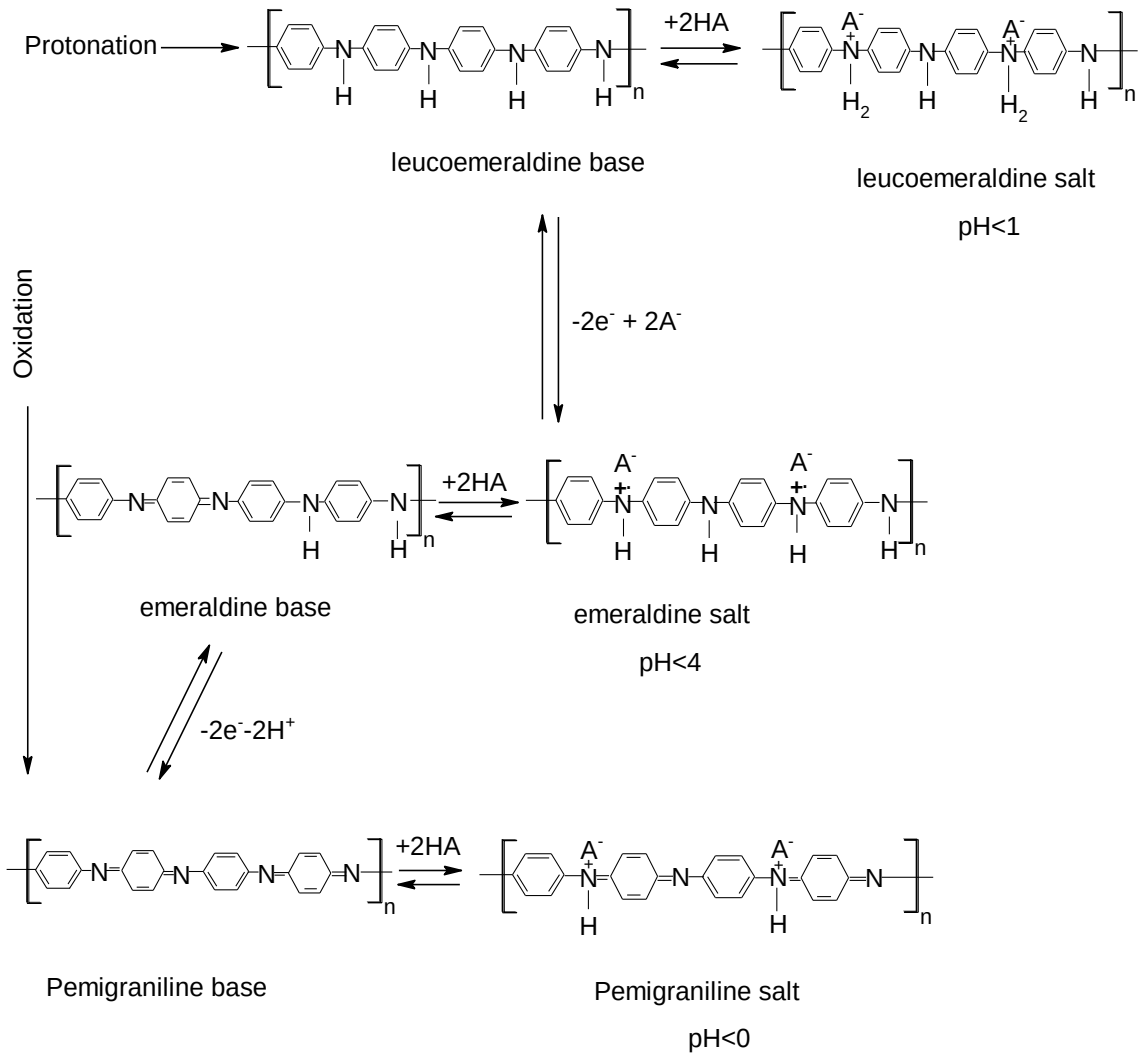

Figure 2.1 Reversible doping and conversion of different oxidation states of polyaniline

(Adapted from Ref 2)

The goal of this work is to develop a novel microarray battery that relies on the properties of polyaniline: conductivity, electrochromics, stability, and low costing.

2.2 Experimental section

2.2.1 Design of experiments

Following the principle of simplicity and miniaturization, a rechargeable microarray battery has been designed in which polyaniline and Ag were deposited electrochemically on the two ends of a microarray Au electrode in a bipolar electrochemical cell sequentially. Owing to the electrochromic properties, polyaniline was reduced with the companying of the color change in the cathodic pole. Simultaneously, the oxidation of Ag was observed in the anodic pole of the bipolar electrodes when a potential was applied on the two driving electrodes. Here the electrochemical cell acted as an electrolytic cell. However, once the power was removed, the electrolytic cell automatically switched to a galvanic cell. The reduced polyaniline thus was re-oxidized and Ag^+ was re-deposited. This process can be repeated based on the reversibility of redox reaction of polyaniline that results in the formation of the rechargeable batteries. Figure 2.2 schematically shows the design of the rechargeable microarray battery.

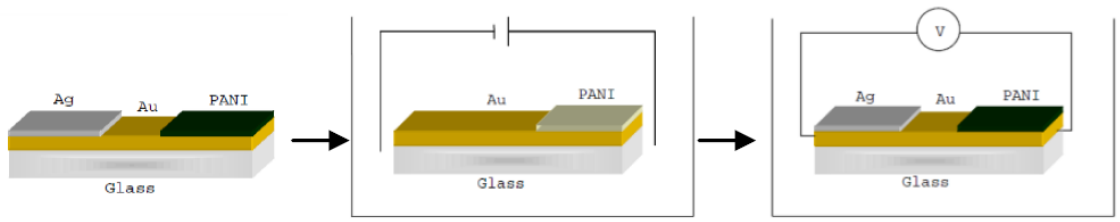

Figure 2.2 Schematic description of the working principle of a rechargeable microarray battery

The advantages of this design are expressed as following: All the microelectrodes can be controlled just by two driving electrodes, thus simplifying the setup of the experiments; all the experiments are operated on the microarray electrodes so that only the small amount of chemical reagents are needed; and the processes of charge-discharge can be observed visually.

2.2.2 Materials and Reagents

Aniline monomer (99.5%), silver nitrate, sulfuric acid, hydrochloric acid, copper sulfate pentahydrate, Dimethylformamide (DMF), N-Methyl-2-pyrrolidone (NMP) and potassium persulfate were purchased from Fisher. Perchloric acid and ceric ammonium nitrate were bought from Sigma-Aldrich. Au film (99.999% purity) was purchased from Alfa. Glassy carbon rods (6mm diameter) were obtained from SPI Supplies. All chemicals were used as received. Deionized water (Mill-Q, 18.2 MΩ.cm) was used to prepare all aqueous solutions.

2.2.3 Substrate Preparation

Microscope slides were ultrasonically cleaned in a deionized water bath and acetone bath for 30 minutes each respectively and dried in a stream of flowing N_2. Au bulk film electrodes were cleaned by immersing them into piranha solution (1:3 v/v 30% H_2O_2 and 18M H_2SO_4) three times for 15 minutes each and then rinsed by deionized water and dried in a stream of flowing N_2.

2.2.4 Synthesis of Polyaniline

The synthesis of polyaniline includes both chemical and electrochemical syntheses. Chemical synthesis can generate polyaniline powder, whereas, electrochemical approach can produce the polyaniline film on the electrodes.

2.2.4.1 Chemical Synthesis

1.67 mL concentrated HCl was added to 20 mmol aniline that was dissolved in 50mL distilled water in a volumetric flask to form Aniline hydrochloride. 25 mmol (6.75g) potassium peroxydisulfate was dissolved in 50ml water. These two solutions were kept at room temperature for 1 hour and then mixed and stirred for 5 minutes. The resulting solution was placed for 24 hours. The solution was filtrated and the precipitate was washed using 0.2M HCl and acetone for 3 times each, respectively. Polyaniline hydrochloride was dried in air for overnight and then under vacuum at 60^0C for 2 hours. Emeraldine-based polyaniline form was acquired by dissolving polyaniline hydrochloride powder in 3% ammonia solution for 8 hours. After being filtered, the emeraldine base was dried under vacuum at room temperature for 24 hours.

2.2.4.2 Electrochemical Synthesis

Two electrochemical methods were employed to synthesize polyaniline, these are, the cyclic voltammetry and the direct current potential amperometry. In a conventional three electrodes cell, the electropolymerization of aniline was carried out using a BAS epsilon potentiostat workstation. An Au foil was used as the working electrode, a Pt net acted as the counter electrode and Ag/AgCl was as the reference electrode. 0.1M aniline in 0.5M sulfuric acid solution was added to the cell and a scan range from -200mV to 1000mV was set. The scan rate was controlled at 50mV/s.

Polyaniline on microelectrodes was synthesized in a bipolar cell. Two stainless steels with areas 1.32 cm^2 were used as driving electrodes that were connected to a Hewlett-Packard model 6010 regulated DC power supply. 0.1 M aniline in 0.5M sulfuric acid solution was added to the cell (diameter 5 cm) and 17V was applied on two driving electrodes for 40 minutes. The polyaniline-coated glass slides were immersed in NMP for a few seconds to wash off the polyaniline formed on the exposed region (Space between the Au electrodes) of Au microarray electrodes.

Different approaches were used to deposit polyaniline on the different electrodes. For the big electrodes, the technique used in conventional electrochemical synthesis was employed; whereas, the deposition of polyaniline on the small electrodes such as microelectrodes has to be obtained utilizing the bipolar electrochemical technique.

2.2.5 Fabrication of Au microarray electrodes

2.2.5.1 Deposition of gold

A 20 nm thick chromium film was sputter coated on the pre-cleaned glass slides as a coherent layer. An Au layer with the thickness of 200 nm was subsequently deposited on the chromium coated glass slides.

2.2.5.2 Transference of microarray patterns

The fabrication of the Au microarray electrodes were implemented using the technique called toner transfer masking in which three things were needed: good-coated microscope slides with designed microarray patterns onto it, a single tone laser printer and a glossy photographic paper. In this work, the microarray patterns with the size of 3.02 x 0.35 mm were printed onto the glossy photographic paper (Photo Basic Gloss, Staples) by a laser printer (HP Laser Jet p3005n), and further transferred onto the Au-coated glass slides. Heat and pressure were employed to ensure that the glossy photographic paper with patterns were stuck to the surface of Au tightly. The glass slides were immersed into a warm water bath to peel away the paper and leave the patterns on the surface of glass slides. Finally, acetone was used to wash off the toner.[12]

2.2.5.3 Etching of gold and chromium

To obtain the microarray electrodes, the exposed areas of glass slides have to be etched. Potassium iodide electrolyte, and the mixture of perchloric acid ($HClO_4$) and ceric ammonium nitrate $(NH_4)_2[Ce(NO_3)_6]$ were used to etch Au and Cr. Potassium iodide electrolyte was dropped onto the glass slides until the color in exposed region changed to gray. After rinsing with water, the glass slides were successively etched using a solution of perchloric acid and ceric ammonium nitrate in order to oxidize

chromium to chromium cation. After a while, a transparent (exposed region) microarray Au electrode was achieved. Figure 2.3 shows the formation of Au microarray electrodes.

2.2.6 Formation of Polyaniline (PANI) on Au Microarray electrodes

Polyaniline film can be acquired through either electrochemical oxidation of aniline on the electrodes or drop coating. Electropolymerization of aniline was performed on Au microarray electrodes in a bipolar electrochemical cell. The approach of drop coating was to drop the solution of polyaniline (emeraldine-base synthesized by chemical approach) in N, N-Dimethylmethanamide (8.6 mg polyaniline in 0.75 ml DMF) solution onto the Au microarray electrodes. Hexadecyl-trimethyl-ammonium bromide (CTAB) was used as surfactant to change the surface property and aided a droplet of polyaniline solution to stabilize itself on the surface of electrodes.

2.2.7 Modification of Au microarray electrodes

Both of the polyaniline and silver were immobilized onto the Au microarray electrodes. Polyaniline was deposited on one end while Ag was coated on the other end of Au microelectrodes by placing the polyaniline-modified microarray electrodes in a bipolar cell with 0.1M fresh-made $AgNO_3$ solution as the electrolyte and applying 16V on the driving electrodes (glass carbon) for 2 minutes.

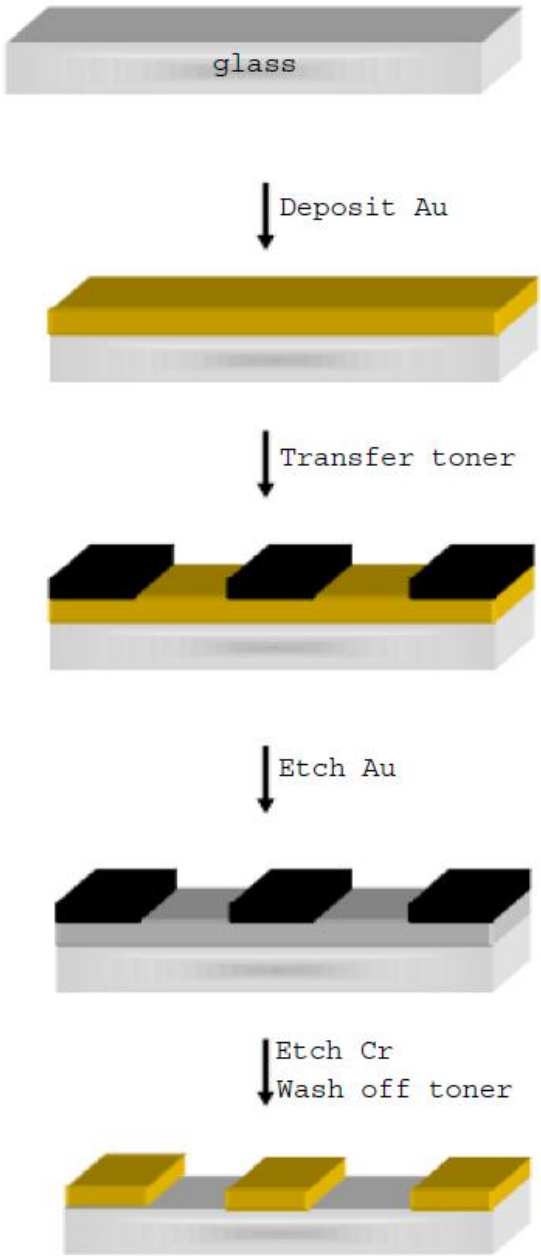

Figure 2.3 Schematic illustration of the fabrication of Au microarray electrodes.

2.2.8 Raman spectroscopy

Raman spectra were measured with a confocal microscopic Raman spectrometer (Renishaw 1000 model) coupling with a CCD detector and a holographic notch filter. Radiations (514 nm, 785 nm) from an air-cooled argon ion laser (Spectra-Physics Lasers, Inc. model 163-C4260) were used for excitation. Laser power is 5 mill watts. The collection time is 20 s and the number of accumulation is 1.

2.2.9 Linear Sweep Voltammetry and Cyclic Voltammetry

Linear sweep voltammetry measurements were performed using a BAS Epsilon Potentiostat workstation. A traditional three-electrode configuration was employed in which the Ag-coated Au bulk film acted as the working electrodes, a Pt net was the counter electrode and Ag/AgCl was the reference electrode. The electrolyte was 0.5M H_2SO_4 aqueous solution.

Unlike the Linear sweep voltammetry measurements, the cyclic voltammetry measurements were implemented using Au foil as working electrodes in 0.1 M aniline-0.5 M H_2S0_4 aqueous solution with the scan rate of 50 mV/s.

2.3 Results and Discussion

2.3.1 UV-visible spectrum of polyaniline

UV-visible absorption spectrum of polyaniline was recorded by a Shimadzu UV-3600 UV–vis-near infrared (UV–vis-NIR) spectrophotometer.

UV-visible spectrum of polyaniline was collected by dissolving polyaniline film in N-Methyl-2-pyrrolidone (NMP). The spectrum exhibits the feature of the emeraldine

base formed upon the de-protonation action of NMP on the Polyaniline hydrochloride. The peak found at 320 nm is attributed to a $\pi - \pi^*$ transition in the benzenoid structure and the peak at 610 nm is assigned to exciton formation in the quinoid rings. [13-16]

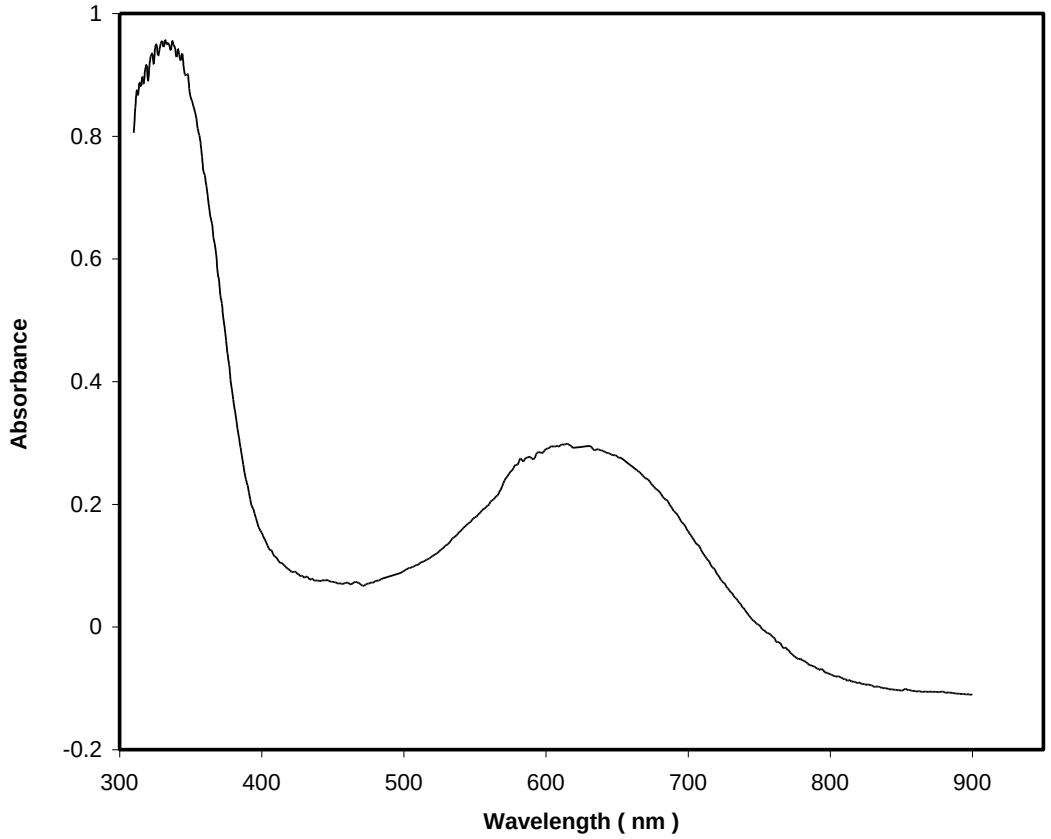

Figure 2.4 UV-visible absorption spectrum of polyaniline

2.3.2 Photographic records to charge-discharge processes of polyaniline

A microarray electrode composed of eight micrometer-scale Au electrodes was used as the bipolar electrode in the construction of the rechargeable batteries. Because of

the electrochromic property of polyaniline, the processes of charge-discharge can be observed visually. Therefore, photography is chosen to record those processes.

Picture 2.1 (a) displays the image of Au microarray electrodes after the polyaniline (blue) and silver (grey) were deposited on two ends of electrodes. A film of polyaniline with the deep blue was formed in anodic pool of bipolar microarray electrodes. The mechanism of this synthesis has been discussed in the chapter one. Briefly, the aniline monomer is firstly oxidized to form cation radicals, and then the cation radicals of aniline monomer react with each other to generate a dimer, oligomer until the polymer is developed. Due to the variety of potential gradient applied on bipolar electrodes at both vertical and horizontal directions, the deposition of the silver on the electrodes is not uniform.

When the modified Au microarray electrodes were placed into 0.5M sulfuric acid solution, the polyaniline film was protonated. Consequently, the green color was observed as exhibited in picture 2.1 (b). In these experiments, the right end with polyaniline film was set as the cathode and the left end coated silver acted as the anode of bipolar electrodes. When a constant potential was applied to the two ends of driving electrodes, the reduction of polyaniline occurred that led to the polyaniline changed from emeraldine to leucoemeraldine form, which can be observed by color change (picture 2.1 (c). Concurrently, the oxidation of silver took place on the anode which resulted in the stripping of silver. In this stage, the electrochemical cell was used as an electrolytic cell. Once the power supply was removed, the electrolytic cell would

automatically convert to a galvanic cell. In the negative pole of the galvanic cell, the polyaniline was oxidized that resulted in the occurrence of the green color, which indicated the recovery of the emeraldine form, while in the positive pole of this battery, the Ag^+ was reduced and the Ag was generated again (picture 2.1 (d). Picture 2.1 (e) was taken after five minutes the power was removed. When a potential is applied onto the driving electrodes for a longer time, Ag^+ formed on the anode of the Au microarray electrodes will migrate towards the cathode of the driving electrodes. Once the power is removed, it needs time for Ag^+ to move back. Therefore, the regeneration of Ag can be observed clearly in picture (e).

2.3.3 Raman Spectroscopy

Raman spectroscopy was used to monitor the conversion of oxidation states of polyaniline under the condition of applying different voltages.

The studies of spectroelectrochemistry were carried out in a glass cell (diameter 5cm) with 0.5M sulfuric acid solution as the electrolyte and glassy carbon electrodes as the driving electrodes (diameter 6 mm) that were connected to a Hewlett-Packard model 6010 regulated DC power supply.

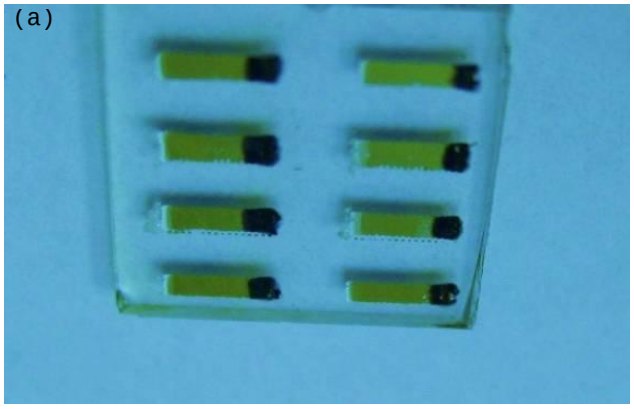
(a)

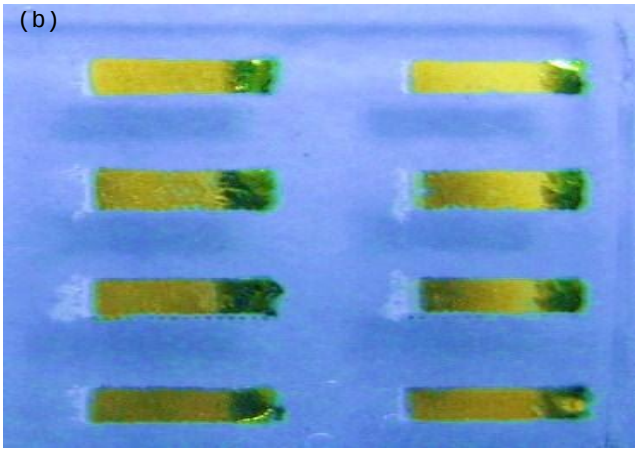
(b)

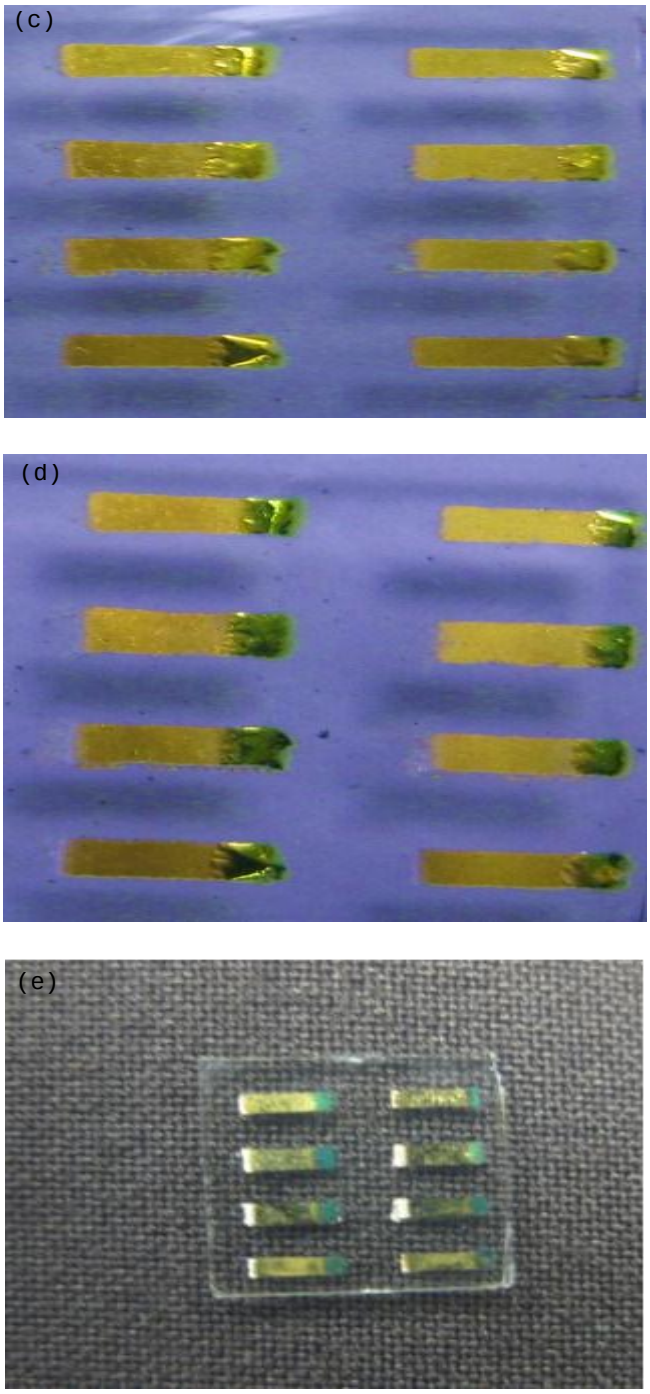

Picture 2.1 Processes of the PANI redox reactions taking place on micro-array electrodes accompanied by the stripping and recovering of Ag.

Figure 2.5 shows the variation of Raman spectra. Green curve represents the spectrum that was collected before applying voltage to the bipolar microarray electrodes, which is the spectrum of oxidized polyaniline. Compared to green curve, the orange one has a lower Raman intensity due to the reduction of polyaniline. After the power supply is removed, the reduced polyaniline is oxidized and Raman intensity restore. The experimental results indicate that the charge-discharge process is reversible. The length of conjugated chain on polyaniline backbone shortens as the polyaniline change from the oxidized state to the reduced state which reduces the polarizability of polyaniline molecules. As a result, the Raman intensities decrease with the conversion of oxidized form to reduced form. The peak at 1181 cm^{-1} is attributed to the C-H bending vibration on the benzenoid ring while the peak at 1351 cm^{-1} corresponds to the C-N stretching vibration of polarons. The peaks at 1597 cm^{-1} and 1514 cm^{-1} are ascribed to the C=N stretching and C=C stretching on the quinoid ring, respectively. The assignments of other Raman bands are showed in table 2.1.

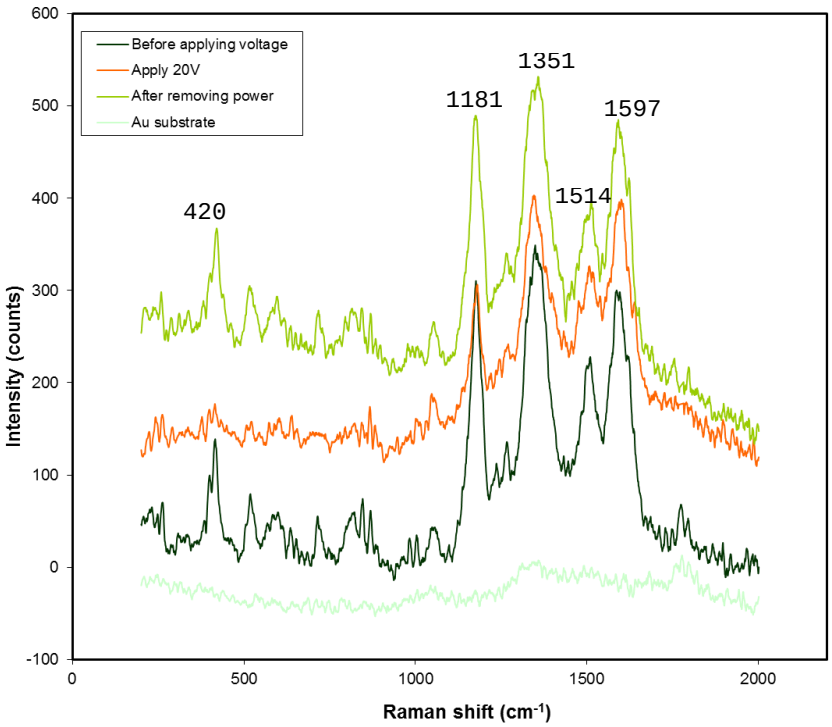

Figure 2.5 Raman spectra of polyaniline with and without an applying potential. The excitation wavelength is 785 nm (Collection time =20 s).

The structures of polarons and bipolarons are shown as follows: [18]

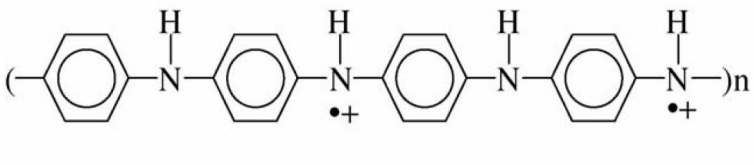

Polarons

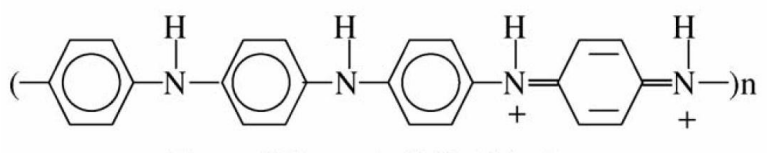

Bipolarons

Table 2.1 Assignment of Raman band of polyaniline[18-20]

Wavenumbers (cm^{-1})	*Assignment*
1597	C= C stretching (quinoid ring)
1514	C= N stretching (quinoid ring)
1351	C-N stretching of Polysemiquinone radical (polarons)
1248	C− N stretching (benzenoid ring)
1181	C− H bending (benzenoid ring)
1044	C-H bending and ring deformation (benzenoid ring)
999	C-H bending and ring deformation (benzenoid ring)
420	C-N-C conformational change in the PANI backbone

Figure 2.6 is the Raman spectra of polyaniline which was formed on the Au microarray electrode acquired by using 514nm laser as the excitation source. As mentioned in Figure 2.4, PANI base exhibits two absorption peaks in UV-vis –NIR spectrum. The peak at 320 nm is assigned to a π-π^* transition in the benzenoid structure and the peak at 610 nm is attributed to excitonic n-π^* transition involving in the benzenoid rings and the quinoid rings.[21] If 785 nm laser is replaced with 514 nm laser, the band originating from the oxidized segments should be relatively decreased due to the resonance Raman effects. Therefore, Raman spectra changes from figure 2.5 to figure 2.6.

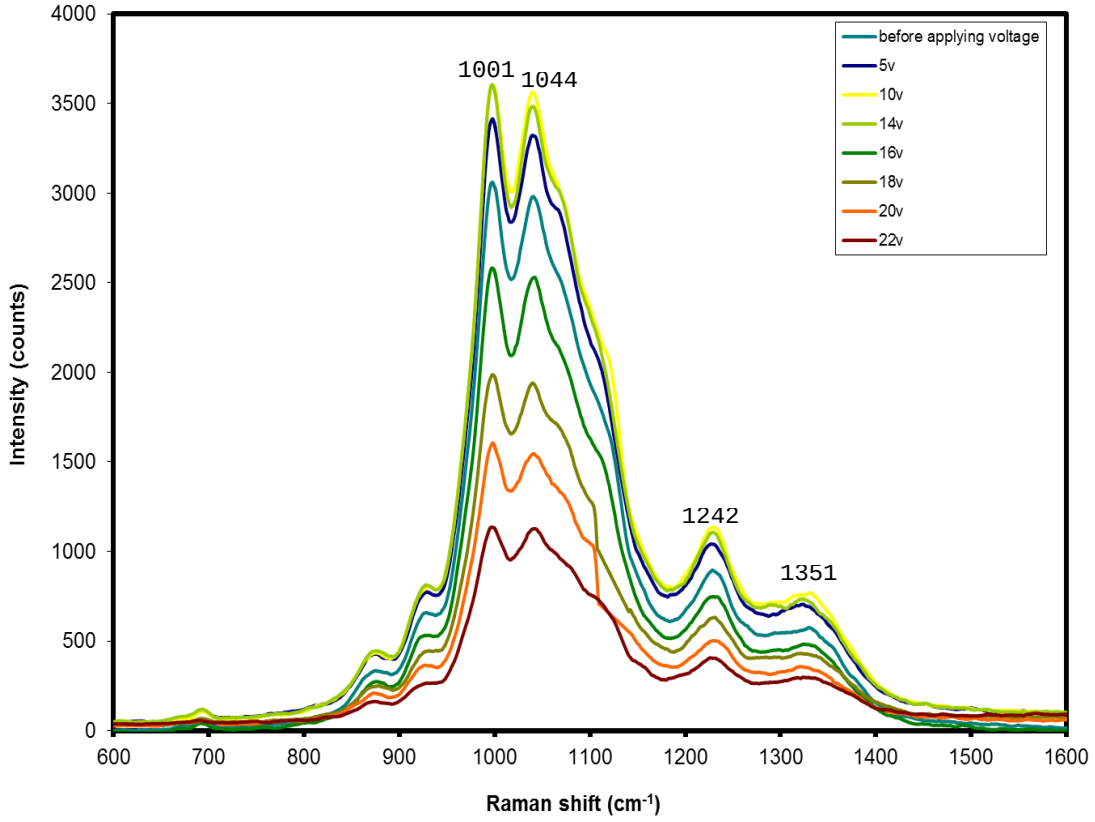

Figure 2.6 Raman spectra of polyaniline with the different applied voltages. The green laser of 514 nm was used as excitation source (Collection time is 20 s).

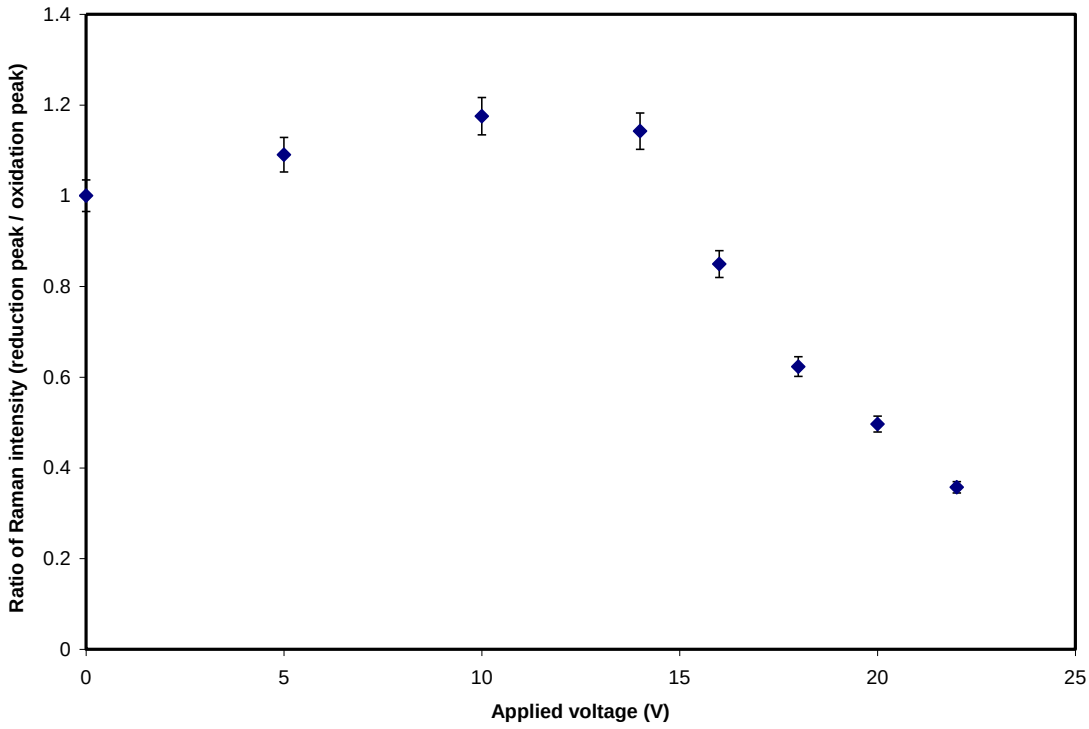

Figure 2.7 Ratio of Raman intensity for reduction peak / oxidation peak of PANI at 1044cm^{-1} as the function of applied voltage. The green laser of 514 nm was used as excitation source (Collection time is 20 s).

Generally, the Raman intensity of polyaniline coated in the cathodic pole of Au bipolar electrode decreases as the voltage increases gradually. To derive figure 2.7, the peak collected before applying voltages is treated as the oxidation peak and the peak collected after applying voltages is treated as the reduction peak. The intensity ratios were calculated from the intensities obtained at other applied voltages divided by the intensity acquired at 0 V. The peak centered at 1044 cm^{-1} is assigned to the C-H bending vibrations and deformation of benzenoid ring. In figure 2.7, a slight rise of intensity is

observed with the applied voltage from 0V to 13V. After that, the intensity ratio decreases which indicates the increasing of extent of reduction for polyaniline. The ratio is dominated by two opposite factors. On one hand, the intensities of C-H bending vibrations on the benzenoid ring increase with the reduction of polyaniline. On the other hand, the reduction of polyaniline decreases the Raman intensity due to the reducing of polarizability of polyaniline molecules. In the first stage, the increasing of the intensity surpasses the decreasing of the intensity and therefore, we see the slight increasing. In the second stage, the decreasing of the intensity plays a main role, and thus, a decreasing of intensity is observed.

Polyaniline is a conjugated polymer, including delocalized π bonds. When the voltages applied on driving electrodes increase, the degree of polyaniline being reduced increases, which causes the variation in electronic structure of polyaniline. The decreasing of conjugated chain in polyaniline increases the band gap energy between ground state and excited state, and decreases the polarizability of molecule which results in the decreasing of Raman intensity.

The fact of Raman intensity dropping as the extent of reduction of polyaniline increases can also be demonstrated by applying a constant voltage onto driving electrodes and subsequential measuring the intensities of different spots away from the end of bipolar electrode where the polyaniline was deposited (figure 2.8 from curve 1 to curve 10).

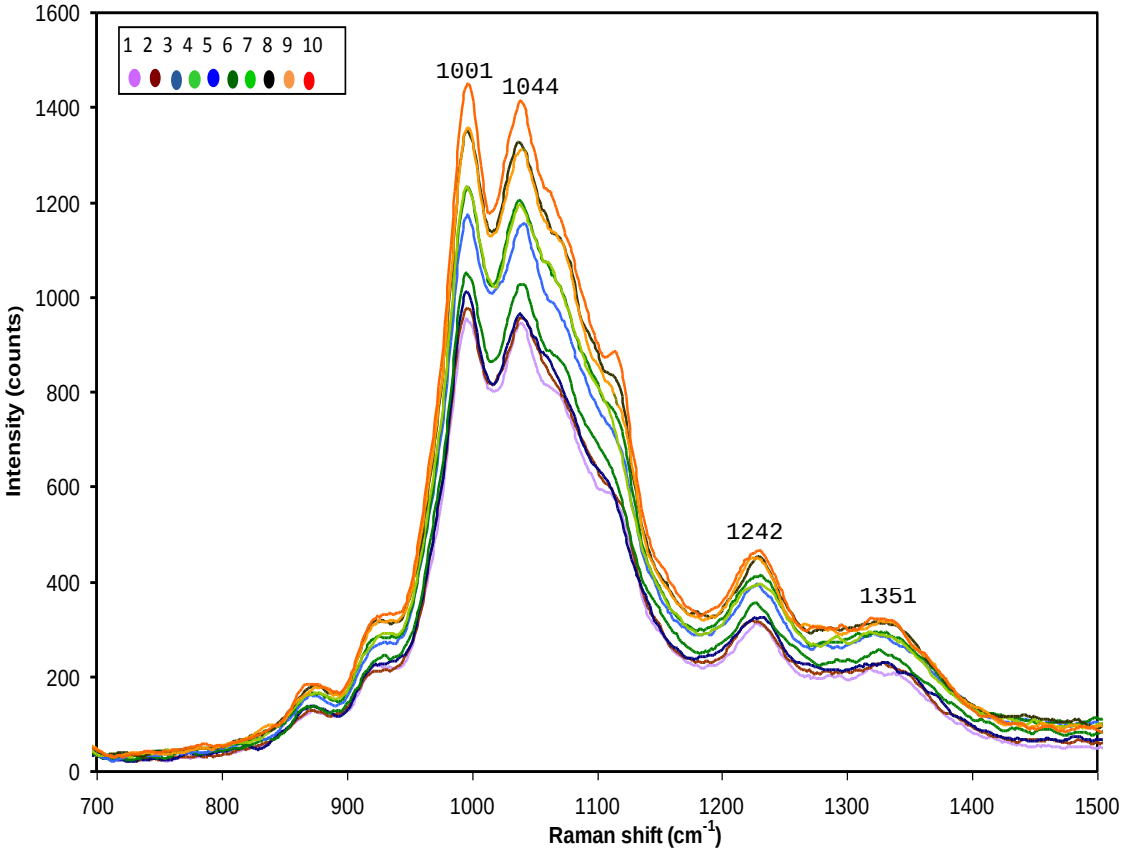

Figure 2.8 Raman spectra of polyaniline collected from different spots along the Au bipolar electrode. The excitation wavelength is 514 nm and the collection time is 20s. Inset stands for a bipolar electrode and the spots from where the Raman signals are collected. The distance between two spots is 50 μm.

Because of the special setup of bipolar electrodes in electrochemical cell (floating in electrolyte), the potential is the length dependent. The overpotential drops along the bipolar electrode from the end to the center. In this case, the degree of polyaniline being reduced decreases from the end to the center of Au bipolar electrodes. By integrating the peaks at 1044 cm^{-1} from figure 2.8, the relationship of Raman intensity of reduced

polyaniline and the distance from detected spots to the end of the polyaniline-modified Au bipolar electrode is achieved. The Raman intensities steadily augment as the measurements are implemented from the end to the center of electrode with a constant voltage applied as shown in figure 2.9.

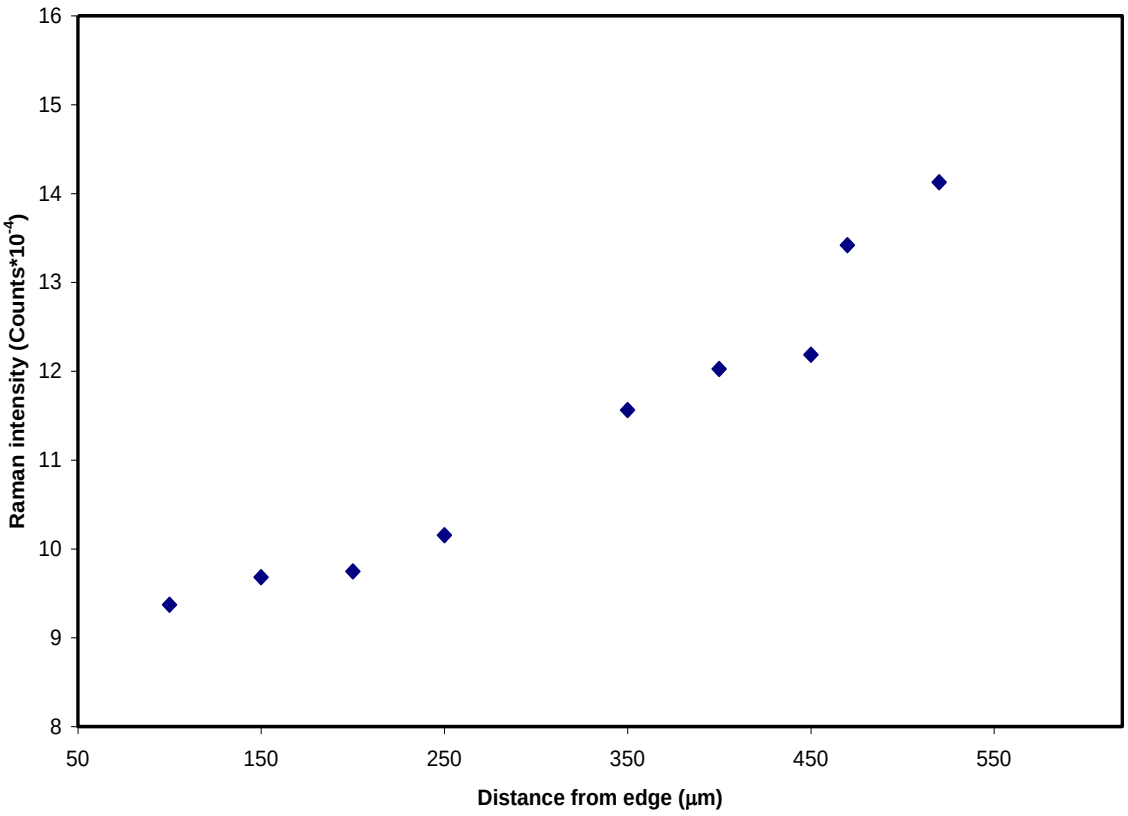

Figure 2.9 Raman intensity of reduced polyaniline as the function of the distance from detected spots to the end of the modified Au bipolar electrode.

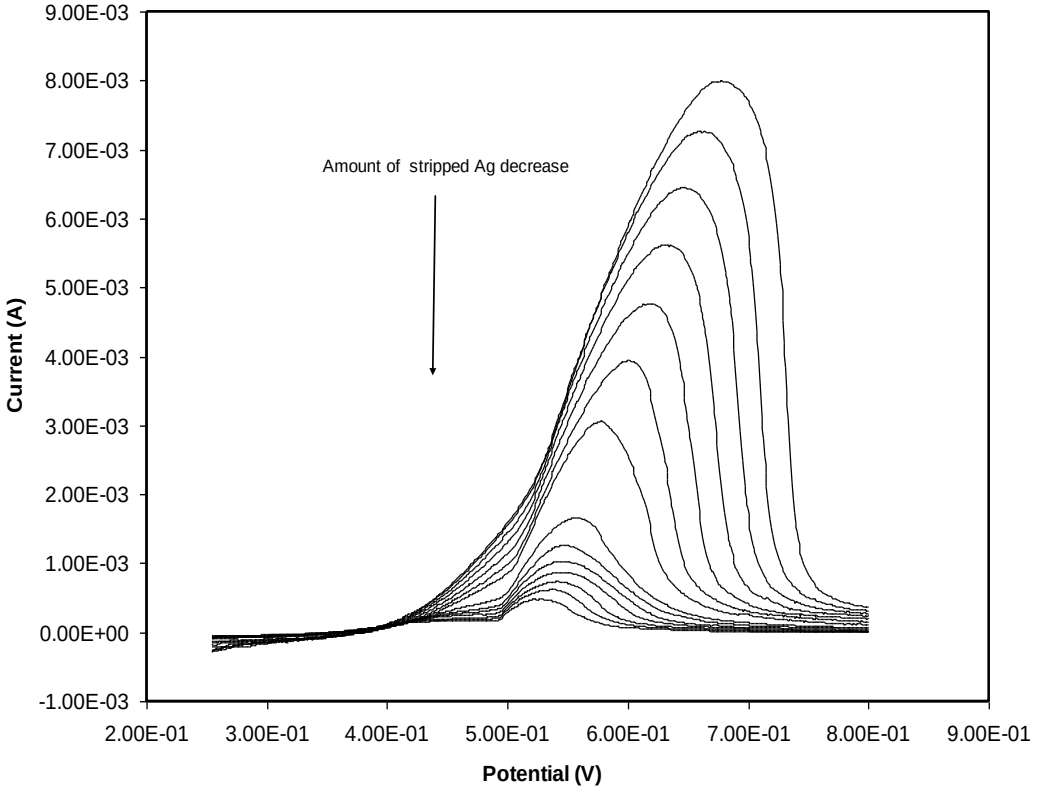

Figure 2.10 Representative of linear sweep voltammograms of Ag. The experiment was performed in 0.5M H_2SO_4 aqueous solution with scan rate 50mV/s

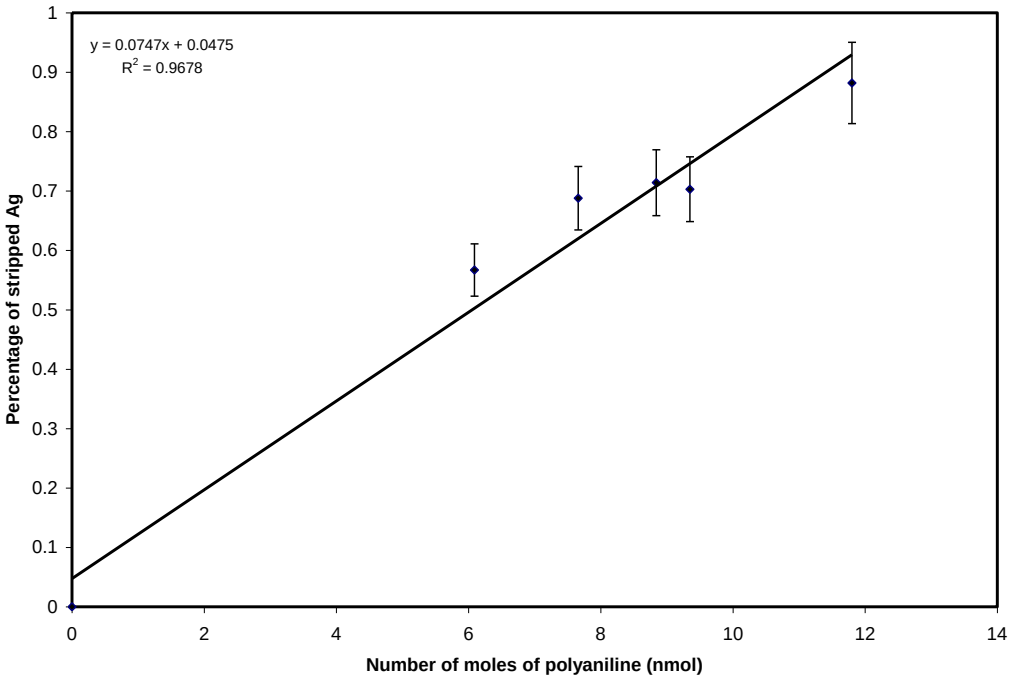

Figure 2.11 Percentage of stripped Ag as the function of the number of mole of polyaniline

2.3.4 Stripping of Ag

To measure the stripping percentage of Ag in the charge processes, a bulk Au foil was utilized as the substrate in which the polyaniline and Ag was immobilized on the two ends. The experiments were performed in a conventional three electrodes system by using the linear sweep voltammetry technique. Figure 2.10 exhibits the linear sweep voltammetry curves. The peak current gradually decreases which means the Ag left on the electrode becomes less and less. When the peak current was reduced to around 0.2 mA, the reaction was ceased. Similar results were also observed for the other samples (data not shown). Comparing the difference in the amount of stripped Ag before and

after the battery was charged, a relationship between the percentage of stripped Ag and the amount of polyaniline was obtained which is shown in figure 2.11.

Figure 2.11 exhibits the linear relationship between the percentage of stripped Ag and the amount of reduced PANI. Due to the requisition of the electro-neutrality, the rates of electron transfer at both of ends of the bipolar electrode must be equal. The amount of current flowing through the bipolar electrode is proportional to the amount of both stripped Ag and reduced PANI. Consequently, the percentage of stripped Ag is proportional to the number of moles of PANI.

Alternatively, the stripping of Ag can be recorded through photography. Figure 2.12 shows the good agreement with the results acquired from the linear sweep voltammetry.

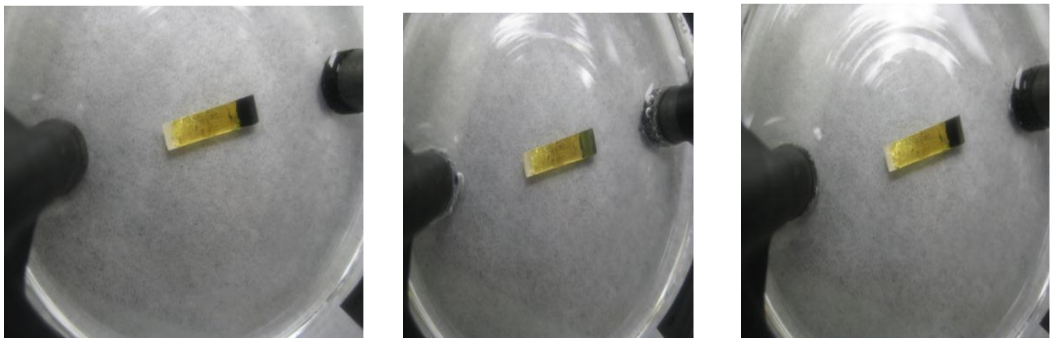

(a)

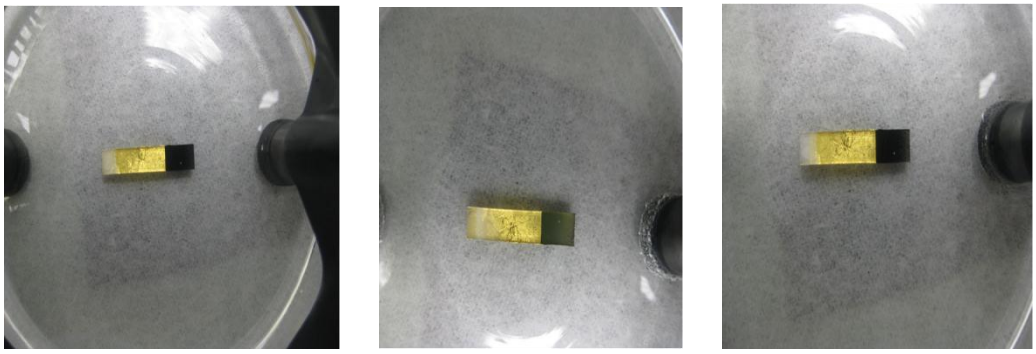

(b)

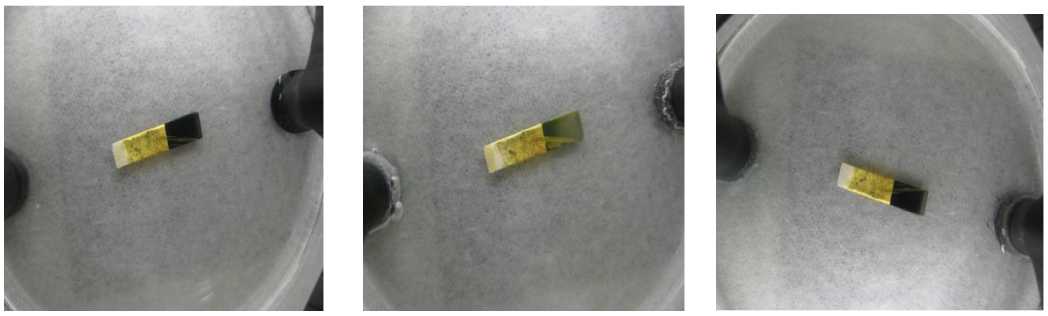

(c)

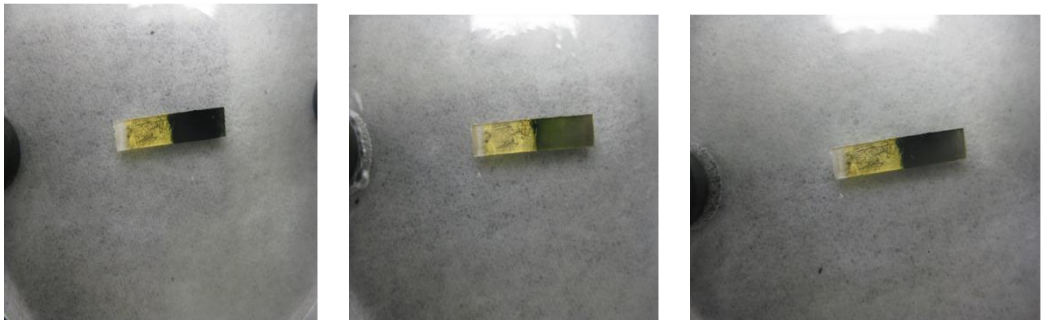

(d)

Picture 2.2 Processes of PANI redox reactions accompanied by stripping and recovering of Ag. The deposited PANI is (a) 9.50 nmol, (b) 15.9 nmol, (c) 17.2 nmol, (d) 21.7 nmol

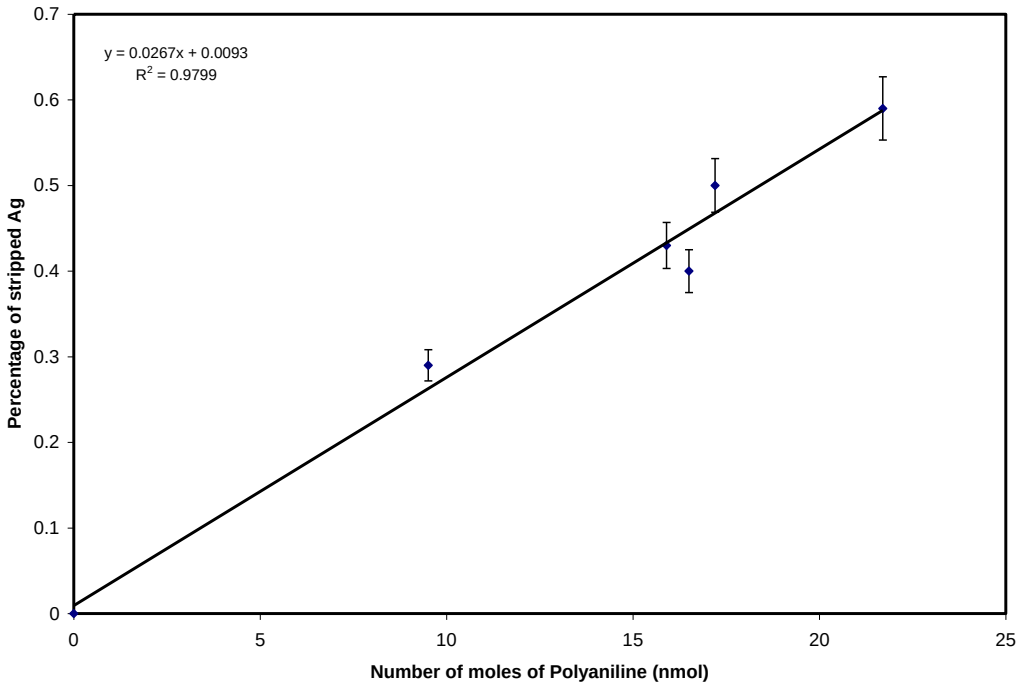

Figure 2.12 Calibration curve

Table 2.2 presents the percentage of stripped Ag with different depositing time of Ag. The percentage of stripped Ag drops from 100% to 45.5% as the results of depositing time being increased from 45 to 75 minutes with a similar amount of PANI on the other end of the electrodes. The amount of PANI being increased from 8.6 nmol to 15.9 nmol causes the arising of percentage of stripped Ag from 45% to 100% with the same depositing time. Further, the experimental results demonstrate the near linear relationship displayed in figure 2.12.

Table 2.2 Percentage of stripped Ag with different depositing time of Ag.

Deposit time (s)	Polyaniline (nmol)	Percentage of stripped Ag
30	6.17	1.00
45	8.73	1.00
75	8.60	0.455
75	15.9	1.00

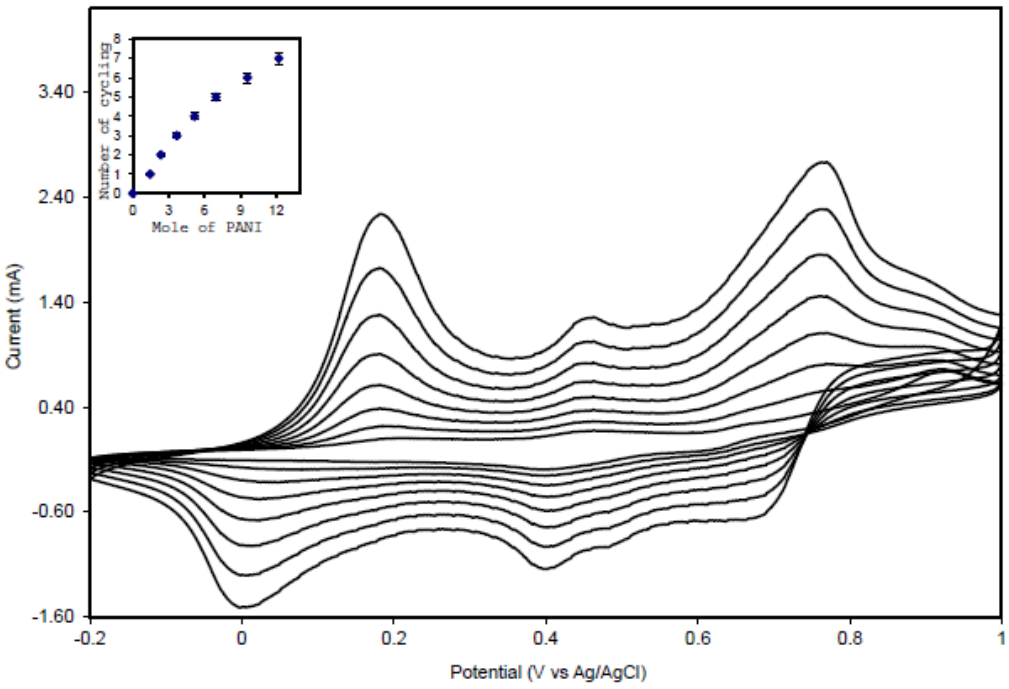

Figure 2.13 Cyclic voltammograms for electropolymerization of aniline in 0.1 M aniline-0.5 M H_2S0_4 aqueous solution: scan rate, 50 mV/s. The number of cycles as the function of the amount of polyaniline is plotted as inset.

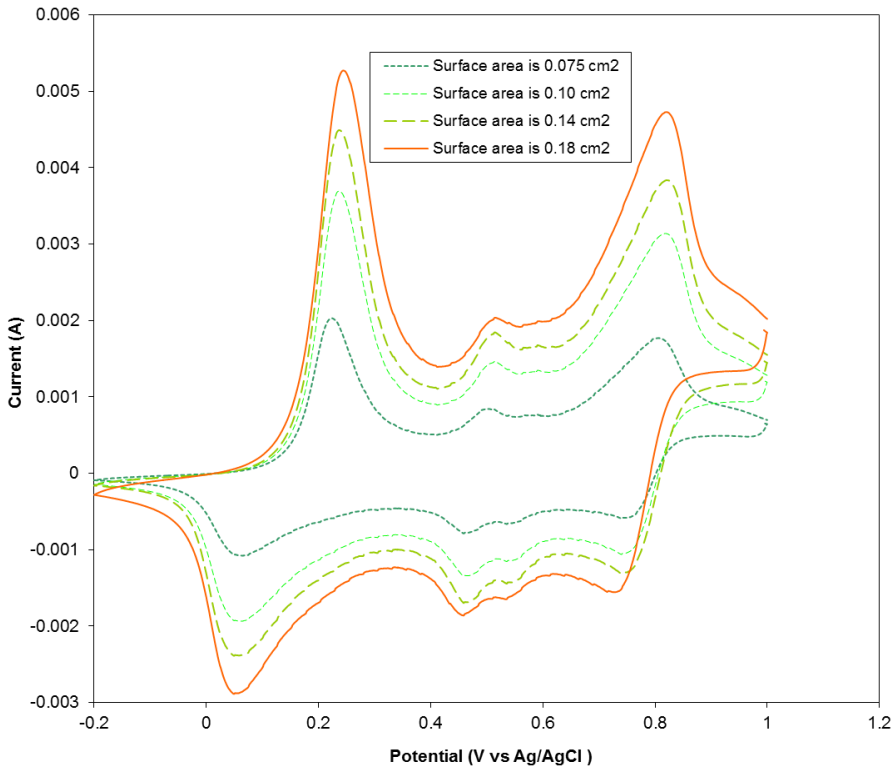

Figure 2.14 Cyclic voltammograms for polyaniline with same thickness and various electrode surface areas.

2.3.5 Cyclic voltammetry

The cyclic voltammograms for electropolymerization of aniline on an Au electrode are shown in figure 2.13. There are two strong anodic peaks occurring at 0.17V and 0.75V sequentially and a weak peak at 0.44V. The peak at 0.17V is assigned to the oxidation of leucoemeraldine to Polyaniline base while the peak at 0.75V is ascribed to the oxidation of Polyaniline base. The weak peak is thought to be the results of the degradation of polyaniline that refers to the formation of benzoquinone and is attributed

to the oxidation of a quinoid structure.[22-23] Inset displays the relationship between the number of cycling and the amount of polyaniline deposited on the surface of Au foil. More scan cycles will produce more polyaniline.

Figure 2.14 is the cyclic voltammograms for polyaniline used in Ag stripping experiments. The electrode surface area is displayed in the graph. The bigger the electrode surface area is, the more the deposited polyaniline there is.

2.3.6 Substrate Effect

In order to investigate the reaction activities of the different metals as substrates in these reactions, four metals were utilized: copper, silver, gold, and platinum. Polyaniline is more noble than Cu and less noble than Ag, and Au as well as Pt. Therefore, once the electrolytic cell is converted into the galvanic cell by removing the power, Ag^{+}(also Au^{3+}, Pt^{4+}) around negative pole will be reduced to Ag (or Au, Pt), while Cu^{2+} in negative pole will not be spontaneously reduced to Cu. Accordingly, Ag, Au and Pt can be used in this kind of battery reactions except for copper. Under the same experimental condition, silver has the highest reaction activity due to its highest reduction ability, and thus having the highest concentration of Ag^{+} around anode of bipolar electrode in electrolytic cell. When the electrochemical cell changes from an electrolytic cell to a galvanic cell, there will be the greatest amount of re-deposited Ag when compared with Au and Pt. The reaction activity of Pt is better than that of Au, because Pt has a stronger ability of reduction than Au's. Picture 2.3 exhibits the redox reactions taking place on the Pt bipolar electrode

accompanied by the stripping of Cu. It can be seen that copper won't redeposit on the positive pole of Pt electrode after removal of the power source.

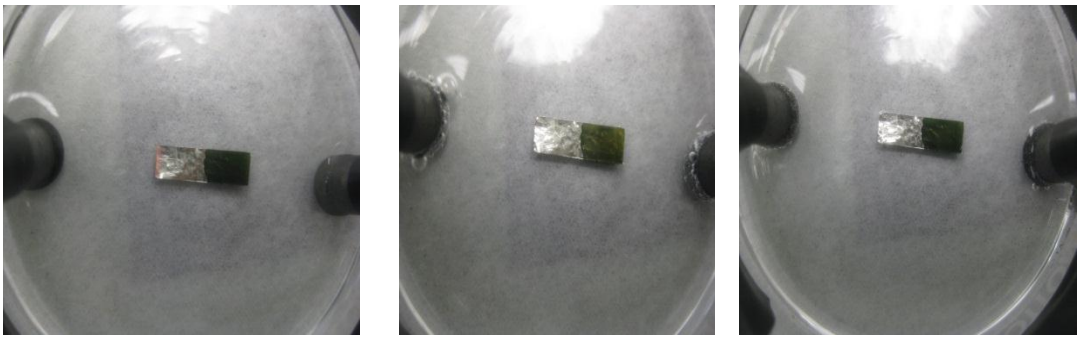

Picture 2.3 PANI redox reactions taking place on the Pt electrode accompanied by the stripping of Cu.

2.4 Conclusions

A rechargeable battery based on the Au microarray electrodes has been fabricated and characterized. The exploration of conductive materials formed on micrometer scale substrates via bipolar electrochemical technique allows us to modify the electrodes with even smaller size. A simple and speedy approach with less costing was used to make microarray electrodes. The Raman intensities of the reduced polyaniline decreased with the increasing of applied potential due to the variation of electronic structure on polymer backbone. The electrochromic properties of polyaniline enables us to monitor the charge-discharge processes visually. The output voltages for Au microelectrodes were measured. The results show that the average value for one Au microarray is 0.2V. The

interesting result reported here is that the voltage of a microarray battery can be controlled by placing the electrodes with the different amounts and the different array patterns on the surfaces of Au substrates, which will let us design batteries with a wide range of voltages.

References

(1) Huang, J. and Kaner, R. B. *Macromolecules* **2005**, 38(2), 317.

(2) Lange, U.; Roznyatovskaya1, N. V.; Mirsky, V. M. *Analytica chimica acta* **2008**, 614, 1–26.

(3) Kobayashi, T.; Yoneyama, H.; Tamura, H. *J. Electroanal. Chem.* **1984**, 161, 419.

(4) Kobayashi, T.; Yoneyama, H.; Tamura, H. *J. Electroanal. Chem.* **1984**, 177, 281.

(5) Kobayashi, T.; Yoneyama, H.; Tamura, H. *J. Electroanal. Chem.* **1984**,177, 293.

(6) Desilvestro, J.; Scheifele, W.; Haas, O. *J. Electrochem. Soc.* **1992**, 139, 2727.

(7) Joo, A.J.; Epstein, K. *Appl. Phys. Lett.* **1994**, 65, 2278.

(8) Xie, D.; Jiang, Y.; Pan, W.; Li, D.; Wu, Z.; Li, Y. *Sens. Actuators B* **2002**, 81, 158.

(9) Mohammad, F. *J. Phys. D: Appl. Phys.* **1998**, 31, 951.

(10) Sakurai, Y.; Jung, H.S.; Shimanouchi, T.; Inoguchi, T.; Morita, S.; Kuboi, R.; Natsukawa, K. *Sens. Actuators B* **2002**, 83, 270.

(11) Hanawa, T.; Kuwabata, S.; Hashimoto, H.; Yoneyama, H. *Synth. Met.* **1989**, 30, 173.

(12) Easley, C. J.; Benninger, R. K. P.; Shaver, J. H.; Heada, W. S, and Piston, D. W. *Lab Chip* **2009**, 9, 1119–1127

(13) Pruneanu, S.; Veress, E.; Marian, I.; Oniciu, L. *Journal of Materials Science* **1999**, 34, 2733 – 2739.

(14) Zach, P. *J. Polym. Sci.* **1972**, 10, 2379.

(15) Rao, C. N. R. “Ultra-Violet and Visible Spectroscopy,” 2nd ed. (Butterworth, Guildford, **1967**).

(16) Monkman, A. P. in “Conjugated Polymeric Materials, Nato ASI Series E: Applied Sciences,” Vol. 182, edited by J. L. Bredas and R. R. Chance (Kluwer, Dordrecht, The Netherlands, **1990**), 273.

(17) Kumar, A. *Nanofibers*, ISBN 978-953-7619-86-2, **2010**, 438.

(18) Bernard, M.C.; Hugot-Le Goff, A. *Electrochimica Acta* **2006**, 52, 595–603.

(19) Gustavo, M.; Nascimento, P.; Kobata, Y. G. and Marcia, L. A. *J. Phys. Chem. B* **2008**, 112, 11551–11557.

(20) Boyer, M.-I.; Quillard, S.; Rebourt, E.; Louarn, G.; Buisson, J. P.; Monkman, A. and Lefrant, S. *J. Phys. Chem. B* **1998**, 102, 7382-7392.

(21) Quillard, S.; Louarn, G.; Lefrant, S.; MacDiarmid, A. G. *Phys. ReV. B* **1994**, 50, 12496

(22) Watanabe, A.; Mori, K.; Iwasaki, Y. and Nakamura, Y. *Macromolecules* **1987**, 20, 1793-1796.

(23) MacDiarmid, A. G.; Chiang, J. C.; Halpern, M.; Huang, W. S.; Mu, S. L.; Somasiri, N. L. D.; Wu, W.; Yaniger, S. I. *Mol.Cryst. Liq. Cryst.* **1985**, 121, 173.

Chapter 3

WIRELESS ELECTROCHEMICAL SENSORS WITH OPTICAL READOUT: DETECTION OF ALCOHOL

3.1 Introduction

The electrochemiluminescence of $Ru(bpy)_3^{2+}$ and its derivatives as detectors have been broadly studied since $Ru(bpy)_3^{2+}$ ECL was firstly observed by Bard's group.[1-2] Danielson et al reported the detection of alkylamines, amino acids, protein, antibiotics, and some other compounds.[3-7] Uchikura and coworkers utilized ECL reaction to determine tryptophan.[8] However, of these studies many works were related to the solution ECL (ECL occurring in the diffusion layer near the electrode surface). Compared with the solution ECL, $Ru(bpy)_3^{2+}$ immobilized on a solid electrode surface can not only reduce the consumption of some expensive chemicals, but also generate a reusable sensor. Many methods are used to immobilize $Ru(bpy)_3^{3+}$ and its derivatives onto the electrodes such as ion exchange interactions, covalent binding, layer by layer self-assembly and the Langmuir-Blodgett technique. Bard et al used Nafion, a cation exchange polymer, to immobilize $Ru(bpy)_3Cl_2$ on the surface of pyrolytic graphite to investigate ECL mechanism via the reactions of electrogenerated $Ru(bpy)_3^{3+}$ with oxalate based on the electrochemical stability of Nafion and high selectivity of polymer to $Ru(bpy)_3^{2+}$.[9-10,11] Nieman et al reported Nafion-modified electrodes used to examine NADH.[12] Cui and coworkers immobilized $Ru(bpy)_3^{2+}$ on Nafion-coated graphite oxide electrode surface and obtained two cathodic ECL peaks under the cyclic voltammetric

conditions.[13] Following these works, we report a wireless alcohol sensor with a simple experimental design and the function of regenerating reagents.

Alcohol measurement is a prime demand for brewing and food industry. For example, plant products such as hexanol, play important roles in plant defense and represent a potential source of natural alternatives to improve the shelf life and the safety food. Several alcohol sensors have been reported based on alcohol dehydrogenase.[14-19] The catalytic reaction is as below:

$$R\text{-}CH_2OH + NAD^+ \xrightarrow{ADH} R\text{-}CHO + NADH + H^+ \quad (3.1)$$

The concentration of alcohol can be measured by directly detecting the reduced form of nicotinamide adenine dinucleotide (NADH).

As we know, an electrically isolated conductor immersed in an electrolyte can act as a bipolar electrode, if a sufficiently large potential difference is applied across the solution. By coupling an electron transfer reaction involving the analyte at one end of the bipolar electrode to a light emitting process at the other end, one can read out the state of the bipolar electrochemical sensor optically and spectroscopically. Such a kind of sensors is reported here. To detect alcohol, the enzyme reaction is combined with ECL reporter. On one hand, the rates of electron transfer at both ends of Pt bipolar electrodes are the same due to the electroneutralization, thus, the concentration of alcohol can be detected by measuring the intensity of ECL. On the other hand, the expensive NAD^+ can be regenerated automatically.

3.2 Experimental section

3.2.1 Chemicals and materials

Multiwalled carbon nanotubes(MWCNTs) with diameter of less than 30nm was purchased from Nanolabs, Inc. Nicotinamide adenine dinucleotide(NAD^+), Alcohol dehydrogenase (EC 1.1.1.1) (ADH), Poly(diallyldimethylammonium chloride) (PDDA), Nafion 117 solution, Tris(2,2'-bipyridyl) dichlororuthenium(II) hexahydrate and platinum foil were obtained from Sigma-Aldrich. All chemicals were used as received.

3.2.2 Preparation of alcohol sensor

Platinum foils (12.5mm×12.5mm) were used as the substrates for the construction of the sensors. Pt foils were polished with aqueous slurries of fine alumina powders (0.05 um) on a polishing cloth, and then rinsed with deionized water and ethanol for 4 minutes each in an ultrasonic bath. Following that, the Pt foils were cleaned electrochemically in a traditional three-electrode cell with 0.05 M H_2SO_4 solution as the electrolyte scanning from -250 to 1250 mV for 1 hour.

Layer by layer self-assembly technique was used to prepare alcohol sensors. Briefly, Pt foil was immersed in a solution that MWCNTs (2 mg) was suspended in 1 mL dimethyformamide (DMF) for 1 hour and then placed into an aqueous solution of 10 mM NAD^+ for overnight. The MWCNTs/NAD^+ -Modified Pt foils were rinsed with deionized water for 3 times and dried under N_2 atmosphere. After that, the Pt foils were further modified by immersing them in (2 mg/ml) ADH in 0.1 M Phosphate buffer (pH=8.12) solution for 1 hour and then rinsed with the PBS buffer solution and deionized H_2O for 3

times subsequently. The last step was to put the Pt foils in 30% PDDA solution for 1 hour, then rinsed and dried under N_2 steam.

2μL Nafion 117 solution was pipetted onto the other end of a modified Pt foil. After being dried, the Pt was immersed in 0.1M H_2SO_4 solution containing 1mM $Ru(bpy)_3Cl_3$ for 1.5 hour and then rinsed with H_2O and dried under N_2 steam. $Ru(bpy)_3Cl_3$ was obtained through the chemical oxidation of $Ru(bpy)_3Cl_2$.

3.2.3 Apparatus and measurements

All the ECL experiments were performed in a bipolar electrochemical cell. The electric field was generated by applying voltage between two Au wires that were inserted into 0.1M phosphate buffer solution (4mL) containing 30% wt CH_3CN and 5mM $K_2S_2O_8$ solution (0.05mL). All the ECL intensities were measured using a confocal microscopic Raman spectrometer (Renishaw 1000 model) with a CCD detector and a holographic notch filter. Radiation of 514 nm from an air-cooled argon ion laser (Spectra-Physics model 163-C4260) was used for excitation. The collection time was 10s.

The measurements of cyclic voltammetry were performed using a BAS epsilon potentiostat workstation. A standard three electrode system was used in which a modified Pt foil acted as the working electrode, a Pt net was the counter electrode and Ag/AgCl served as the reference electrode.

3.3 Results and discussion

3.3.1 Characterization

3.3.1.1 Modification of one end of Pt bipolar electrode.

In this study, the reasons for MWCNTs being chosen as the first layer lie in its special electronic structure and ability to facilitate electron transfer reactions. MWCNTs, NAD^+, ADH and PDDA were immobilized on the anodic pole of Pt bipolar electrode by the layer-by-layer self-assembly technique. The adsorption of NAD^+ onto MWCNTs is considered to be the strong π–π stacking interaction between the adenine subunit in the NAD^+ molecule and delocalized π in MWCNTs.[22] The ADH shows negative charge when ADH is dissolved in 0.1M pH 8.14phosphate buffer solution. Therefore, by specific binding (between ADH and NAD^+) as well as electrostatic interaction, ADH and PDDA can be subsequently adsorbed onto NAD^+/ FMWCNTs-modified Pt surfaces.

Figure 3.1 displays the Raman spectra of MWCNTs (brown curve), NAD^+/MWCNTs (blue curve), ADH/ NAD^+/ MWCNTs (orange curve) and PDDA/ ADH/ NAD^+/ MWCNTs (green curve) achieved on the surface of Ag. (Incident light was focused on the black spot). The two Raman bands of MWCNT called D-band from the disorder induced mode and G-band from the tangential mode occur at 1360cm^{-1} and 1598cm^{-1} resepectively.[20] The Peaks at 2720 cm^{-1} and 2956 cm^{-1} correspond to the second-order bands: 2D and D+G.[21] The intensities of Raman spectra gradually decrease with the assembling of layer by layer.

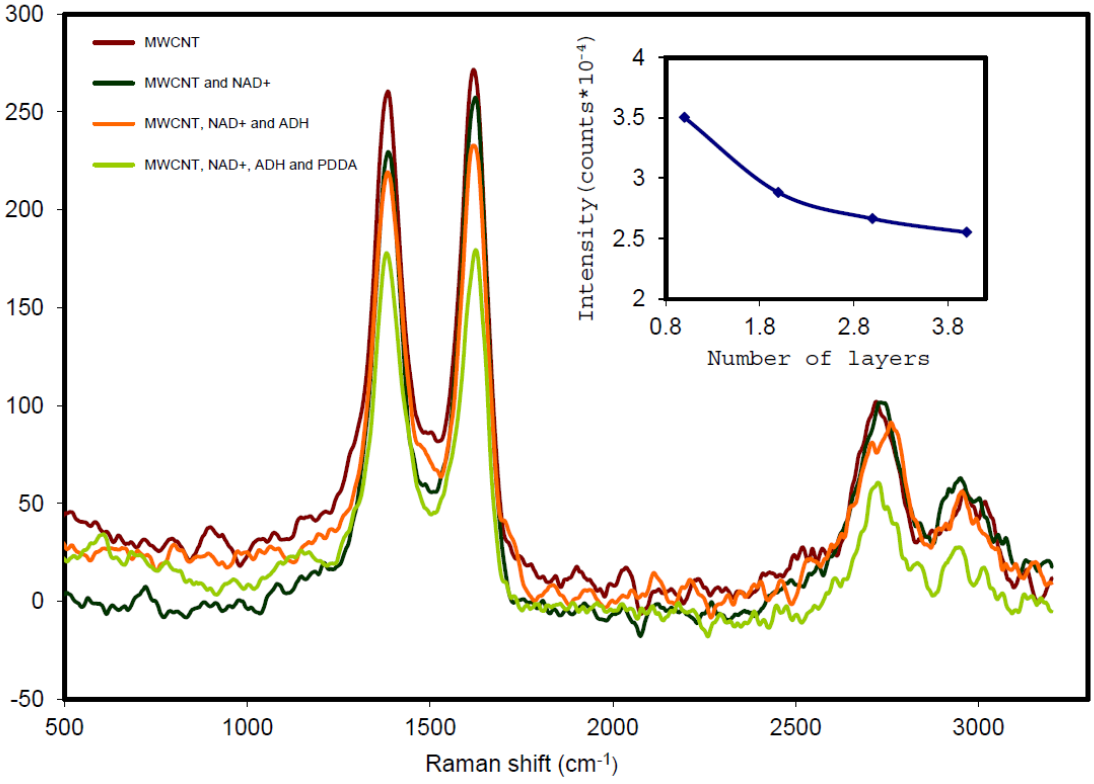

Figure 3.1 The Raman spectra of MWCNTs, NAD^+, ADH and PDDA immobilized on the surface of silver foil.

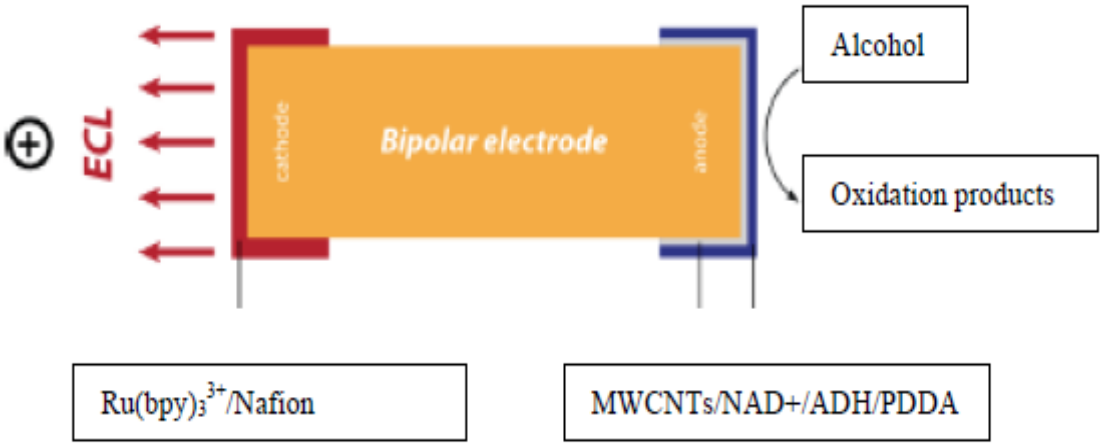

Scheme 3.1 Chemical modified bipolar electrode for the detection of alcohol

3.3.1.2 Fabrication of alcohol sensor

Scheme 3.1 depicts the formation of alcohol sensor. PDDA, ADH, NAD^+ and MWCNTs are adsorbed on the anodic pole and $Ru(bpy)_3^{3+}$-doped Nafion is coated on the cathodic pole. The state of the sensor is indicated by the ECL intensity.

Picture 3.1 is the Optical image showing ECL from cathodic pole of BPE after alcohol was added into the bipolar electrochemical cell. The light emission demonstrates that the alcohol sensor has been successfully fabricated.

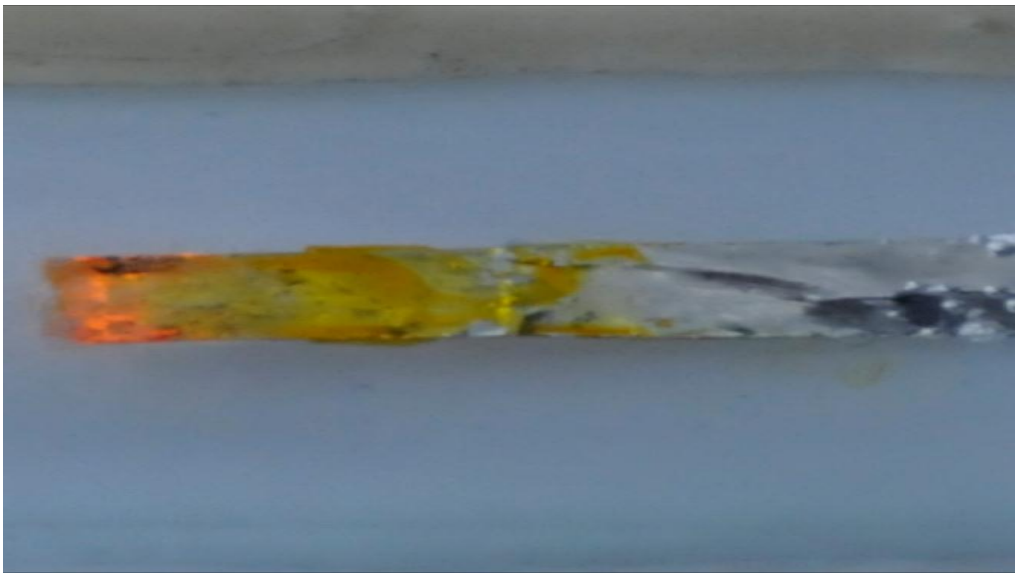

Picture 3.1 The ECL image obtained from cathodic pole after alcohol was added into the bipolar electrochemical cell.

3.3.2 Quantitative response of alcohol sensor to ethanol

We measured the cyclic voltammogram of ethanol using modified Pt as working electrode in 0.1M pH 8.12 phosphate buffer solution with a scan rate of 50 mV/s. Two oxidation peaks were acquired (see figure 3.2). The peak located at 0.3V is ascribed to the formation of acetaldehyde while the second peak occurred at 0.67V is attributed to the reaction that ethanol is oxidized to generate acetic acid.

When a potential is applied between the two driving electrodes, the potential of solution will drop gradually as the distance from the driving electrodes gradually increases due to the solution resistance. Thus, a potential gradient is formed through the solution. Figure 3.3 describes the potential of solution as the function of the distance from the driving electrodes. In this experiment, the input voltage was 13V and the experiment

was carried out in a glass cell (diameter 3.6cm) filled with 0.1M pH 8.12 phosphate buffer solution by measuring the potential difference of solution at different position between two driving electrodes. The results indicated that the potential difference was 2.1V when the bipolar electrode was place 1.2cm far from the two driving electrodes.

Cui and coworkers observed two cathodic ECL peaks of $Ru(bpy)_3^{2+}$ at -0.99 V and -1.8V (vs. saturated calomel electrode). The first oxidation potential of ethanol from our experiment results is 0.3V. Consequently, the enzyme catalytic oxidation reaction of ethanol monitored by ECL will take place, once a more than 13V voltage is applied on the driving electrodes.

In order to study the intensity of ECL that is subject to the response of alcohol sensor to ethanol, Raman microscopy was employed to collect the fluorescence spectrum generated by ECL. As discussed before, because of the requirement of charge balance at two ends of bipolar electrodes, the velocities of faradaic processes occurring at both anode and cathode are the same. Hence, the velocity of anodic reaction is related to the photon flux at cathodic pole. Figure 3.4 exhibits the linear relationship between the ECL intensity and the concentration of ethanol.

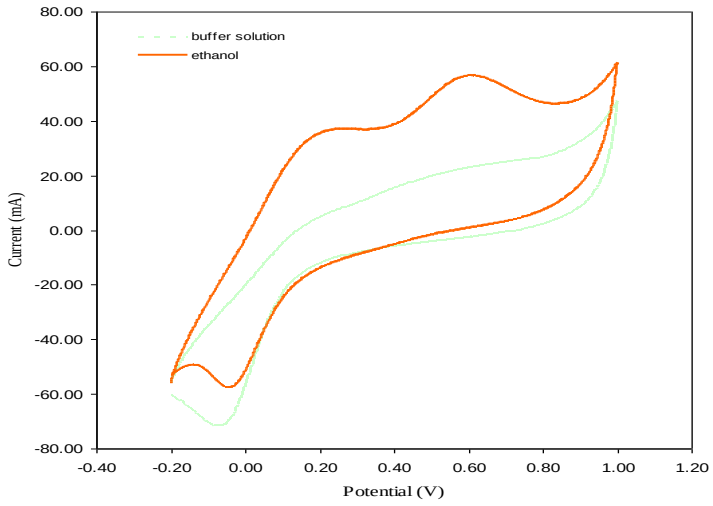

Figure 3.2 Cyclic voltammogram of modified Pt in 0.1M PH=8.12 Phosphate buffer solution after adding 9mM ethanol.

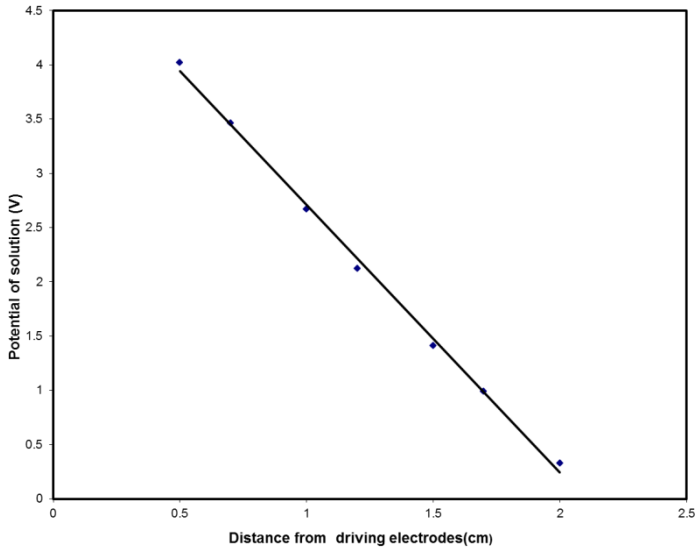

Figure 3.3 Potential of solution is the function of distance from the driving electrodes. The input voltage is 13V and the electrolyte is 0.1M pH 8.12 phosphate buffer solution.

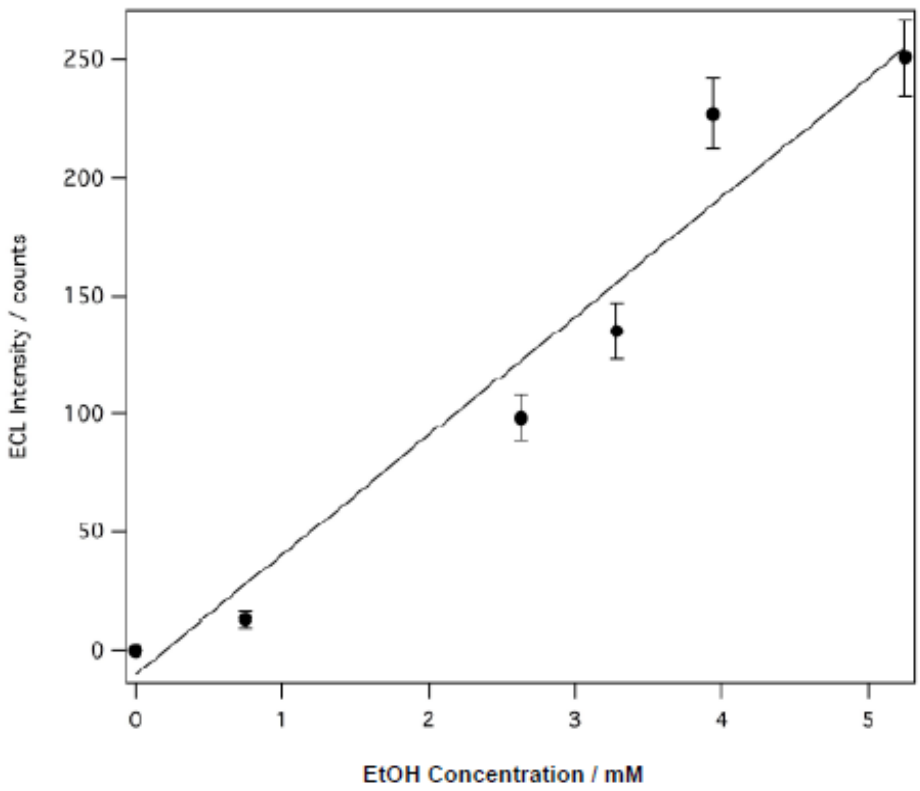

Figure 3.4 Calibration curve of ethanol sensor

3.3.3 Influence of pH on the enzymatic activity of ADH

The mechanism of ADH with coenzyme ADH^+ catalyzing the oxidation of alcohol involves the electrostatic stabilization of the alcohol's oxygen by a zinc atom from ADH, which makes the proton on the alcohol more acidic. A basic medium will facilitate the hydride to transfer from alcohol to NAD^+, and thus resulting in the increasing of ADH activity. However, a strong basic solution might cause the denaturation of protein that reduces the activity of ADH. Figure 3.5 depicts the pH dependence of ADH activities.

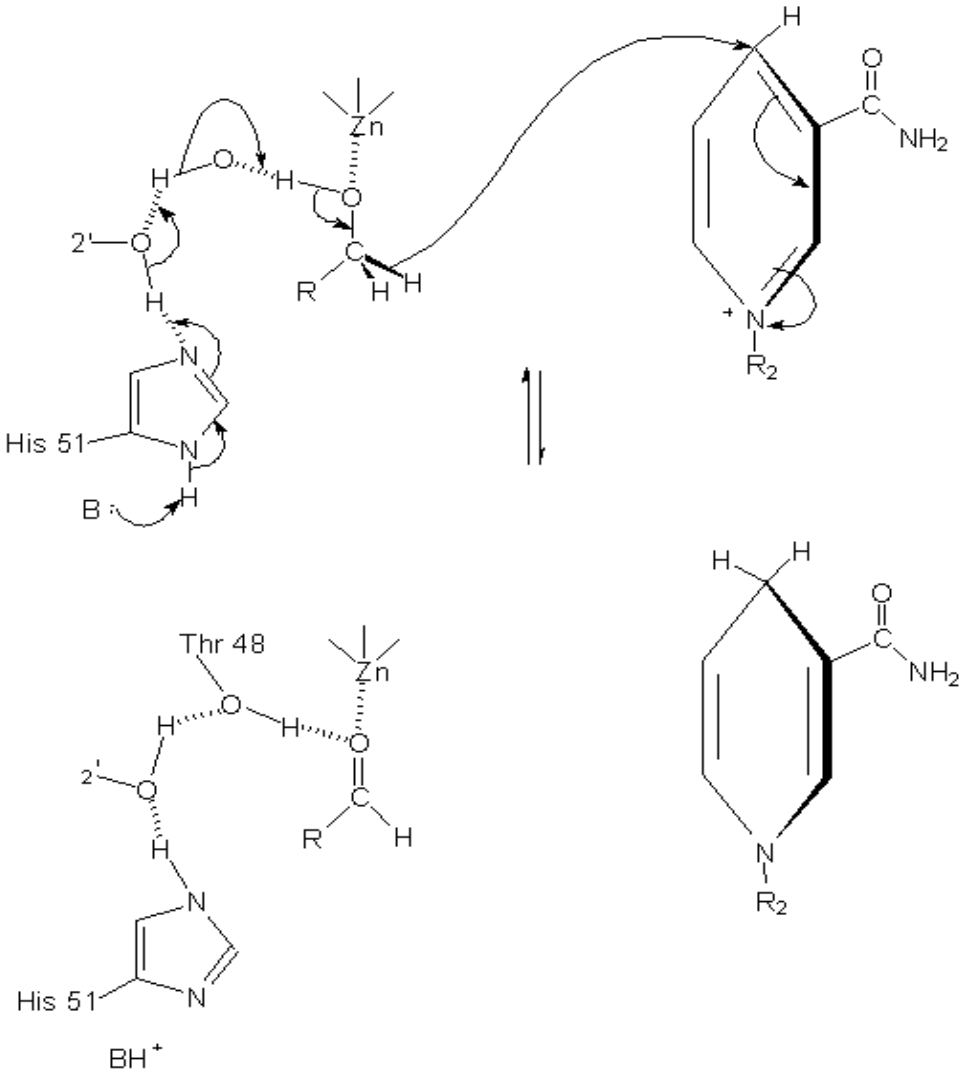

Scheme 3.2 Mechanism of ADH with coenzyme NAD^+ catalyzing the oxidation of alcohol.

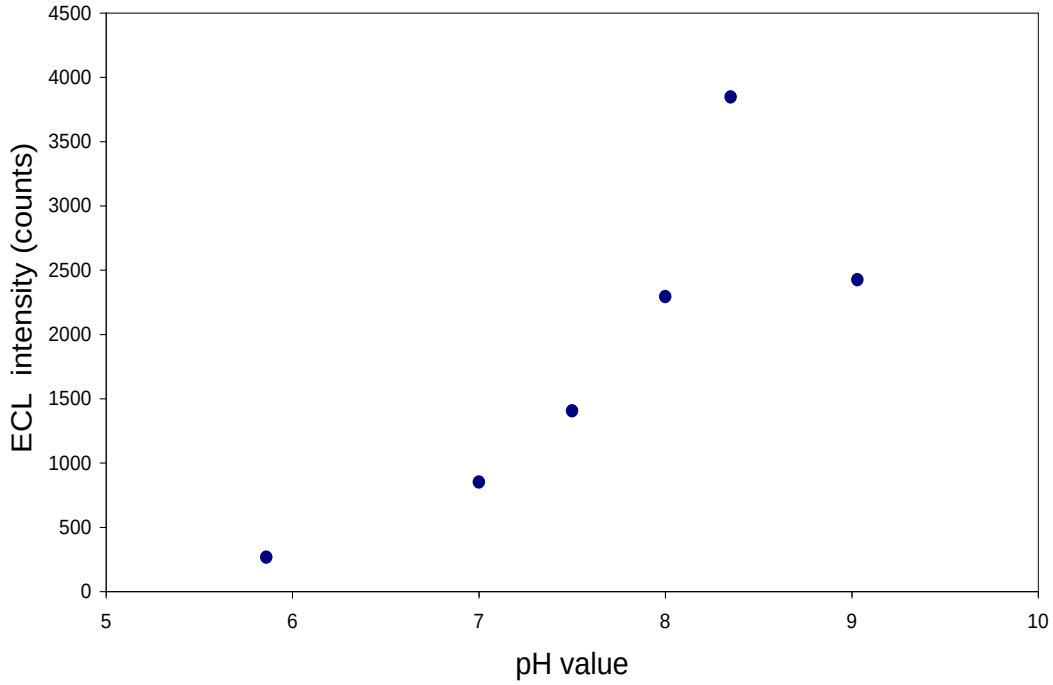

Figure 3.5 ECL intensity as a function of pH value of buffer solution

We measured the ECL intensities of six modified Pt foils with same surface areas in the different pH buffer solutions. The experimental results are displayed in figure 3.5.

The ECL intensity increases and then decreases with the increasing of pH value of the buffer solution. The results indicate that the optimum pH is 8 to 9 for this enzymatically catalyzed reaction, which is consistent with the optimum pH of ADH.

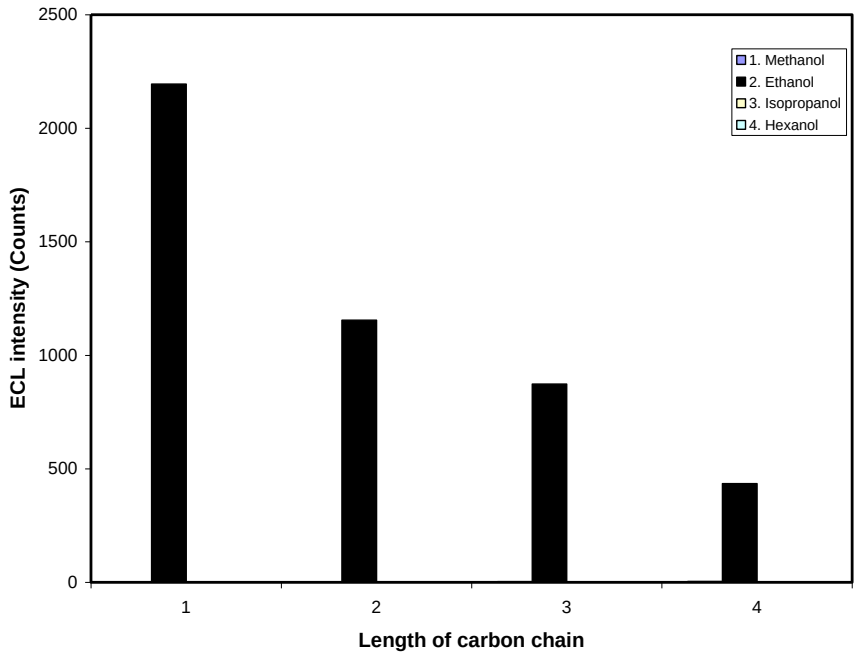

Figure 3.6 Comparison of ECL intensity from different alcohol oxidation reactions. Four modified Pt foils were placed in bipolar electrochemical cell containing 0.1M pH 8.12 phosphate buffer solution.

3.3.4 Effect of chain length of alcohol on ECL intensity

Four alcohols with different lengths of carbon chain were investigated. The oxidation of methanol resulted in the highest ECL intensity, whereas the oxidation of hexanol generated the lowest ECL intensity, which can be explained as follows: Based on the mechanism of ADH with coenzyme NAD^+ catalyzing the oxidation of alcohol, the products of the hydrogen atom on methanol being substituted by alkyl group will be more different to transfer hydride to NAD^+, because the alkyl group that belongs to the group of providing electrons weakens the acidity of proton on the alcohol. Thus, when

these oxidation reactions are performed in bipolar system, the oxidation of hexanol will need the highest input voltage. In other words, the oxidation reaction of methanol will generate the highest ECL intensity at the same experimental condition. Platinum has strong catalysis for the oxidation of methanol. The high ECL intensity of methanol partially derives from the contribution of catalysis of Pt.

3.3.5 Mechanism

Figure 3.7 shows the change of ECL intensity as the ethanol was added continuously to the bipolar electrochemical cell. The ECL intensity increases at the first stage in which the concentration of $Ru(bpy)_3^{3+}$ is high, while the concentration of $Ru(bpy)_3^{+}$ augments gradually with the process of the oxidation reaction of ethanol, therefore more and more $Ru(bpy)_3^{2+}$* are formed that cause the increment of ECL intensity. When the concentration of $Ru(bpy)_3^{+}$ reaches the critical value that is equal to the concentration of $Ru(bpy)_3^{3+}$, the highest ECL intensity is attained. After that, the annihilation reaction will be controlled by $Ru(bpy)_3^{3+}$. The concentration of $Ru(bpy)_3^{3+}$ decreases with the progress of the reaction. Accordingly, ECL intensity decreases" at the second stage as shown in figure 3.7.

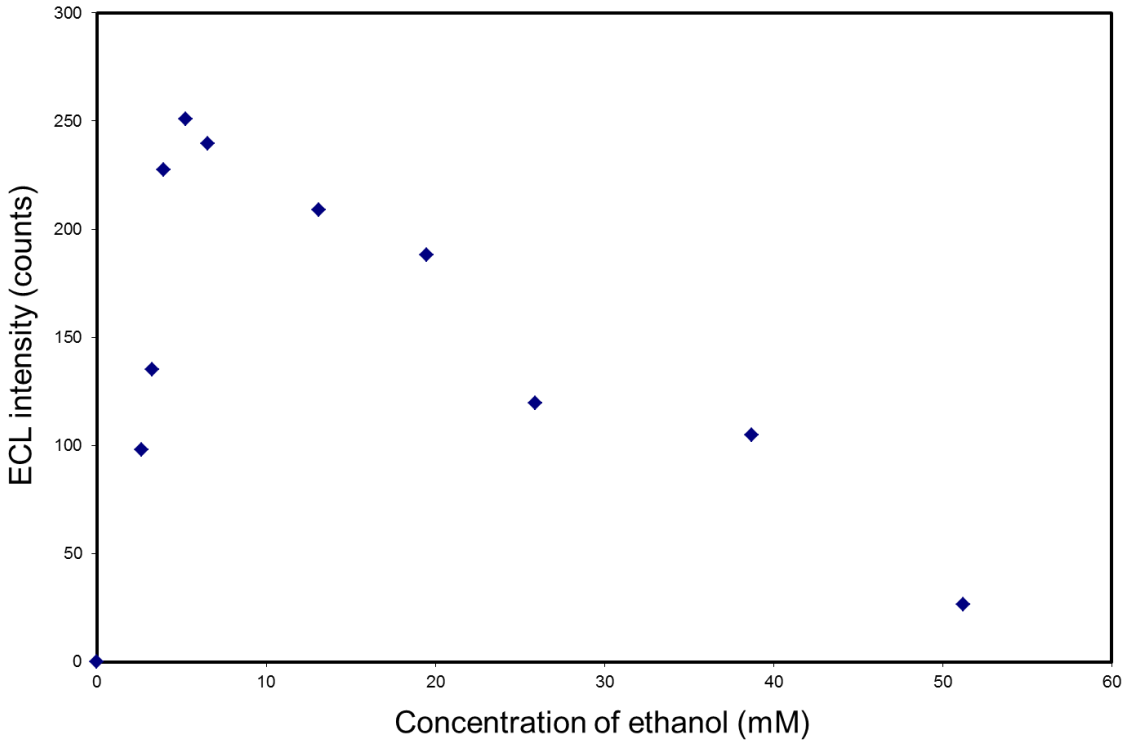

Figure 3.7 Loss of ECL intensity at higher ethanol concentrations.

The experimental results suggested the annihilation mechanism of cathodic ECL. $Ru(bpy)_3^{2+}$ was pre-oxidized using PbO_2 as the oxidant in 0.1M H_2SO_4 solution to form $Ru(bpy)_3^{3+}$. The produced $Ru(bpy)_3^{3+}$ was absorbed to the matrix of Nafion by immersing the Nafion-modified Pt (Au) into the $Ru(bpy)_3^{3+}$ solution. When a potential was applied on the driving electrodes, $Ru(bpy)_3^{3+}$ was reduced to generate the $Ru(bpy)_3^{+}$ on the surface of the bipolar electrode. Based on the standard electrode potential, E^0 $Ru(bpy)_3^{3+}$ / $Ru(bpy)_3^{2+}$ is bigger than E^0 $Ru(bpy)_3^{2+}$ / $Ru(bpy)_3^{+}$. Both of $Ru(bpy)_3^{3+}$and $Ru(bpy)_3^{+}$

are not stable and easy to react with each other to produce $Ru(bpy)_3^{2+}$ with the accompanying of the light emission.

$$2Ru(bpy)_3^{2+} + PbO_2 + 4H^+ \rightarrow 2Ru(bpy)_3^{3+} + Pb^{2+} + 2H_2O \quad (3.1)$$

$$Ru(bpy)_3^{2+} + e^- \rightarrow Ru(bpy)_3^{+} \quad (3.2)$$

$$Ru(bpy)_3^{3+} + Ru(bpy)_3^{+} \rightarrow Ru(bpy)_3^{2+*} + Ru(bpy)_3^{2+} \quad (3.3)$$

$$Ru(bpy)_3^{2+*} \rightarrow Ru(bpy)_3^{2+} + h\nu \quad (3.4)$$

$$Ru(bpy)_3^{2+} - e^- \rightarrow Ru(bpy)_3^{3+} \quad (E°Ru^{2+/3+} = +1.2 \text{ V vs SCE}) \quad (3.5)$$

$$Ru(bpy)_3^{2+} + e^- \rightarrow Ru(bpy)_3^{+} \quad (E°Ru2+/1+ = -1.4 \text{ V vs SCE}) \quad (3.6)$$

3.3.6 Photo-enhanced ECL

Figures 3.8, 3.9, 3.10 describe the phenomenon of photo-enhanced ECL (brown curve represents the ECL spectra after adding ethanol and the rest curves stand for the spectra of background). Comparing the spectrum (brown curve) obtained from no laser shone on the cathode of modified Pt (Au) electrode, the spectrum (brown curve) shows a higher ECL intensity when the cathode of the bipolar electrode is illuminated by a laser. Further, the stronger laser power brings about the higher ECL intensity.

From equation (3.3), $Ru(bpy)_3^{3+}$ can react with $Ru(bpy)_3^{+}$ to form the exited state $Ru(bpy)_3^{2+*}$ and the ground state $Ru(bpy)_3^{2+}$. If the surface of Pt(Au) foil is illuminated by a beam of light, the ground state $Ru(bpy)_3^{2+}$ will absorb photons and thus increasing the population of $Ru(bpy)_3^{2+*}$ which leads to the increment of ECL intensity.

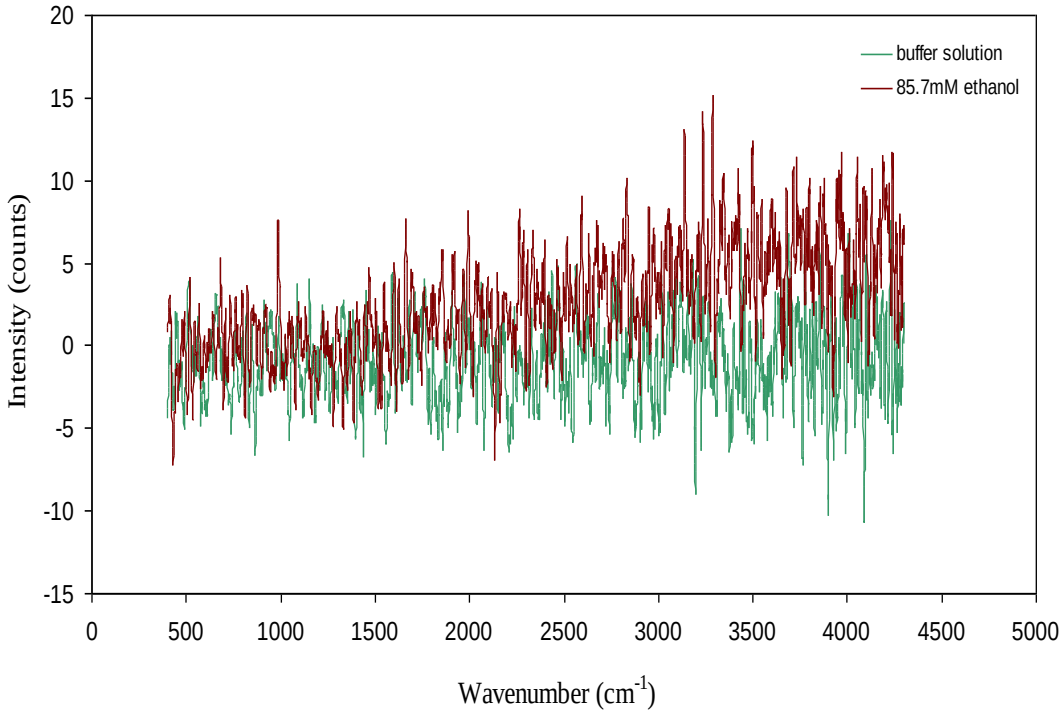

Figure 3.8 Phenomenon of photo-enhanced ECL without laser

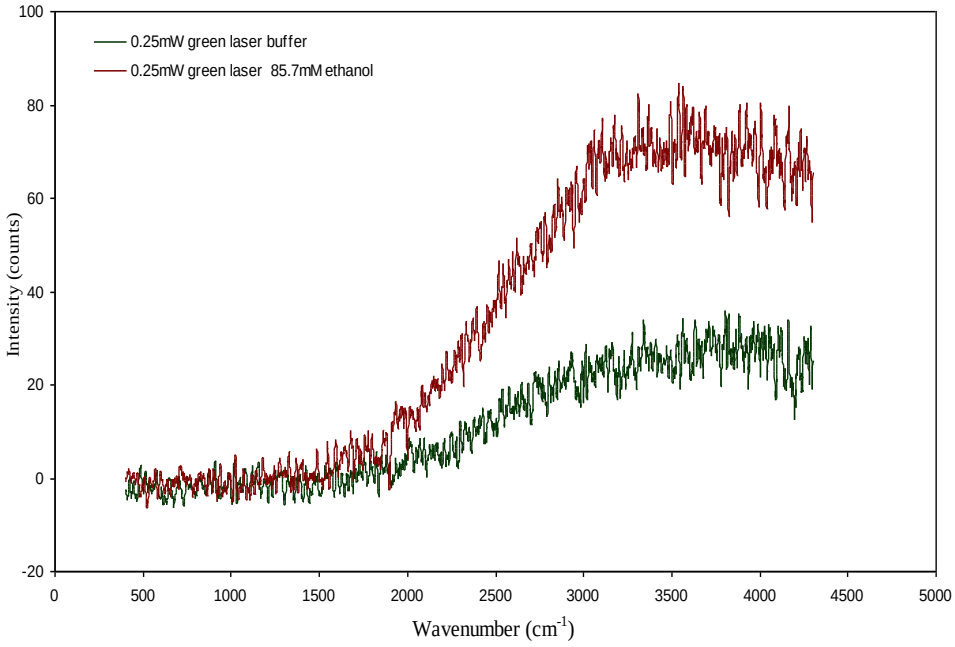

Figure 3.9 Phenomenon of photo-enhanced ECL with 0.25 mW laser

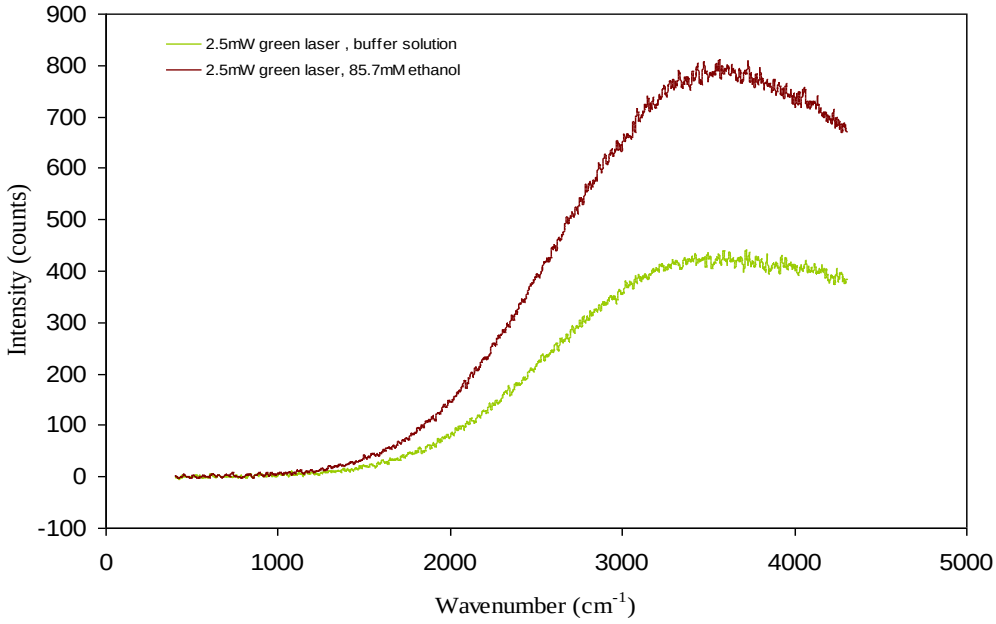

Figure 3.10 Phenomenon of photo-enhanced ECL with 2.5 mW laser

3.4 Conclusions

A novel wireless alcohol sensor with ECL as a reporter has been successfully fabricated and characterized. The concentration of alcohol was detected by monitoring the ECL intensity. The experimental results indicated the linear relationship of the concentration of alcohol and ECL intensity in some concentration range and demonstrated the ECL annihilation reaction mechanism. By illuminating the alcohol sensor in bipolar electrochemical cell, the Photo-enhanced ECL can be observed. The feature of the sensor is that the sensing of alcohol can be observed visually.

In contrast to the ECL emitted from the anode, cathodic ECL from the surface-confined $Ru(bpy)_3^{2+}$ has the advantages of less consumption of chemical reagents as well as no participating of coreactant and the ability to regenerate the sensors. The studies of cathodic ECL will open a new window for people to design the new sensing systems.

The design reported here is sample and extremely flexible: it can be implemented as a small, portable hand-held device; as a detector element for use in microfluidic separation and in a highly multiplexed multi-analyte detection platform.

References

(1) Rubinstein, I.; Martin, C. R; Bard, A. J. *Anal. Chem.* **1983**, 55, 1580-1582.

(2) Ege, D.; Becker, W. G.; Bard, A. J. *Anal. Chem.* **1984**, 56, 2413-2417.

(3) Noffsinger, J. B.; Danielson, N. D. *Anal. Chem.* **1987**, 59, 865-868.

(4) He, L.; Cox, K. A; Danielson, N. D. *Anal. Lett*. **1990**, 23, 195-210.

(5) Danielson, N. D.; He, L.; Noffsinger, J. B.;Trelli, L. *Pharm. Biomed*. **1989**,

(6) Targove, M. A; Danielson, N. D. *J. Chromatogr. Sci*. **1990**, 28, 505-509.

(7) Holeman, J . A; Danielson, N. D. *Anal. Chim. Acta*. **1993**, 277, 55-60,

(8) Uchikura, IC; Kirisawa, M. *Chem. Lett*. **1991**, 1373-1376.

(9) Rubinstein, I.; Bard, A. J. *J. Am. Chem. Soc.* **1980**, 102, 6641.

(10) Rubinstein, I. and Bard, A. J. *J. Am. Chem. SOC.* **1981**,103, 5009.

(11) Downey, T.M.; Nieman, T.A. *Anal. Chem.* **1992**, 64, 261

(12) Downey, T. M. and Nieman, T. A. *Anal. Chem.* **1992**, 64, 261-266

(13) Cui, H; Zhao, X.Y.; Lin, X.Q. *Luminescence* **2003**, 18(4), 199-202.

(14) Sprules, S. D.; Hartleya, I. C.; Wedge, R.; Harta, J. P.; Pittsonb, R. *Analytica Chimica Acta* **1996**, 329, 215-221

(15) Williams, A. K. and Hupp, J. T. *J. Am. Chem. Soc.* **1998**, 120, 4366-4371

(16) Barzegar, A.; Moosavi-Movahedi, A. A.; Ganjali, M. R. *J Appl Electrochem* **2009**, 39:1111–1116

(17) Pandey, P. C.; Upadhyay, S.; Tiwari, I. and Tripathi, V. S. *Analytical Biochemistry* **2001**, 288, 39–43.

(18) Leca, B.; Marty, J.L. *Analytica Chimica Acta* **1997**, 340, 143-148.

(19) Leca, B.; Marty, J.L. *Biosensors& Bioelectronics* **1997**, 12, 1083-1088.

(20) Zhang, H.; Lin, G.; Zhou, Z.; Dong, X.; Chen, T. *Carbon* **2002**, 40, 2429–2436.

(21) Al-Khedher1, M.; Pezeshki, C.; McHale, J.; Knorr, F. *J. Mater. Sci. Technol* **2011**, 27(4), 301-308

(22) Zhou, H.J.; Zhang, Z.P.; Yu, P. *Langmuir* **2010**, 26(8), 6028-6032.

Chapter 4

STUDIES ON THE REACTION OF ANTIBODY AND ANTIGEN

4.1 Introduction

Antibody-antigen interactions are analogized to the relationship of a lock and key which implies the feature of high specificity and affinity.[1] Specificity is the ability of an antibody reacting with a specific antigen, while the binding strength between an epitope of an antigen and an antigen binding sites in an antibody is defined as affinity. Antibody-antigen interactions are reversible due to the non-covalent binding between antibodies and antigens. The binding strength is formed by the balance of the attractive and repulsive forces including van der Waals interactions, hydrogen bonds, ionic interaction, and hydrophobic interaction. Two approaches are used to quantitatively study antibody-antigen interactions, namely, the thermodynamic and kinetic approaches. Antibody-antigen interactions can be expressed as

$$\text{Antibody(Ab)} + \text{Antigen(Ag)} \underset{K_d}{\overset{K_a}{\rightleftharpoons}} \text{antibody-antigen complex (Ab-Ag)}$$

where K_a denotes the association constant and K_d is the dissociation constant.

At equilibrium,

$$Ka = [Ab\text{-}Ag] / [Ab][Ag] \quad (4.1)$$

If θ is the fraction of Ag binding onto Ab, thus,

$$[Ab\text{-}Ag] / [Ab] = \theta / 1- \theta \quad (4.2)$$

Equation (4.1) is substituted by equation (4.2), then

$$K_a = \theta / (1- \theta)*C \quad (4.3)$$

$$\theta = K_aC/ (1+K_aC) \quad (4.4)$$

$$\log (\theta/(1- \theta)) = \log K_a + \log C \quad (4.5)$$

where C is the concentration of free antigen.

From a plot log (θ/ (1- θ)) with respect to log C, the association constant K_a can be derived.

To study the interactions of antibodies and antigens, the first step is to immobilize antibodies onto the surface of a sensor. There are many methods employed in the immobilization of antibody. Summarily, these methods are divided into two categories: covalent immobilization and physical adsorption.

In physical adsorption, the antibodies are adsorbed on the surfaces of sensors by means of van der Waals interactions, hydrogen bonds, and hydrophobic interaction. Owing to the weak binding force between the antibodies and surfaces, the antibodies bound on the surfaces are unstable.

Covalent immobilization relies on the structure of the antibody. Antibody is a "Y" shape protein with two terminals, N-terminal containing amine group and C-terminal possessing carboxyl group. Antibodies are immobilized by the two kinds of functional groups reacting with the surfaces. In addition, by reducing carboxyl group, antibodies can provide other functional groups, formyl groups, to participate in the immobilization.

Figure 4.1 depicts the mechanism of the molecules containing amine group being grafted onto the SAMs with carboxyl group. EDC/NHS is used to activate the carboxyl group.

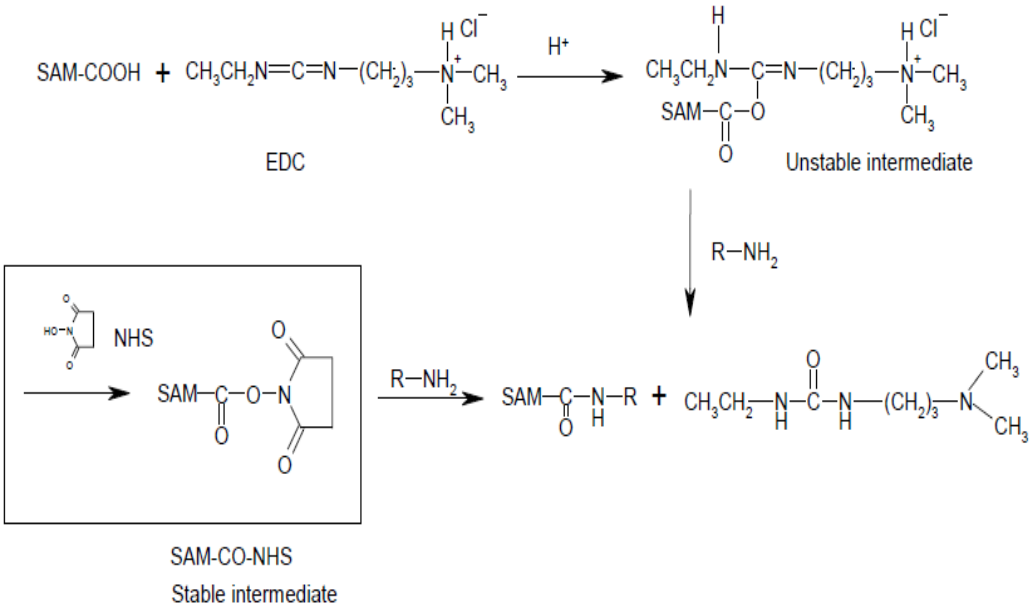

Figure 4.1 Mechanism of the SAMs with carboxyl group reacting with molecules containing amine group

The work presented here is to immobilize the anti-IgG on the surface of Au-coated MSPs that act as a magnetostrictive sensor to detect antigen. Based on the equation (1.3),[2] ($\Delta f = f - f_0 = - f_0 \Delta m/2m_s$), the variation in the resonance frequency of the sensor is proportional to the Δm (mass load), which is the amount of bound antigen.

Accordingly, the frequency shift is proportional to the concentration of antibody-antigen complex. Hence, this equation can be written as

$$\Delta f = K_{new} [Ab\text{-}Ag] \quad (4.6)$$

Substituting $\theta = [Ab\text{-}Ag] / [Ab]_0$ into equation (4.6), a new equation is acquired

$$\Delta f = K_{new} [Ab]_0 \theta \quad (4.7)$$

where $[Ab]_0$ is the initial concentration of antibody, θ is the fraction of antigen binding onto antibody.

$\theta=0$ means no antigen bound to antibody, $\Delta f = f_0$. $\theta = 1$ represents maximum binding, $\Delta f = \Delta f_{max}$. Therefore,

$$\Delta f = \Delta f_{max} \theta \quad (4.8)$$

Replacing θ in equation (4.8) with equation (4.4), a new equation is obtained.

$$\Delta f / \Delta f_{max} = K_a C / 1+K_a C \quad (4.9)$$

4.2 Experimental section

4.2.1 Materials and Reagents

Alkaline phosphatase conjugated monoclonal anti-rabbit IgG (γ-chain-specific) (rAb*), rabbit IgG (rAg), tetrachloroauric acid ($HAuCl_4$) and sodium borohydride ($NaBH_4$), $Ru(NH_3)_6Cl_3$ were purchased from Sigma-Aldrich. 4-nitrophenylphosphate disodium salt (99 %), Gold(I) sodium thiosulfate hydrate (99.9% metals basis), Formaldehyde (37%w/w aq. soln., stab, with 7-8%methanol) and sodium sulfide were bought from Alfa Aesar. Potassium phosphate monobasic (KH_2PO_4), potassium

phosphate dibasic (K_2HPO_4), Sodium chloride, magnesium chloride, silver nitrate, sulfuric acid, hydrochloric acid and sodium hydroxide were bought from Fisher-Scientific. Tris(hydroxymethyl)aminomethane and Tween-20 were bought from ACROS. N-hydroxysuccinimide (NHS), N-(3-Dimethylaminopropyl)-N'-ethylcarbodiimide hydrochloride (EDC), Sodium azide, 16-Mercaptohexadecanoic acid, 1-Octadecanethiol were purchased from Sigma-Aldrich. Metglas™ 2826MB in a ribbon form (MSPs) was obtained from Honeywell International (Conway, SC). All chemicals were used as received without further purification.

4.2.2 Pre-treatment of magnetostrictive particles (MSPs)

The different size SiC paper (400, 4000), diamond paste (15um, 3um, 1um) and 0.05um alumina were used to polish the surface of MSPs and then the polished MSPs were ultrasonically cleaned in deionized water and acetone for 5 minutes each, respectively, and dried in a stream of flowing nitrogen.

4.2.3 Deposition of Au on MSPs

The pre-treated MSPs were immersed into 0.029 M $AgNO_3$ aqueous solution for 4 minutes. Then, the MSPs were rinsed using water for 3 times and dried in a stream of flowing nitrogen. After which, the MSPs were placed in the solution composed of 0.625 M HCHO, 0.127M Na_2SO_3, and $7.9x10^{-3}$ M $Na_3Au(S_2O_3)_2$ with temperature being controlled to 28^0C for 24 hours., Au-coated MSPs were then rinsed with water and annealed.

4.2.4 Annealing of Au-deposited MSPs

In order to increase the adhesion of Au on MSPs, the Au-deposited MSPs were put into a quartz glass tube that was further placed in an oven with temperature being controlled at 350 ^{0}C for 2.5 hours under a stream of flowing nitrogen.

4.2.5 Preparation of antibody-based MSPs sensors

Au-deposited MSPs were soaked in 1mM mixed ethanol solution [$SH(CH_2)_{15}COOH$:$SH(CH_2)_{17}CH_3$=8:2] for a period of 24 hours to form the self-assembled monolayers and then rinsed using ethanol for three times and dried in a stream of flowing nitrogen. To active the carboxyl group, the SAMs-assembled MSPs were immersed in 2mg/ml EDS-NHS solution for 1.5 hours and then rinsed using the distilled water for 3 times and dried.

In our experiments, we used PBS buffer solution (pH=7.33) with 0.13M NaCl and 1% (v/v) Tween-20 to dissolve anti-IgG. The activated MSPs were placed in 5 μg/mL alkaline phosphatase conjugated monoclonal anti-rabbit IgG PBS buffer solution for 24 hours at room temperature. Finally, the sample was rinsed using PBS buffer for 3 times and dried.

4.2.6 Synthesis of 4-Aminophenyl phosphate (pAPP)

4-Aminophenylphosphate (pAPP) was synthesized according to the literature.[3] 2.81 g 4-nitrophenyl phosphate disodium salt (Na_2pNPP) was dissolved in 5.6 mL distilled water and pH was adjusted to 9 with NaOH solution. 5.11g $Na_2S•9H_2O$ was added and the resulting mixture was heated to 90 – 95 °C in an oil bath for 1 hour. The solution was cooled and acidified with concentrated HCl (pH < 2). The acidified solution was filtered

and the pH of the acid filtrate was adjusted to 4-5 by 25% NaOH solution. The fluffy white crystals were collected (i.e. the monosodium salt of pAPP) and recrystallized from boiling methanol to remove inorganic impurities. The product pAPP was kept in a refrigerator for use later.

4.2.7 Cyclic Voltammetry Measurement

Cyclic voltammetry measurements were conducted under a stream of flowing nitrogen in a traditional three-electrode cell in which the modified MSPs acted as the working electrodes, a Pt net was utilized as the counter electrode and Ag/AgCl was the reference electrode. 4 mM 4-Aminophenyl phosphate in 0.1 M Tris buffer including 1mM $MgCl_2$ and 0.02% w/v NaN_3 (pH=9.0) solution was used as the support electrolyte.

4.2.8 Surface Enhanced Raman Spectroscopy (SERS)

SERS spectra were measured with a confocal microscopic Raman spectrometer (Renishaw 1000 model) with a CCD detector and a holographic notch filter. Radiation of 514 nm from an air- cooled argon ion laser (Spectra-Physics model 163-C4260) was used for excitation. Laser power was 1.75 mill watts. The collection time was 20s and accumulated 8 times.

4.2.9 Contact Angle Measurement

The contact angle measurements of deionized water (Mill-Q, 18.0 MΩ.cm) on the surfaces of modified MSPs were carried out at room temperature and ambient humidity by the sessile drop method using Standard Goniometer (Model No.: 200-00-115, Rame-hart, Inc.) and drop image standard, ver. 1.5.02 (software).

4.2.10 Measurement of Frequency

The frequency measurements were performed in a coil-wound tube using a network analyzer (HP 87511) controlled by a personal computer. A DC magnetic field was generated by placing a magnet outside of the tube. The solution containing antigens was forced to flow through the tube where the antibody-modified MSPs was placed. The resonance frequency was recorded as the function of time.

4.3 Results and Discussion

4.3.1 Comparison of different methods for depositing Au onto MSPs

To explore a simple approach to deposit Au on magnetostrictive particles, two chemical methods have been tested. One is to use replacement reaction to deposit Au.[4] The reaction equation is expressed as

$$Fe(s) + AuCl_4^-(aq) \rightleftharpoons Au(s) + Fe^{3+(}aq) + 4Cl^-(aq) \qquad (4.10)$$

A pre-treated MSPs was dipped into $HAuCl_4$ solution for 2 seconds and then rinsed using the distilled H_2O and dried under the N_2 stream. This approach is very simple and by using which a uniform Au layer (single molecular layer) can be obtained. But the disadvantage of this method is that the atoms can exchange between the inner layer and the outer layer which causes some Fe atoms moving to the surface when annealed at 250^0c.

The other one is electroless Au plating.[5-7] Firstly, MSPs reacts with $AgNO_3$ to generate a layer of Ag atoms, and then the Ag reacts with $Au(S_2O_3)_2^{3-}$ to form Au which is used as nucleation sites for the subsequent growing of Au generated by the oxidation of

HCHO. The following chemical reaction equation shows the reaction process of electroless Au plating.

$$Fe + 3Ag^{+} \rightleftharpoons Fe^{3+} + 3Ag \quad (4.11)$$

$$Ag + Au(S_2O_3)_2^{3-} \rightleftharpoons Au + Ag(S_2O_3)_2^{3-} \quad (4.12)$$

$$2Au^{+} + HCHO + 3OH^{-} \rightleftharpoons HCOO^{-} + 2Au + 2H_2O \quad (4.13)$$

Compared with the Au deposition through replacement reaction, electroless Au plating is relatively complicated and has a much longer reaction time. However, Ag in this system plays a role of adhesion between Au and MSPs. Moreover, the possibility of Fe atoms switching with the outermost Au atoms decreases that ensures the purity of Au on the MSPs surfaces due to the formation of multilayer Au atoms. Therefore, the problem occurring in Au deposition derived from replacement reaction will not be concerned when the annealing is implemented. Consequently, electroless Au plating is chosen to deposit Au onto MSPs in this work. The results from EDS verify the deposition of Au on the surface of Fe (figure 4.2).

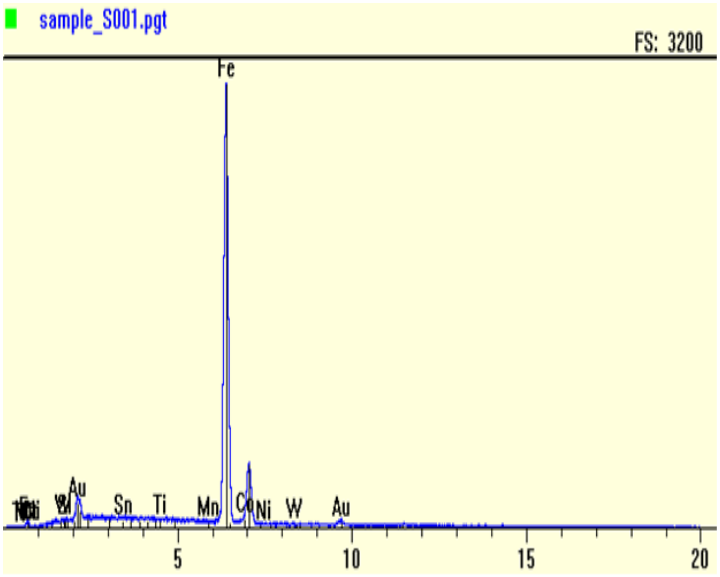

Figure 4.2 EDS of Au-coated Fe

4.3.2 Surface modification

Self-assembled monolayers (SAMs) are monomolecular films formed spontaneously on a substrate by strong interactions between the substrate surface and the head group of assembled molecules. It is possible to introduce any special functional groups by organic synthesis to tailor organic and organometallic structures at the surface of substrate, and thus controlling the chemical composition as well as properties of surfaces. Because of well-defined structure, low defected density, and chemical stability, SAMs especially thiol-based SAMs have attracted a considerable scientific interest and been broadly used to construct sensors.[8-11]

To modify MSPs with antibodies, some functional groups such as −COOH have to be introduced to Au-deposited MSPs. Even though the more −COOH group may bring

about the more population of antibodies, the −COOH group can penetrate the surface layer of MSPs. Hence, a mixed solution of $SH(C_{15}H_{30})COOH$ and $C_{18}H_{37}SH$ would be a good choice. Here, $C_{18}H_{37}SH$ not only adjusts the concentration of $SH(C_{15}H_{30})COOH$ on the surface of MSPs, but also makes the monolayers of $SH(C_{15}H_{30})COOH$ more orderly. The mixed ethanol solution of $SH(C_{15}H_{30})COOH$ and$C_{18}H_{37}SH$ with the ratio 8:2 was used to produce self-assembled monolayers in this work.

4.3.3 Characterization of MSPs-based sensors

Antibody- modified MSPs were examined by using the cyclic voltammetry and contact angle measurement, Raman and frequency measurement. The results are displayed as follows.

4.3.3.1 Cyclic voltammetry

Figure 4.2 is the cyclic voltammograms of alkaline phosphatase conjugated anti-rabbit IgG-modified MSPs in 0.1M Tris buffer containing 4-aminophenyl phosphate (pAPP). The pAPP hydrolyzes under the catalysis of alkaline phosphatase (AP) to generate 4-aminophenol (equation 4.14).

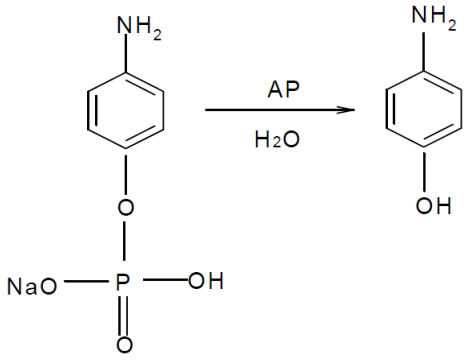

(4.14)

4-aminophenol is electrochemically active,[12-13] and the electrochemical oxidation reaction is showed in equation 4.15. Owing to the sensitivity of 4-aminophenol to light and oxygen, the subsequent electrochemical measurement was performed in the nitrogen atmosphere and the cell was covered by aluminum film. Antibody-modified MSPs was nonconductive, so an Au ball was used as the working electrode that was placed as close as possible to the antibody-modified MSPs.

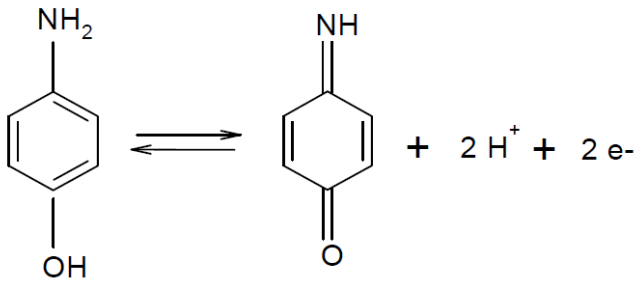

(4.15)

The cyclic voltammograms of antibody-modified MSPs is showed in figure 4.2. The orange line in figure 4.2 represents the cyclic voltammogram of antibody-modified MSPs in Tris buffer solution containing pAPP, while the dot line corresponds to the electrochemical behavior of antibody-modified MSPs in Tris buffer solution. The anodic peak at 0.1V indicates the oxidation of 4-aminophenol, and thus, demonstrates the immobilization of antibody on the MSPs

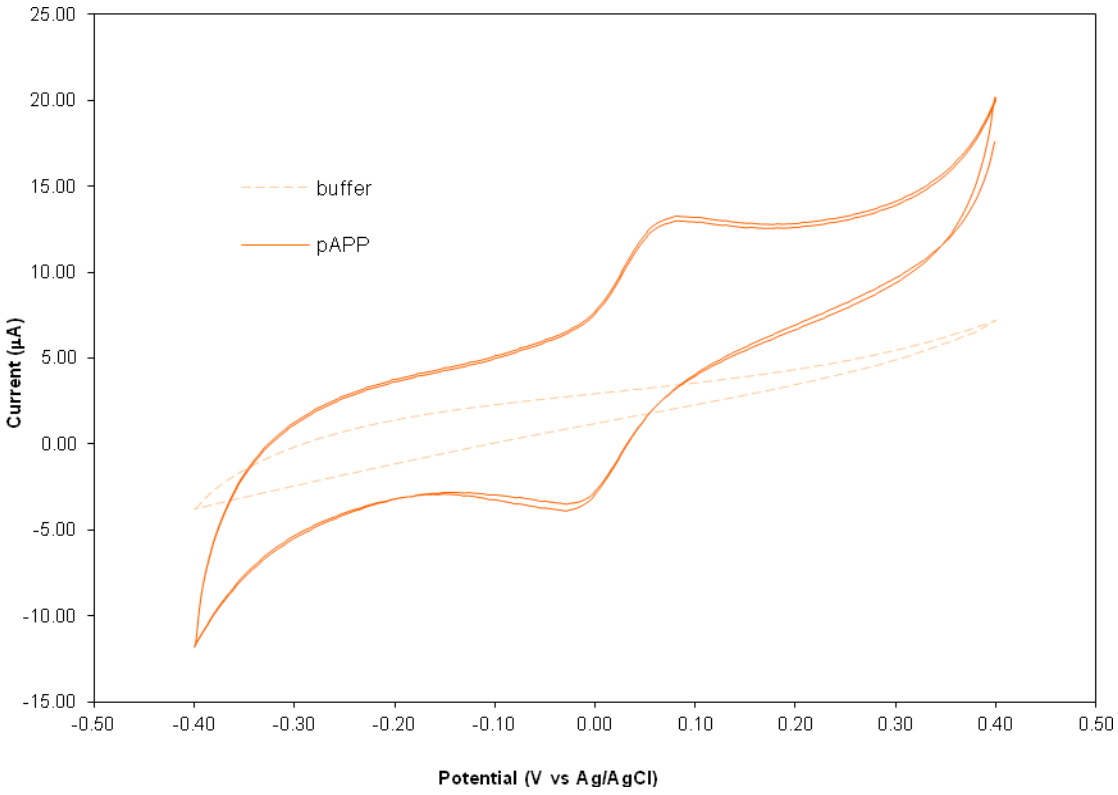

Figure 4.3 Cyclic voltammograms of antibody-modified MSPs. The electrolyte contains 4 mM 4-Aminophenyl phosphate in 0.1 M Tris buffer solution with 1mM $MgCl_2$ and 0.02% w/v NaN_3 (pH=9.0). Scan rate 50mv/s.

4.3.3.2 Contact Angle Measurement

The different surfaces display different surface properties such as wettability. Therefore, bare Au and modified Au are expected to have various values in the measurements of contact angles.[14-16] The contact angle is the angle between liquid and solid interfaces which reflects the strength of interaction of liquid and solid molecules. A strongly hydrophilic surface will exhibit a low value of contact angles due to the strong

interaction between solid and liquid (H_2O) molecules. Whereas, highly hydrophobic surfaces will display high values for contact angle measurements. Normally, the water contact angle is smaller than 30^0 on the highly hydrophilic surface and larger than 90° on the hydrophobic surface. For some superhydrophobic surface, the water contact angle can even be higher than 150^0.

Picture 4.1 exhibits the wettability of different surfaces. (a) The surface of Au-coated MSPs has the highest contact angle value. (b) The contact angle decreased when mixed SAMs (9:1) were assembled onto Au-coated MSPs, because the hydrophilic carboxyl groups were introduced to the surface. (c) The immobilization of antibody onto the surface resulted in the contact angle decreasing more due to the more hydrophilic functional groups were grafted onto the surface.

Table 4.1 is the summary of contact angle measurements. As expected, $-CH_3$ group terminated SAMs have the highest contact angle that is 118.2^0 for 1-Octadecanethiol (C18). Mendoza et al reported the contact angle of 109^0 and 111^0 for decanethiol (C10) and hexadecanethiol (C16) respectively.[17] In contrast, the surface property of -COOH group terminated SAMs is more difficult to control. A wide range of contact angles have been reported.[18-19] Roughness of surfaces, interaction between molecules can alter the contact angles. As displayed in table 4.1, the contact angles increase with the increasing of the concentration of $C_{18}H_{37}SH$ in a mixture ethanol solution, which indicates the increasing of hydrophobic properties on the surface. When the SAMs are formed by pure $C_{18}H_{37}SH$ molecules, the strongly hydrophobic surfaces are generated

which cause the highest contact angle value. The contact angles are reduced via introducing more hydrophilic functional groups coming from antibody.

Table 4.1 Contact angle measurement (^{0}C)

The ratio of mixed SAMs	After Packing SAMs	After packing SAMs and antibody
$SH(CH_2)_{15}COOH$	59.8±1.76	26.8±2.19
$SH(CH_2)_{15}COOH:C_{18}H_{37}SH$=9:1	75.0±2.50	39.7±5.02
$SH(CH_2)_{15}COOH:C_{18}H_{37}SH$=8:2	87.9±2.68	45.5±5.56
$SH(CH_2)_{15}COOH:C_{18}H_{37}SH$=5:5	96.9±0.625	52.5±5.72
$SH(CH_2)_{15}COOH:C_{18}H_{37}SH$=3:7	98.1±1.65	64.8±3.35
$C_{18}H_{37}SH$	118.2±4.97	----

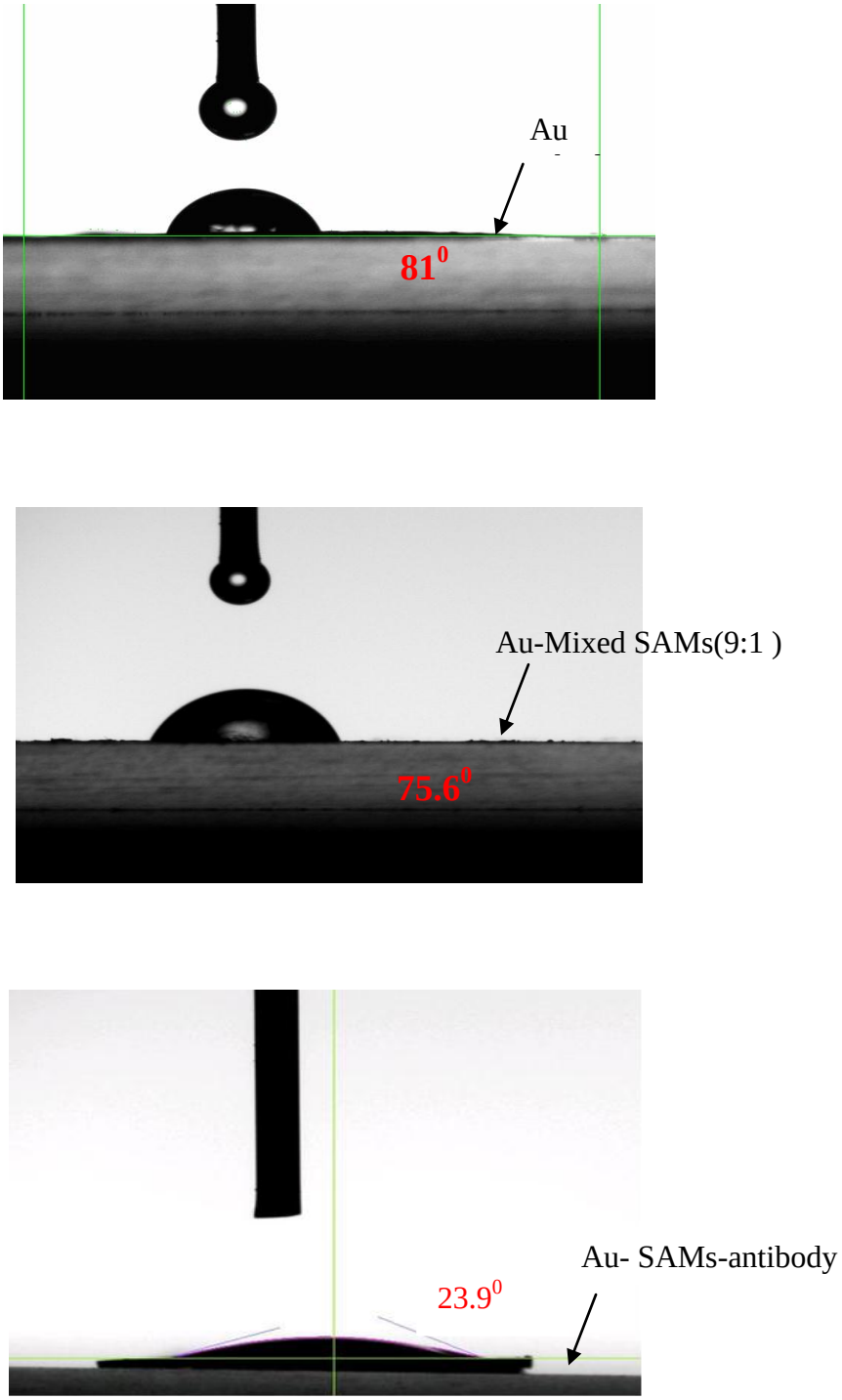

Picture 4.1 Contact angles on the different surfaces.

4.3.3.3 Raman spectroscopy

In the measurements of Raman spectra, silver developer solution composed of Tween 80(final concentration 0.5%), $AgNO_3$ (final concentration 1mM) and ascorbic acid (final concentration 1mM) was used to enhance the Raman signals.[20] The modified MSPs were immersed into freshly prepared Ag developer solution for 2 minutes and then rinsed with the deionized water for three times and dried in N_2 stream.

Figure 4.4 shows the Raman spectra of modified MSPs. The red line corresponds to the spectrum of mixed SAMs modified MSPs and the yellow line represents the spectrum attained from anti-IgG immobilized MSPs. The peak at 702 cm^{-1} is attributed to C-S stretching vibration, while the peak at 883cm^{-1} is related to C-C stretching vibration. The C-H vibration occurs at 1423cm^{-1}. The peak at 2854-2931 cm^{-1} is assigned to the C-H stretching vibration which shows a large enhancement after anti-IgG react with SAMs. The peak at about 1620 cm^{-1} is ascribed to amino acid residue (phenylalanine) from anti-IgG. These evidences indicate the formation of antibody on MSPs.[21-22]

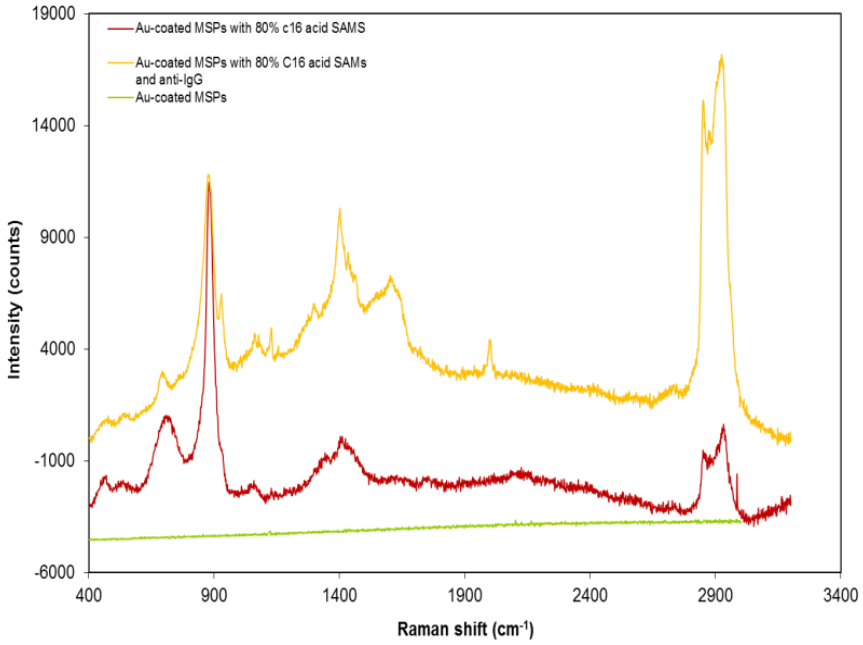

Figure 4.4 Rama spectra of modified MSPs

4.3.4 Frequency measurement

The studies of interactions between ligands and receptors taking place on the interfaces of solid and liquid allow the employment of some surface sensitive techniques such as acoustic techniques, surface plasmon resonance, and electrochemical impedance spectroscopy etc.[23] Here, magnetostrictive particles are used as the sensor platform based on the property that the frequency of the sensor will change as the sensing reactions take place in a magnetic field. By monitoring the frequency change, the information related to the binding of antigen to antibody can be acquired.

Frequency measurements were performed in a flow injection system with a flow rate of 30 μl/min. Prior to detecting antigen, the PBS buffer solution (pH=7.33) was used to flow through the test chamber in which the antibody-modified MSPs was placed at a position with the strongest frequency response until the stable frequency response was reached. Following, the antigens were injected into the test chamber with the concentration from low to high. The resonance frequency was measured during the entire detection period with an interval of 30 seconds.

Figure 4.5 reveals the resonance frequency response of antibody-immobilized MSPs to the increasing concentration of antigen. The resonance frequency was recorded as the function of time. As shown in figure 4.5, the resonance frequency of the sensor increases until the maximal frequency (saturated state) is obtained which means that the mass load derives from the interaction between antibody and antigen and the reaction reaches the dynamic equilibrium.

Table 4.2 Concentration of antigen and resonance frequency shifts

Concentration of antigen (μg/mL)	0.469	0.938	1.88	3.75	7.50	75.0
Frequency shift (Δf) (Hz)	313	438	563	625	688	750
$\Delta f / \Delta f_{max}$	0.417	0.584	0.751	0.833	0.917	1.00

Table 4.3 Association constant (K_a) and disassociation constant (K_d) of antibody-antigen interaction

$K_a(M^{-1})$	2.28±0.152 $\times 10^8$	2.25±0.152 $\times 10^8$	2.42±0.152 $\times 10^8$	2.0±0.152 $\times 10^8$	2.21±0.152 $x10^8$	2.23±0.152 $\times 10^8$
$K_d(M^{-1})$	4.38±0.319 $\times 10^{-9}$	4.45±0.319 $\times 10^{-9}$	4.14±0.319 $\times 10^{-9}$	5.01±0.319 $\times 10^{-9}$	4.53±0.319 $x10^{-9}$	4.50±0.319 $\times 10^{-9}$

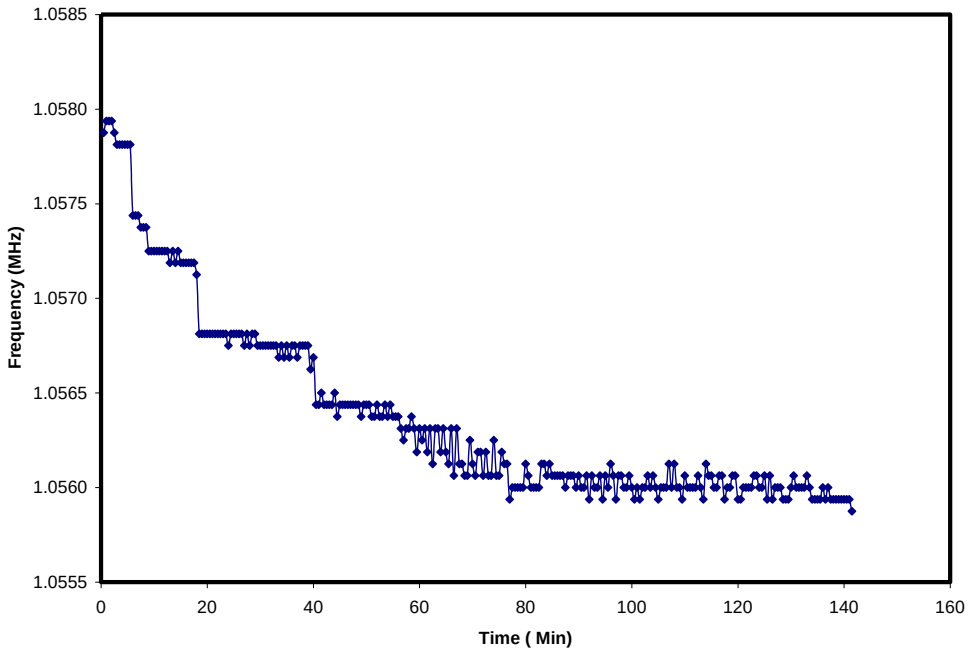

Figure 4.5 Resonance frequency responses of antibody-immobilized MSPs (2.0 mm × 0.3 mm × 15 μm) to the increasing concentration of antigen.

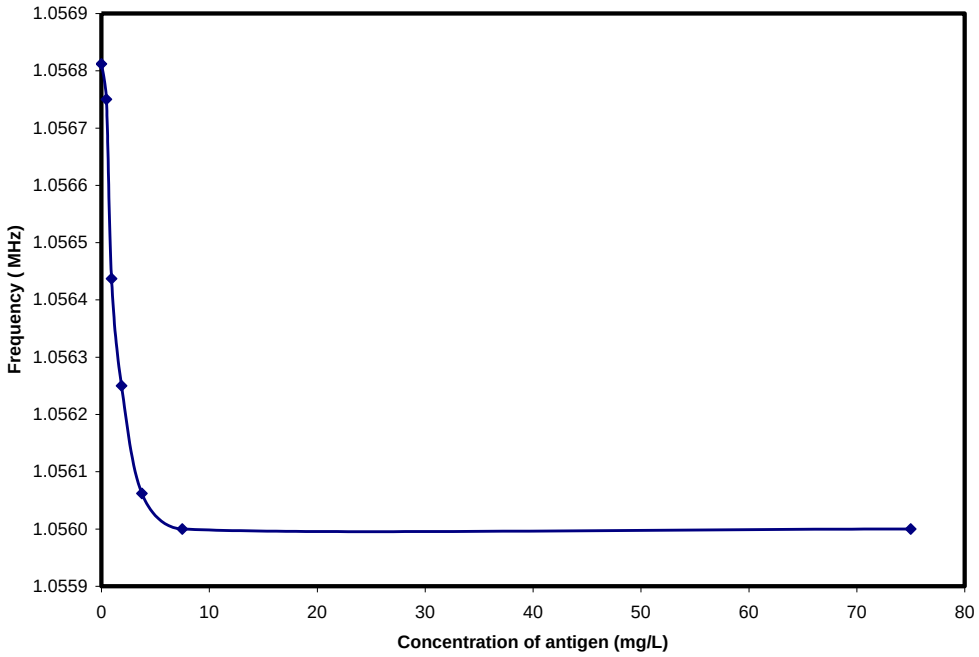

Figure 4.6 Frequency response of antibody-modified MSPs after continuously adding antigen of the different concentration.

Figure 4.6 is the frequency response of antibody-modified MSPs after continuously adding antigen with the different concentration. The frequency drops as antigens of the different concentration are added successively until it reaches the saturated state. Table 4.2 displays the resonance frequency shifts and the concentration of antigen. Combining the results shown in table 4.2 and the equation 4.9, the association constant K_a and disassociation constant K_d of antibody-antigen interaction can be derived,[24-28] which are displayed in Table 4.3. The K_a and K_d of anti-IgG-antigen interactions agree with the values reported in the literature.[24] The experimental results indicate the high affinity of antibody-antigen interaction.

4.4 Conclusions

A wireless magnetostrictive particles-based sensor has been fabricated. Two kinds of approaches for chemically depositing Au were investigated. Electroless Au plating was utilized to deposit Au onto the MSPs with the size (1mm, 2mm, 4mm and 6mm long). In order to obtain a well-controlled and functional surface, a mixed $SH(CH_2)_{15}COOH$:$C_{18}H_{37}SH$=8:2 ethanol solution were used to form self-assembled monolayers. The anti-IgG immobilized MSPs sensors have been successfully employed for the studies of antibody-antigen interactions. The association constant is $2.23\pm0.152\times10^{8}$ M^{-1} which indicate the high affinity of this binding reaction.

References:

(1) Tseng, W.L.; Chan, H.T.; Hsu, S.M.; Chen, R.J.; Lin, S.M. *Electrophoresis* **2002**, 23, 836–846

(2) Grimes, C.A.; Mungle, C.S.; Zeng, K.F.; Jain, M.K.; Dreschel, W.R.; Paulose, M.; Ong, K.G. *Sensors* **2002**, 2, 294-313

(3) Zhang, J.; Cass, A. E. G. *Analytica Chimica Acta*. **2000**, 408, 241.

(4) Sun, Y.G. and Xia, Y.N. *J. Am. Chem. Soc*. **2004**, 126, 3893.

(5) Oldenburg, S. J.; Averitt, R. D.; Westcott, S. L.; Halas, N. J. *Chem. Phys. Lett.* **1998**, 288, 243.

(6) Jackson, J. B.; Halas, N. J. *J. Phys. Chem. B* **2001**, 105, 2743.

(7) Bischoff, M. M. J.; Yamada, T.; Quinn, A. J.; Van der Kraan, R. G. P. and Kempen, H. V. *Physical Review Letters* **2001**, 87(24), 246102-246105.

(8) Gooding, J. J.; Hibbert, D. B. *Trends Anal. Chem.* **1999**, 18, 525.

(9) Gooding, J. J.; Erokhin, P.; Hibbert, D. B. *Biosensors Bioelectronics* **2000**, 15, 229.

(10) Bardea, A.; Katz, E.; Willner, I. *Electroanalysis* **2000**, 12, 731

(11) Stora, T.; Hovius, R.; Dienes, Z.; Pachoud, M.; Vogel, H. *Langmuir* **1997**, 13, 5211.

(12) Ruan, C.; Li, Y., *Talanta* **2001**, 54, 1095.

(13) Francisco, M. S. P.; Cardoso, W. S.; Kubota L. T.,; Gushikem, Y. *Journal of Electroanalytical Chemistry* **2007**, 602, 29–36.

(14) Wang, M. S.; Palmer, L. B.; Schwartz, J. D. and Razatos, A. *Langmuir* **2004**, 20(18), 7754.

(15) Mendoza, S. M.; Arfaoui, I.; Zanarini, S.; Paolucci, F. and Rudolf, P. *Langmuir* **2007**, 23(2), 582-588.

(16) Wang, H.; Chen, S.F.; Li, L.Y. and Jiang, S.Y. *Langmuir* **2005**, 21(7), 2634.

(17) Sandra, M.; Imad, M.; Zanarini, A. S.; Paolucci, F.; and Rudolf. P. *Langmuir* **2007**, 23, 582-588.

(18) Wang, M. S.; Palmer, L. B.; Schwartz, J. D.; and Razatos, A. *Langmuir* **2004**, 20, 7753-7759.

(19) Wang, H.; Chen, S. F.; Li, L. Y.; and Jiang, S. Y. *Langmuir*, **2005**, 21(7), 2633-2636.

(20) Manimaran1, M.; Jana, N. R. *Journal of Raman spectroscopy*, **2007**, 38.1326-1331.

(21) Fagnano', C.; and Fini, G. *Journal of Raman spectroscopy* **1992**, 23. 637-639.

(22) Ahernt, A. M.; and Garrell, R. L. *Langmuir* **1991**, 7, 254-261.

(23) Saha, K., Bender, F., Gizeli, E. *Anal. Chem*. **2003**, 75, 835–842.

(24) Mitsakakis, K.; Gizeli, E. *Biosensors and Bioelectronics* **2011**, 26, 4579– 4584.

(25) Duschl, C.; Sevin-Lándais, A.-F.; Vogel, H. *Biophys. J.* **1996**, 70, 1985–1995.

(26) Andrade, J.D.; Hlady, V. *Advances in Polymer Science*, **1986**, 79. Springer, ISBN 978- 3-540-16422-7, 1–63.

(27) Goodrich, J.A.; Kugel, J.F. *Binding and Kinetics for Molecular Biologists*. Cold Spring Harbor Laboratory Press, New York, ISBN 0-87969-736-9, **2007**.

(28) Karlsson, R.; Michaelsson, A.; Mattsson, L. J. *Immunol. Methods* **1991**, 145, 229–240.

Chapter 5

STUDIES OF AN ALKANE PHOSPHONATE SAMs –BASED NOVEL SENSING PLATFORM

5.1 Introduction

Corrosion of iron and iron-based materials is a crucial concern in many areas such as petrochemical industry. Every year, thousands of millions of dollars are lost due to the corrosion of metals, especially iron and iron-based materials. It is important to understand the generation and protection of corrosion. The corrosion mechanism of iron is shown in figure 5.1. The corrosion of iron is an electrochemical oxidation process. As shown below, iron is oxidized in anode while the oxygen reduction reaction takes place in cathode. The products (Fe^{2+} and OH^{-1}) from both of the electrochemical reactions react with each other to produce $Fe(OH)_2$ that is unstable and easily oxidized to generate $Fe(OH)_3$. Finally, $Fe(OH)_3$ decomposes to form $Fe_2O_3 \cdot xH_2O$, the main form of rust. Because of the large damage resulting from corrosion, it is a vital issue to protect iron-based materials against corrosion. Figure 5.2 is the summary of the methods for the corrosion protection.

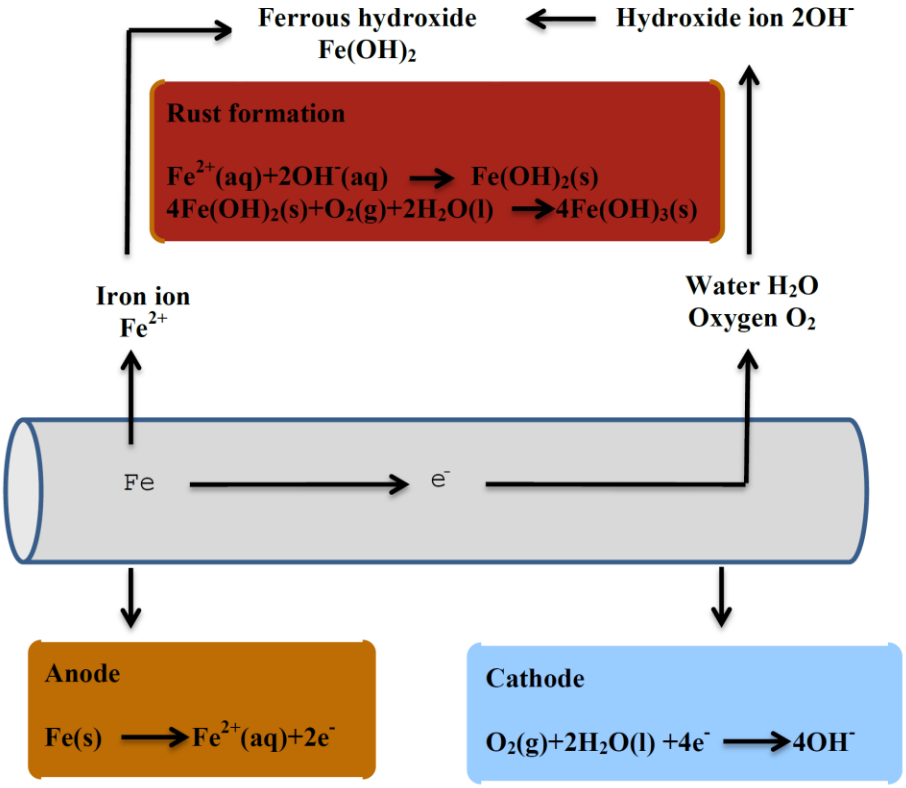

Figure 5.1 Corrosion mechanism of Iron

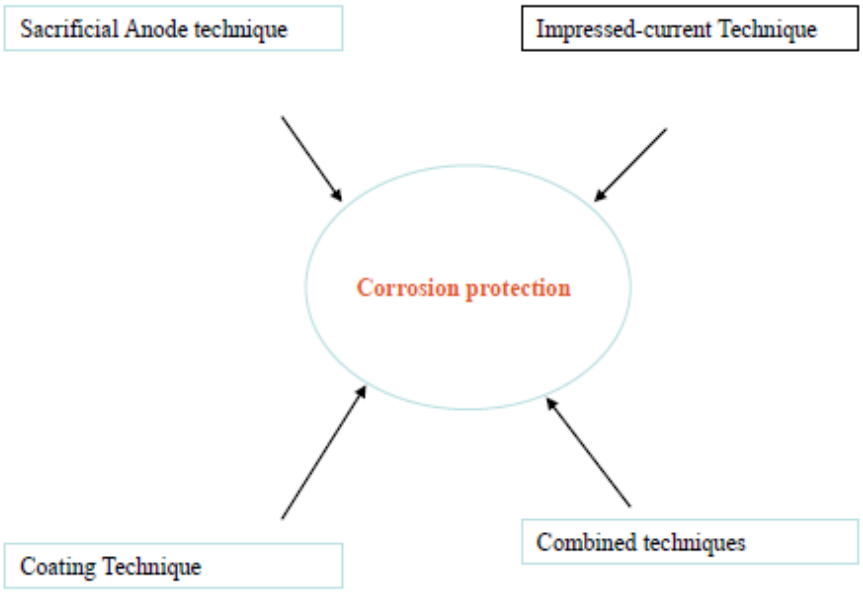

Figure 5.2 Schematic depict the approaches of corrosion protection.

Several methods are employed to prevent the Fe-based materials from corrosion. Sacrificial Anode technique is a technique in which a more active metal is connected to the Fe-based material. The new metal acts as an anode instead of Fe because of its more negative electrode potential and the Fe-based materials play a role of a cathode. Hence, the introduced metal is oxidized and the Fe-based materials survive the attack of corrosion. Two approaches are used to deposit the other metals onto Fe. Chemical deposition also called electroless plating in which chemical reactions are used to deposit

the other more active metals on the surface of Fe. Whereas, electroplating is to implement the deposition in an electric field.

Impressed-current technique is also known as impressed-current cathodic protection technique. In this technique, the anode is connected to a power supply in order to provide the current for the protected system. Usually, this technique is applied to big structures such as the protection of pipelines.

Coating technique is used to change the surface properties via immobilizing other molecules on the surface of materials. Organic compounds are widely accepted inhibitors for corrosion protection. The organic layers formed on the surface of materials efficiently attenuate the electron transfer reactions between the materials and the surrounding and thus, protect the materials from corrosion.[1-4]. The organic compounds are coated on the surface of materials by means of covalent bindings, van der Waals interactions, hydrogen bonds, and hydrophobic interactions. Therefore, the organic molecular electronic structures and functional groups play an important role in binding efficiency.[5-6] Some atoms in functional groups such as oxygen, nitrogen, and sulfur facilitate the adsorption of organic molecules to substrates.[7] For example, the compounds containing thiol functional group such as alkanethiols can be immobilized on the surface of Fe via a strong covalent binding to form the Fe-S σ-bonds,[8-11] which is similar to the Au-S σ-bonds formed on the Au surfaces.

Recently, new types of corrosion inhibitors have been reported. Gomez and coworkers studied the inhibitive properties of amino acids through density functional

theory indexes.[12] As an environmental friendly compound; amino acid will be a promising alternative for the organic corrosion inhibitors.

Self-assembled monolayers are thin films spontaneously formed on the surface of solid substrates through chemisorptions. In contrast with other deposition approaches such as chemical vapor deposition and molecular beam epitaxy (complex instruments and ultrahigh vacuum are needed), the technique to prepare self-assembled monolayers is simple and low costing.

Self-assembled monolayers are the most elementary form of a nanometer-scale organic thin-film material. Typically, the thickness of a SAM is 1-3 nm. The atomic composition of the SAM relies on the composition of the molecular components of the SAM. Therefore, it is possible to introduce any special functional groups by organic synthesis onto the surface of substrate and thus control the chemical composition as well as properties of the surface. SAMs can be formed on substrates of all sizes, for example, thin film, colloids, etc. The adsorption of multi-component monolayers on the substrate can enhance the control over surface functionality.

Figure 5.3 is the Schematic diagram of an ideal, single-crystalline SAM of alkanethiolates supported on a gold surface with a (III) texture.[13] SAMs consist of terminal functional group, alkane chain and head group.

Terminal groups, as shown in figure 5.3, usually are function groups that determine the surface properties and applications of the modified materials, by which the other compounds can be immobilized on the pre-modified materials to act as sensors for

the detection of various gases, protein etc. Thus, a multifunctional sensor platform can be designed via introducing more than one functional group onto the surfaces of substrates to improve the sensing efficiency.

Alkane chains determine the thickness of the film and vary the electronic properties of substrates. Head groups containing oxygen, nitrogen, and sulfur atoms react with the substrates to form strong bonding between head groups and substrates. The SAMs of alkanethiolates are the most studied films formed on the surface of Au, with strong bond energy of about 40-45Kcal/mol for Au-S σ-bond.[13-15] Based on the characteristics of very high density of the functional groups, few number of defects, and well-defined structure, SAMs have been widely used to construct the sensors.

Alkane phosphate SAMs and alkane phosphonate SAMs formed on the different substrates have been reported in the review papers.[16-24] More recently, Tosstti and co-workers have studied the poly(ethylene glycol) functionalized alkane phosphate SAMs produced on titanium oxide surfaces for preventing the nonspecific adsorption of proteins, bacteria, and cells.[25-26]

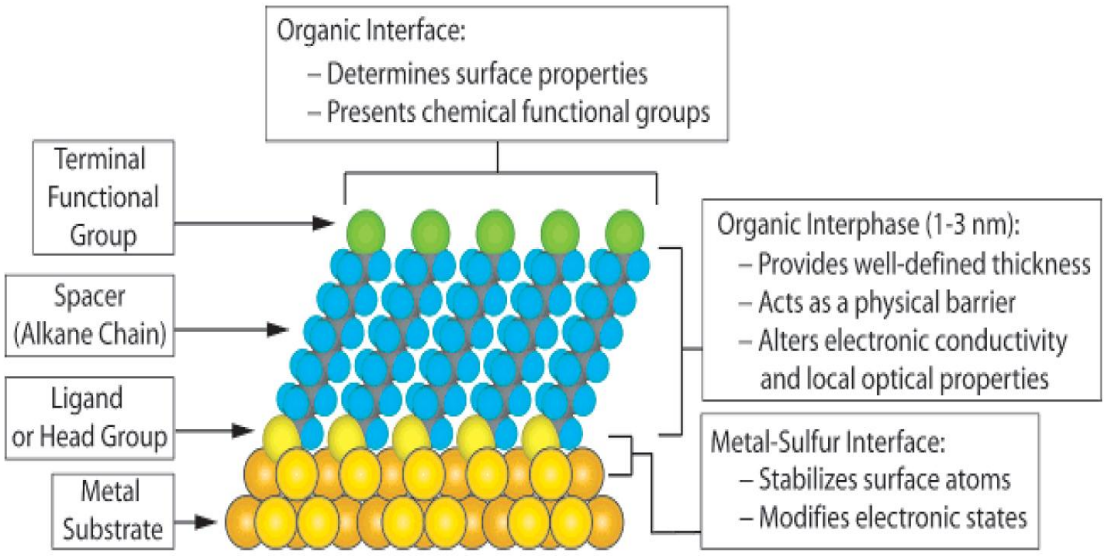

Figure 5.3 Schematic diagram of an ideal, single-crystalline SAM of alkanethiolates supported on a gold surface with a (111) texture.

(Copied from Ref 13 with ACS permission)

However, the studies of alkane phosphonate SAMs formed on Fe or Fe-based materials are barely reported. The object of this work is to explore the formation of alkane phosphonate SAMs on the surfaces of Fe-based materials and its application as a multifunctional sensing platform.

5.2 Experimental section

5.2.1 Chemicals and Reagents

1-Tetradocylphosphonic acid (98%), Hexaammineruthenium chloride (98%), 16-phosphonohexadecanoic acid, Fe wire (99.99% diameter 0.5mm), Fe foil (99.99%,

thickness 0.25mm) potassium nitrate were purchased from Sigma-Aldrich. Magnetostrictive particles (Metglas brand 2826MB in a ribbon form) were obtained from Honeywell International (Conway, SC). All chemicals were used as received.

5.2.2 Pre-treatment of Fe and magnetostrictive particles (MSPs)

Iron and MSPs were polished using the different size SiC paper (400, 4000), diamond paste (15μm, 3μm, 1μm) and 0.05μm alumina sequentially and then were ultrasonically cleaned in both deionized water bath and acetone bath for 5 minutes each respectively and dried in a stream of flowing nitrogen.

Two methods were used to further treat the Fe and MSPs surfaces. First, prior to the treatment, the sodium borate buffer solution was bubbled using a stream of flowing Ar for 20 minutes. Pre-treated Fe (MSPs) was placed in a conventional electrochemical cell containing sodium borate buffer solution with pH of 8.30, controlling current density 40 $\mu A/cm^2$ for 10 minutes and then holding the potential at 380 mV(vs. Ag/AgCl) for 40mins. The oxidized Fe (MSPs) was rinsed with deionized water and ethanol subsequently and dried in Ar stream. Second, instead of a sodium borate buffer solution, 0.5 M H_2SO_4 solution was used as the supporting electrolyte. The cleaned Fe (MSPs) was treated in the 0.5M H_2SO_4 solution by holding the potential at -120mV for 20s, followed by a double-stepwise ORC at -370mV for 15s and then by controlling the potential at -750mV for 20s.

5.2.3 Formation of alkane phosphonate SAMs

Pre-treated Fe(MSPs) were immersed in 1mM phosphonic acid ethanol solution for 24 hours, then the immobilized Fe (MSPs) were rinsed to wash off the unreacted molecules using ethanol for 3 times and dried for the later use.

5.2.4 Electrochemistry

Cyclic voltammetry measurements were conducted by using a BAS-Epsilon workstation in a traditional three-electrode cell in which the modified Fe-based materials acted as the working electrodes, a Pt net was utilized as the counter electrode and Ag/AgCl was the reference electrode. 0.1M KNO_3 solution was used as the supporting electrolyte.

Bipolar electrochemical measurements were performed in a glass cell (diameter 3.6cm) with two Au wires as driving electrodes connected to a Hewlett-Packard model 6010 regulated DC power supply to apply 10.5V across the two driving electrodes. Phosphate buffer solution with a pH of 7.0 was used as supporting electrolyte solution.

5.2.5 Surface Enhanced Raman Spectroscopy (SERS)

SERS spectra were measured with a confocal microscopic Raman spectrometer (Renishaw 1000 model) with a CCD detector and a holographic notch filter. Radiation of 785 nm from an air- cooled argon ion laser (Spectra-Physics model 163-C4260) was used for excitation. Laser power is 1.75 mill watts. The collection time was 20s and accumulated 2 times.

5.3 Results and discussion

The properties of surfaces will vary as the different treatments are applied. Table 5.1 is the summary of three approaches.

Table 5.1 Pre-treatment of Fe surfaces

Sample	Treatment	Comments
1	Mechanically polished	SiC paper, diamond paste, 0.05 μ alumina
2	ORC	0.5 M H_2SO_4 (a) –0.12 V, 20 s; (b) –0.37 V, 15 s; (c) –0.75 V, 20 s
3	Passivation layer	Borate buffer (pH 8.3), controlled potential +0.38 V, 1 h.

The passivation curve is displayed in Figure 5.4. The extent of passivation gradually rises with the proceeding of oxidation reaction of Fe. The passive film blocks the electron transfer, and thus, the current gradually decreases until it reaches a saturated state.

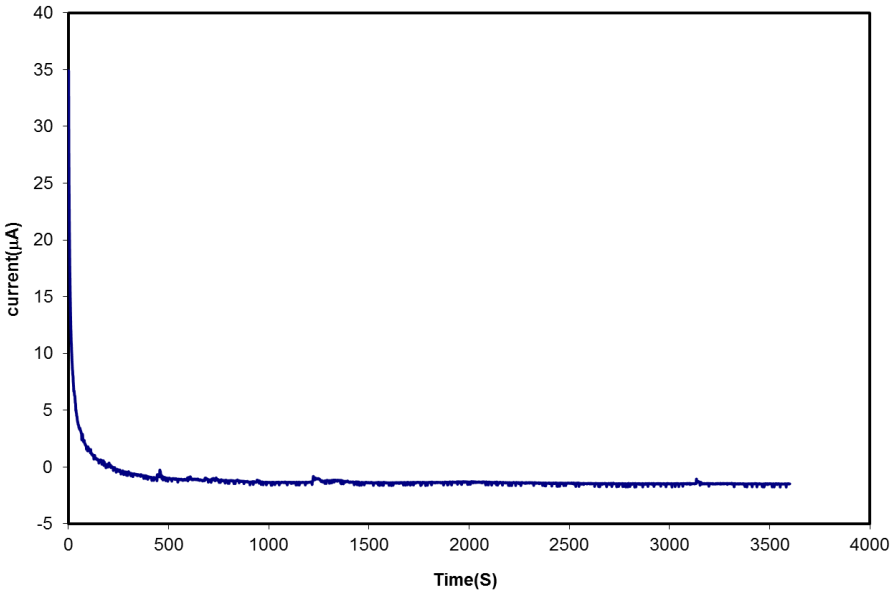

Figure 5.4 Passivation curve of Fe.

The experiment was performed in a sodium borate buffer solution with a pH of 8.30, controlling current density 40 $\mu A/cm^2$ for 10 minutes and then holding the potential at 380 mV (vs. Ag/AgCl) for 40 minutes.

To investigate the change of electrochemical properties after the formation of alkane phosphonate SAMs on Fe surfaces, an electrochemical probe $Ru(NH_3)_6Cl_3$ was introduced. As shown in figure 5.5, $Ru(NH_3)_6^{3+}$ can be easily reduced on the bare Fe electrode, whereas SAMs-modified Fe electrodes inhibit the $Ru(NH_3)_6^{3+}$ from capturing electrons and thus a weak peak current is expected.

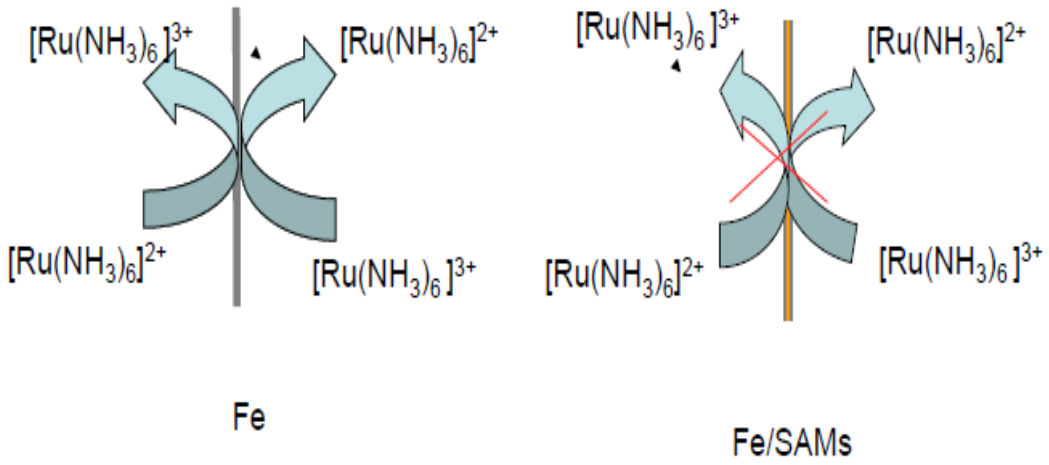

Figure 5.5 Assessing surface using electrochemical probes.

Figure 5.6 is the cyclic voltammograms from Fe electrodes pretreated by three different approaches. The anodic peak current is summarized in table 5.2.

Table 5.2 Comparison of anodic peak current before and after immobilizing SAMs on Fe surfaces.

	Current(A) from figure5.6(a)	Current(A) from figure5.6(b)	Current (A) from figure5.6(c)
Bare Fe electrode	$2.74x10^{-5}$	$5.41x10^{-5}$	$3.41x10^{-5}$
SAMs modified Fe electrode	$3.99x10^{-6}$	$1.25x10^{-5}$	$9.7x10^{-7}$

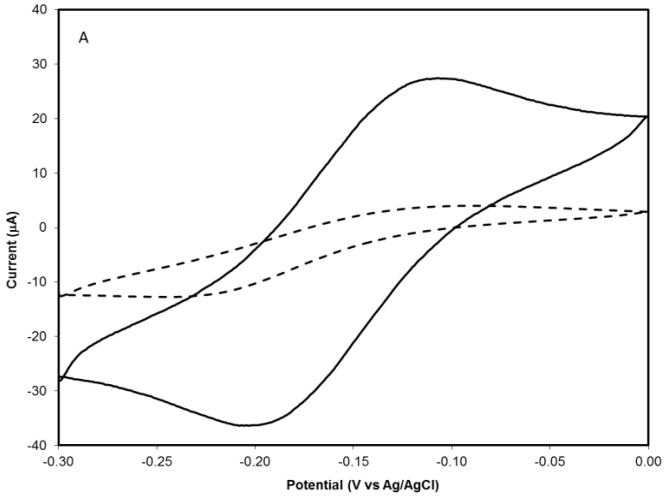

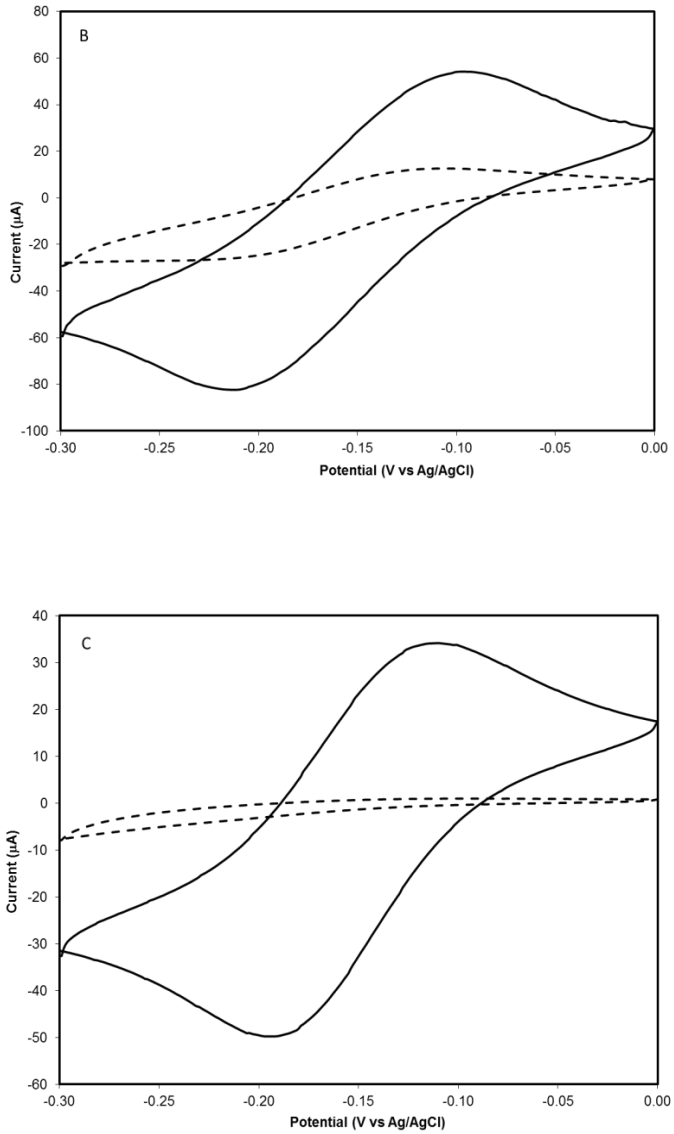

Figure 5.6 Cyclic voltammograms of different Fe electrodes in a 0.1M KNO_3 solution containing 1mM $Ru(NH_3)_6Cl_3$. Scan rate is 50mV/s. (a). Fe surface was mechanically polished, (b). Fe surface was treated by ORC method in 0.5M H_2SO_4 solution. (c). Fe surface was passivated in a borate buffer solution with a pH of 8.30. The solid curves represent the electrochemical behavior of bare Fe and the dotted curves correspond to the cyclic voltammograms obtained from phosphonate SAMs modified Fe electrodes.

In figure 5.6 (a), the anodic peak current of the Fe electrode decreases before and after immobilizing phosphonate SAMs from $2.74x10^{-5}$ to $3.99x10^{-6}$A. This means that the peak current reduces 85%, while the peak current reduces 76.9% in figure 5.6 (b). Compared with figures (a) and (b), the peak current in figure (c) is found to decrease the most about 97.2%. The experimental results indicate that the most efficient assembling take place on the passivated Fe surfaces.

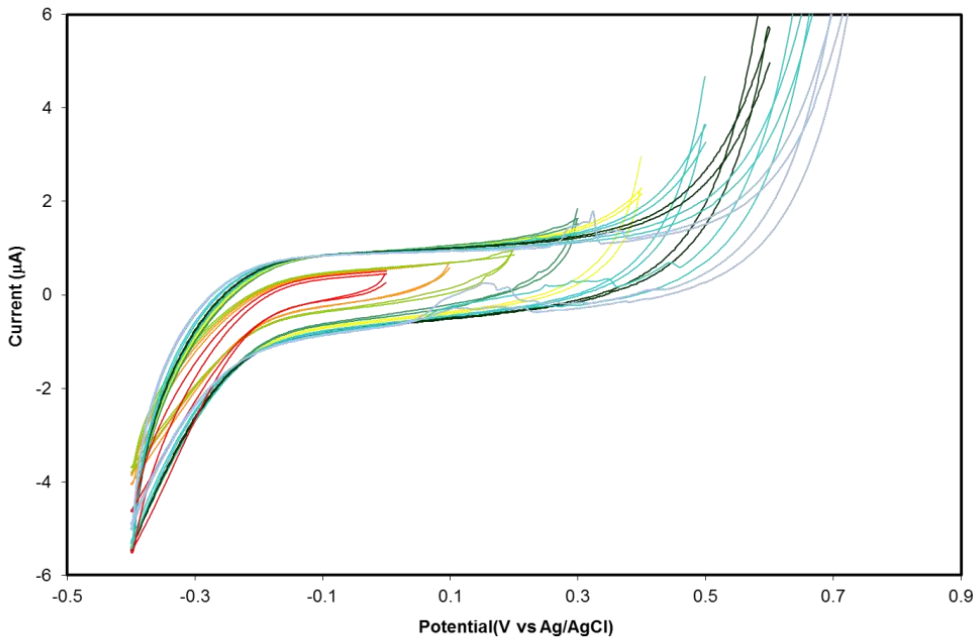

Figure 5.7 Stability of Phosphonate SAMs formed on the mechanically polished Fe surface. The experiments were performed in 1mM $Ru(NH_3)_6^{3+}$- 0.1M KNO_3 solution with Scan rate:50mV/s.

In order to test the stability of SAMs, the following experiments were implemented. SAMs formed on three different surfaces were electrochemically damaged by scanning towards positive potential until 0.8V. Figure 5.7 shows that the current increases with the increased potential. In this experiment, the SAMs were formed on the mechanically polished Fe surface. The SAMs were damaged as the potential was gradually increased which resulted in an increase in surface area of Fe electrode. As a result, the current gradually increased.

The stability of SAMs formed on the electrochemically pre-treated Fe surfaces via ORC approach is exhibited in figure 5.8. The SAMs are stable up until the point when the potential exceeds 0.4V. After that, the current declines due to the passivation. Figure 5.9 shows the stable film adsorbed on passivated surfaces. From these results, one can conclude that the SAMs formed on electrochemically pre-treated surfaces are more stable than those formed on the mechanically polished ones, and the most stable self-assembled monolayers can be formed on the passivated Fe surfaces.

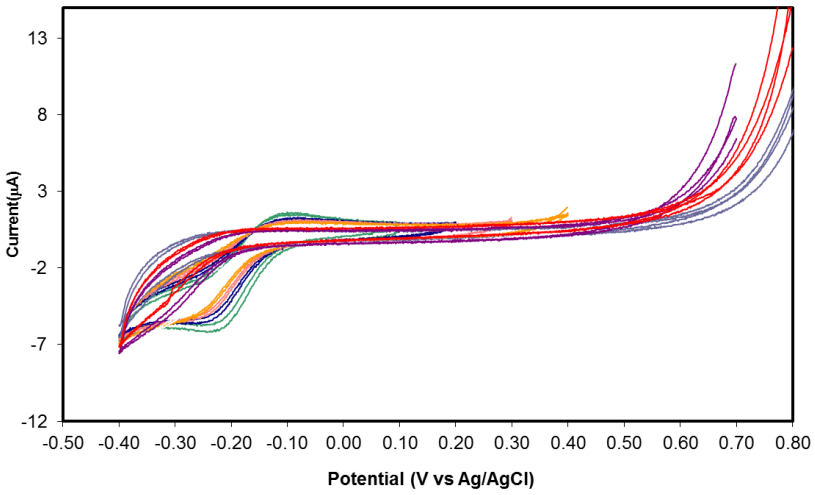

Figure 5.8 Stability of Phosphonate SAMs formed on electrochemically pre-treated Fe surface via ORC approach. The experiments were performed in 0.1M KNO_3 solution containing 1mM $Ru(NH_3)_6^{3+}$. The scan rate is 50mV/s.

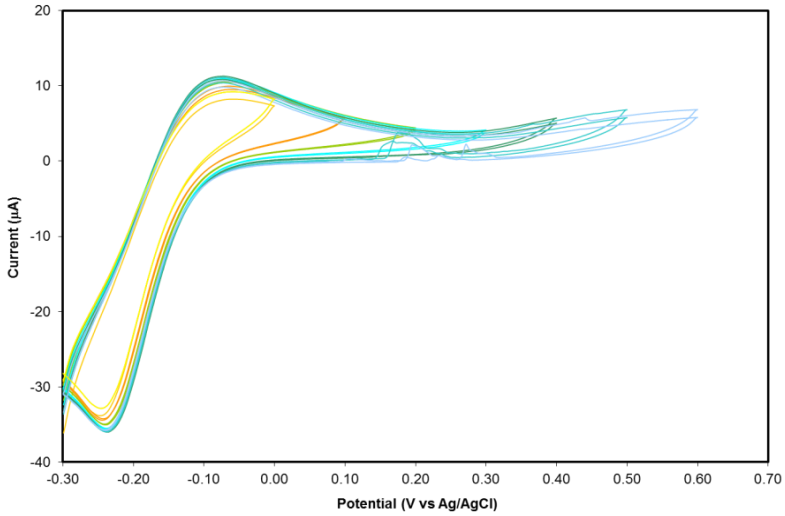

Figure 5.9 Stability of Phosphonate SAMs formed on passivated Fe surface. The experiments were carried out in 0.1M KNO_3 solution containing 1mM $Ru(NH_3)_6^{3+}$.The scan rate is 50mV/s.

Table 5.3 Assignment of Raman peaks of 1-Tetradocylphosphonic acid

Wavenumbers (cm^{-1})	Assignment
2900	ν (C-H) stretching
1460	δ(C-H) scissoring
1308	ω(C-H) wagging
1120	ν(C-C) stretching
1100	ν (C-C) stretching
1059	ν(C-C) stretching
960	ν(P-O) stretching
885	ν(C-C) stretching
790	γ(O-H) rocking

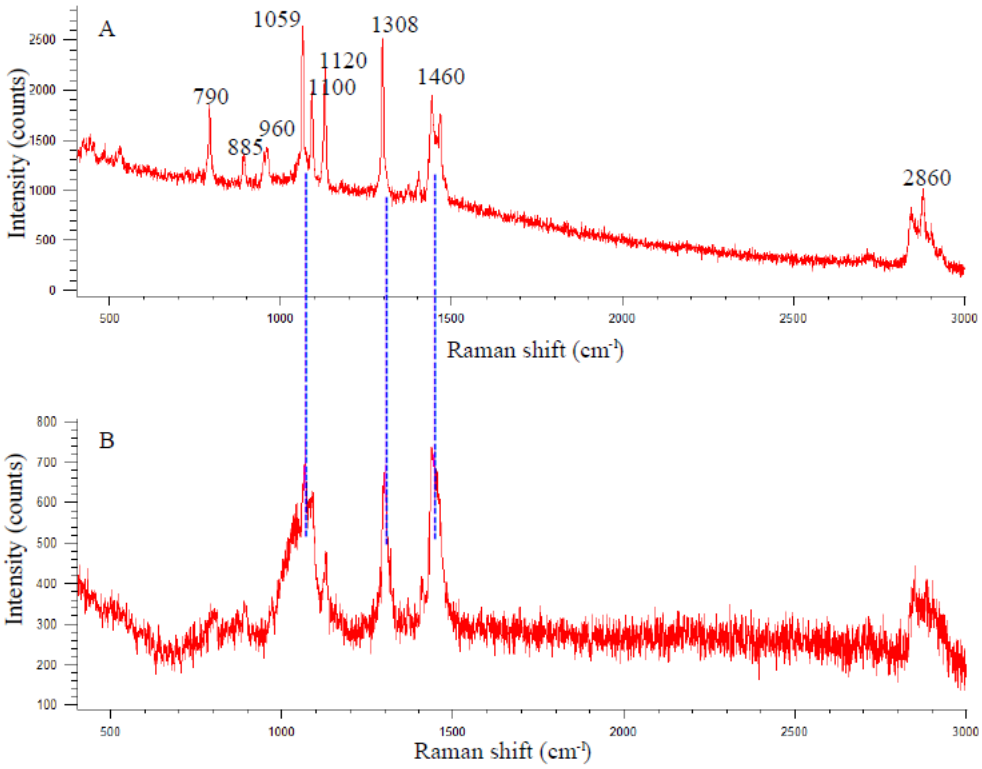

Figure 5.10 Raman spectrum of (a) 1-Tetradocylphosphonic acid powder (b) 1-Tetradocylphosphonic acid modified Fe. The excitation wavelength is 785nm and collection time is 20s.

Raman spectroscopy is a useful tool to study the molecular vibrations of alkane phosphonate SAMs formed on Fe surfaces. Figure 5.10 shows the Raman spectra of 1-Tetradocylphosphonic acid powder and phosphonate SAMs. The two spectra are the similar except the peak width increases in SAMs-modified Fe surfaces, which indicates the reduction of resolution of Raman detection on the monolayers. The peak occurring at 2900 cm^{-1} is attributed to the C-H stretching vibration while the peak at 1460 cm^{-1} is ascribed to the C-H scissoring motion. The peak at 1308 cm^{-1} is assigned to the C-H

wagging motion. The C-C stretching of trans conformation of Alkyl chain takes place at 1059 cm^{-1}. The assignment of Raman peaks of 1-Tetradocylphosphonic acid is shown in table 5.3.[27-29]

The binding of phosphonic acid on the metal oxide surfaces is a condensation reaction between P-O-H and H-O-metal accompanied with the release of a water molecule. Pawsey et al reported that the heat treatment increased the stability of monolayers because the binding reaction is temperature dependent.[30] Scheme 5.1 shows some possible binding modes of phosphonic acid on the metal oxide surfaces.[31]

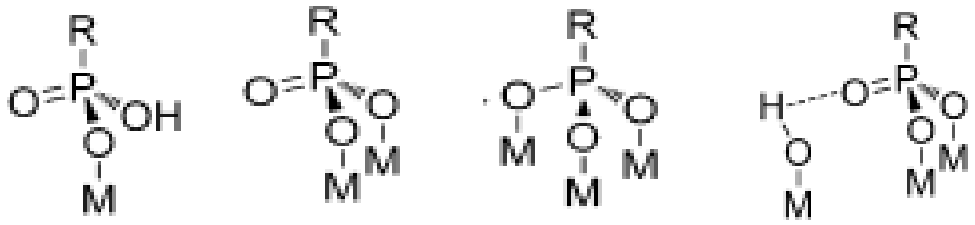

Scheme 5.1 Possible binding modes of phosphonic acid upon adsorption on metal oxide surfaces, ranging from simple hydrogen bonding interactions to tridentate coordination.

Luschtinetz and coworkers studied the mechanism of alkylphosphonic acid bound to Aluminum surface,[32] and other authors reported the binding of alkylphosphonic acid to Fe oxide nanoparticles.[33-35] These results revealed that the acid bound to the Fe oxide surfaces through two symmetric P-O-Fe bonds. The evidence that Raman peak at 790 cm^{-1} disappears in figure 5.10 (b) confirms the bidentate bonding mechanism.

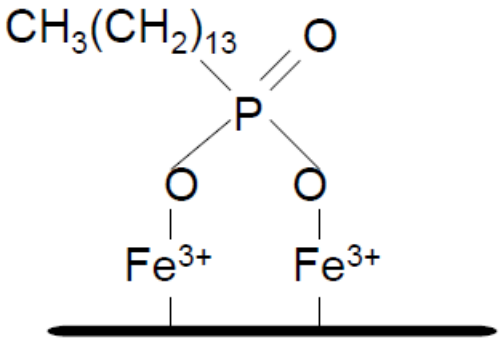

Scheme 5.2 Bidentate bonding mechanism of alkylphosphonic acid to Fe oxide surface.

5.4 Application

The formation of phosphonate SAMs on Fe surfaces can be extended to any Fe-based materials such as MSPs. By combining it with bipolar technique, a multifunctional sensing platform can be fabricated.

5.4.1 Design of Experiments

To obtain multifunctional groups on one solid substrate, a simple approach is exhibited here. Phosphonohexadecanoic acid-modified MSPs were placed in a bipolar electrochemical cell acting as the bipolar electrodes. When a potential was applied on the two driving electrodes, the reduction reactions would take place in the cathode of the bipolar electrode. Thus, the carboxyl groups were reduced and a new kind of functional group, formyl, was produced.

Raman spectroscopy can be used to detect the changes occurring on the MSPs surfaces, however, the weak intensity confines the applications. Raman signals collected on some rough metal surfaces such as Ag, Au, Cu can be enhanced as much as 10^{10} to 10^{11} times comparing to traditional Raman spectrum.[36-37] Therefore, $Ag(NH_3)_2^+$ was introduced in this work to generate Ag onto the surfaces. $Ag(NH_3)_2^+$ as a mild oxidizing reagent would not damage the film, which explains why $Ag(NH_3)_2^+$ rather than Ag^+ was chosen as the oxidant.

Because of the characteristics of bipolar electrodes, the reduced products displayed a concentration gradient along the electrodes that can be monitored by surface enhanced Raman spectroscopy. A trend of Raman intensities reducing along the bipolar electrodes from the end to center was expected.

Scheme 5.3 depicts the detection process. Firstly, $PO_3C_{15}H_{32}COOH$-modified MSPs were electrochemically reduced in a bipolar cell to form $PO_3C_{15}H_{32}CHO$. Then, $PO_3C_{15}H_{32}CHO$ adsorbed on MSPs was chemically oxidized by using $Ag(NH_3)_2^+$ to regenerate $PO_3C_{15}H_{32}COOH$. Finally, Raman signals were detected.

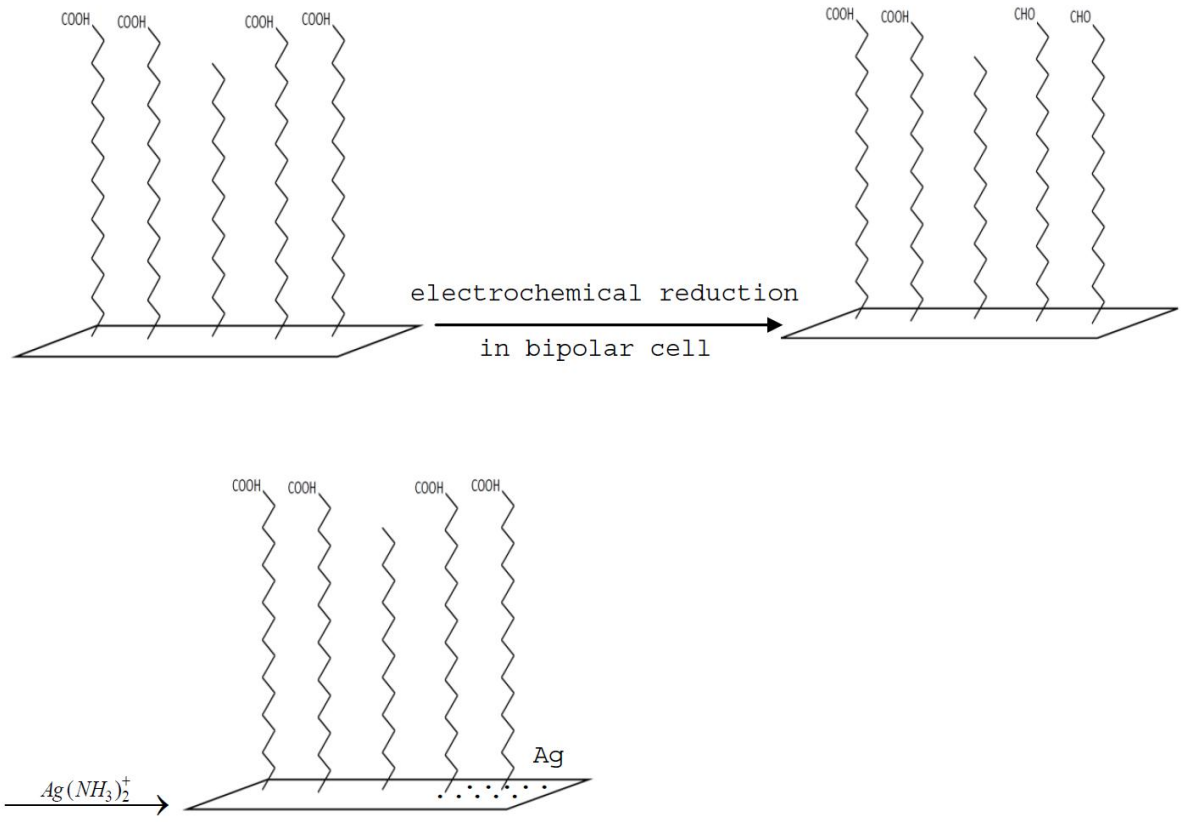

Scheme 5.3 Design of a multifunctional sensing platform

The reaction equations can be expressed as

$$PO_3C_{15}H_{32}COOH + 2H^+ + 2e^- \rightarrow PO_3C_{15}H_{32}CHO + H_2O \quad (5.1)$$

$$PO_3C_{15}H_{32}CHO + Ag(NH_3)_2^+ + H_2O \rightarrow PO_3C_{15}H_{32}COOH + Ag + 2NH_4^+ \quad (5.2)$$

5.4.2 Results and Discussion

16-phosphonohexadecanoic acid-modified MSPs (1.0cm x 0.4cm) were placed in a bipolar electrochemical cell with 0.1M phosphate buffer solution (pH=7.0) as the supporting electrolyte. Two Au wire were used as driving electrodes. A voltage of 10.5 V was applied onto the driving electrodes for 5 minutes. The reduced MSPs was rinsed with deionized water and dried. 29 mM $Ag(NH_3)_2^+$ 0.05mL was dropped onto the surface of modified MSPs. Then, the MSPs were placed into an oven of 30^0c for 40 minutes, which was followed by the rinsing and drying of MSPs.

Surface enhanced Raman spectra are displayed in figure 5.11 and 5.12. In figure 5.11, a new peak occurs at 1605 cm^{-1} that represents the asymmetric carboxylate stretche.[38] In figure 5.12, the Raman signals were collected from the end to the center of modified MSPs with an interval of 40μm. Owing to the features of bipolar electrode, the concentration of reduced –COOH groups decreases that results in the decreasing of the concentration of oxidized –CHO groups and the declining of the enhancement of Raman signals along the electrode from the end to the center and therefore, the Raman intensity gradually reduces. Figure 5.12 clearly exhibits this trend. On the other end of modified MSPs, no redox reaction of SAMs occurs on the surface. Consequently, no Raman scattering is detected as shown in figure 5.13.

Figure 5.14 was obtained by plotting the intensities of the C-C stretching (1059 cm^{-1}) vs. the distance from the detected spots to the end of MSPs. In general, the Raman intensities decrease with the increasing distance. The experimental results demonstrate the formation of two functional groups on the surface of MSPs.

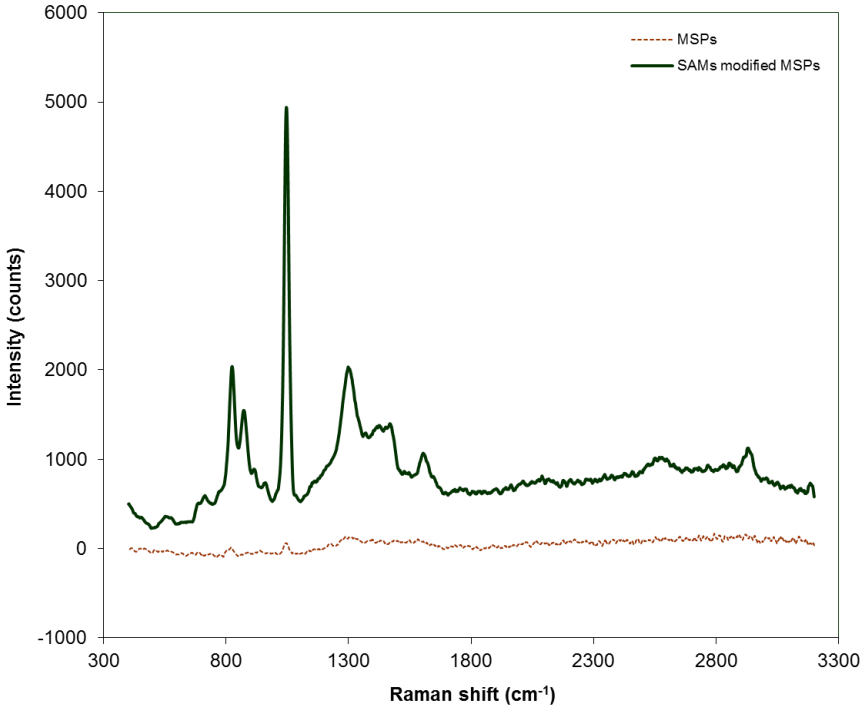

Figure 5.11 Raman spectra of mixed SAMs (molar ratio of 16-phosphonohexadecanoic acid: 1-Tetradocylphosphonic acid is 8:2) formed on MSPs surfaces. A 514 nm laser was used as the excitation source. Collection time: 20s.

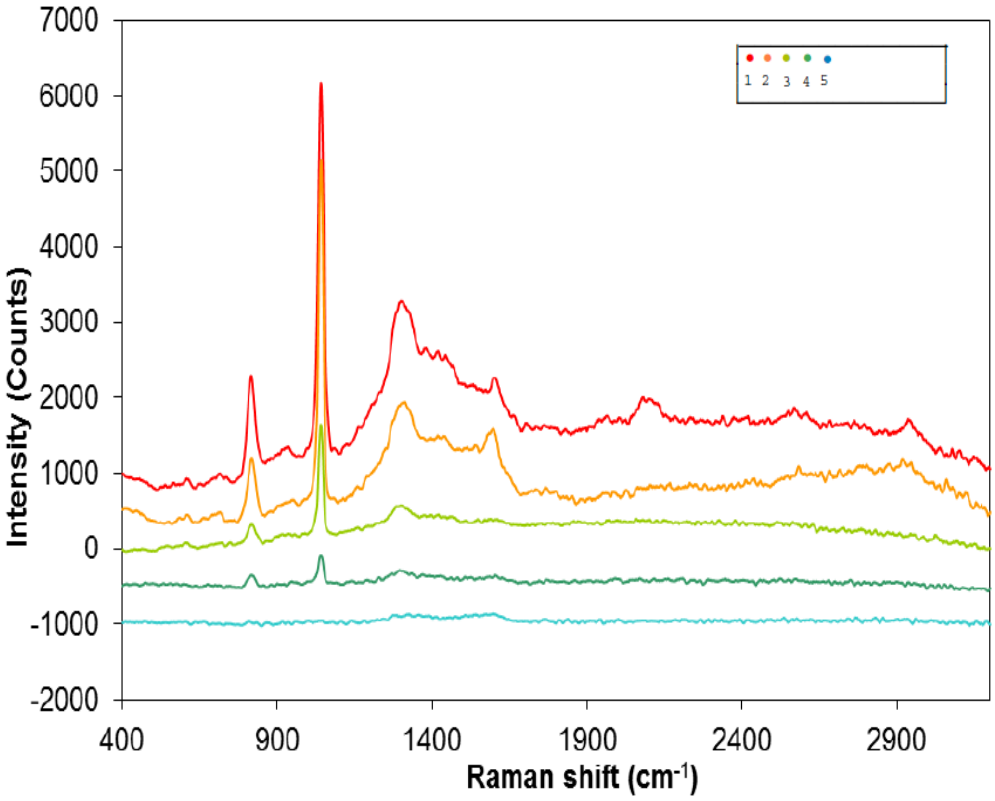

Figure 5.12 Representative Raman spectra of Mixed SAMs collected from different spots. The excitation wavelength is 514 nm and collection time is 20s. Inset stands for a bipolar electrode and the spots where the Raman signals are collected. The distance between two spots is 40μm.

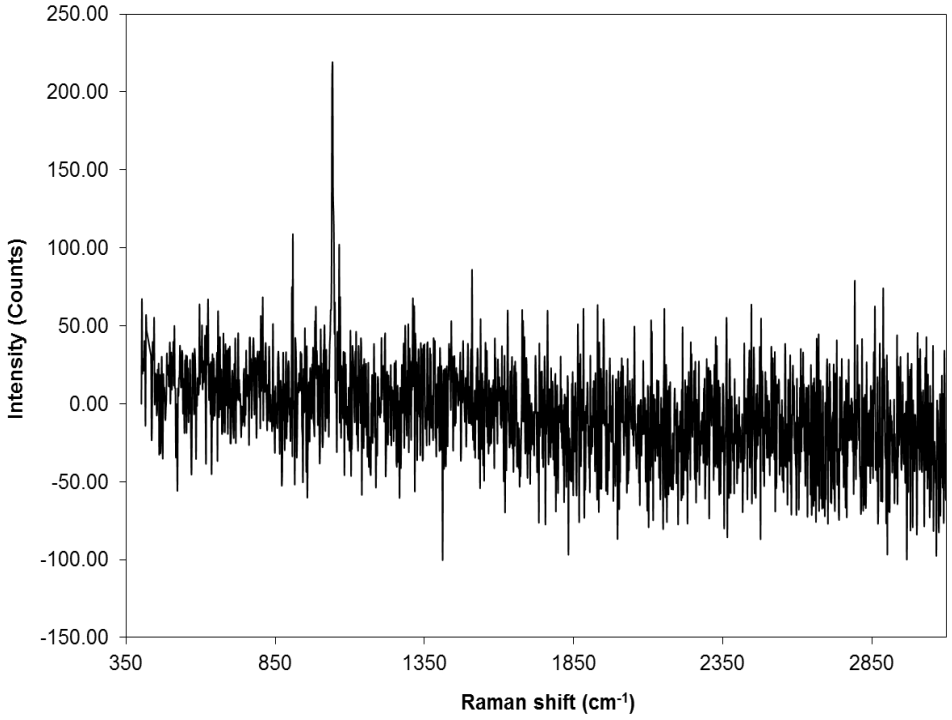

Figure 5.13 No Raman signal is detected on the other end of SAMs modified MSPs surfaces

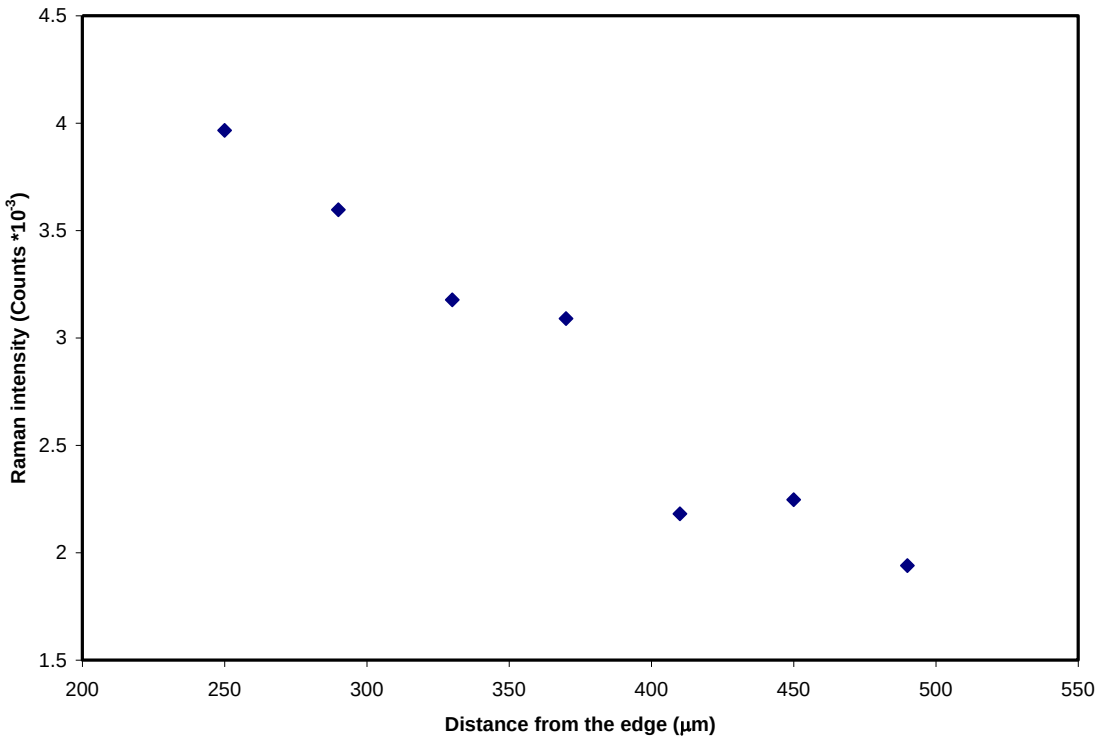

Figure 5.14 Raman intensities decrease with the increasing of distance from the detected spots to the end of the bipolar electrode (modified MSPs.) Intensities are obtained by integrating the C-C peaks at 1059 cm^{-1}.

5.5 Conclusions

The results of this experiment indicate the feature of bipolar electrodes. The voltage applied on bipolar electrodes is the length dependent. The voltage gradually decreases along the bipolar electrode from the end to the center which causes the amount of reduced $PO_3C_{15}H_{32}CHO$ decreasing from the end to the center. As a result, the Raman

intensities reduce with the increasing of distance from the detected spot to the end of the MSPs.

Phosphonate SAMs formed on the surface of Fe have been studied via cyclic voltammetry and surface enhanced Raman spectroscopy. Three approaches used to pre-treat Fe surfaces were discussed. The reaction mechanism is in agreement with the previous reports. The results reveal that the surface passivation can facilitate the adsorption of phosphonate SAMs on Fe.

As an application of phosphonate SAMs, this work exhibits a simple way to construct a multifunctional sensor platform. Two different functional groups from both ends of the bipolar electrodes can be acquired. Therefore, people can detect two different analytes on a sensor.

References

(1) Quan, Z.; Chen, S.; Li, Y.; Cui, X. *Corros. Sci.* **2002**, 44, 703.

(2) Ka´lma´n, E. *Electrochim. Acta* **2001**, 46 (24/25), 3607.

(3) Polewska, W.; Vigt, M.R.; Magnussen, M.O.; Behm, R.J. *J. Phys. Chem. B* **1999**, 103 (47), 10440;

(4) Zamborini, F. P.; Crooks, R.M. *Langmuir* **1998**, 14 (12), 3279.

(5) Granese, S. L. *Corrosion* **1988**, 44, 322.

(6) Bentiss, F.; Traisnell, M.; Lagrenee, M. *J. Appl. Electrochem.* **2001**, 31, 41.

(7) Abd-El-Nabey, B. A.; Khalil, N.; Mohamed, A. *Surf. Technol.* **1985**, 24, 383.

(8) Kataby, G.; Prozorov, T.; Koltypin, Y.; Cohen, H.; Sukenik, C.N.; Ulman, A.; Gedanken, A. *Langmuir* **1997**, 13 (23), 6151.

(9) Volmer, M.; Stratmann, M. *Appl. Surf. Sci.* **1992**, 55, 19.

(10) Zamborini, F.P.; Campbell, J.K.; Crooks, R.M. *Langmuir* **1998**, 14 (3), 640.

(11) Cavalleri, O.; Kind, H.; Bittner, A.M.; Kern, K. *Langmuir* **1998**, 14 (25), 7292.

(12) Go´mez, B.; Likhanova, N. V.; Domı´nguez Aguilar, M. A.; Olivares, O.; Hallen, J. M. and Martı´nez-Magada´n, J. M. *J. Phys. Chem. A* **2005**, 109, 8950-8957.

(13) Love, J. C.; Estroff, L. A.; Kriebel, J. K.; Nuzzo, R. G. and Whitesides, G. M. *Chem. Rev.* **2005**, 105, 1103-1169

(14) Bain, C. D.; Troughton, E. B.; Tao, Y. T.; Evall, J.; Whitesides, G. M.; Nuzzo, R. G. *J. Am. Chem. Soc.* **1989**, 111, 321-335.

(15) Nuzzo, R. G.; Allara, D. L. *J. Am. Chem. Soc.* **1983**, 105, 4481-4483.

(16) Brovelli, D.; Ha¨hner, G.; Ruiz, L.; Hofer, R.; Kraus, G.; Waldner, A.; Schlosser, J.; Oroszlan, P.; Ehrat, M.; Spencer, N. D. *Langmuir* **1999**, 15, 4324- 4327.

(17) Ha¨hner, G.; Hofer, R.; Klingenfuss, I. *Langmuir* **2001**, 17, 7047-7052.

(18) Hofer, R.; Textor, M.; Spencer, N. D. *Langmuir* **2001**, 17, 4014-4020.

(19) Textor, M.; Ruiz, L.; Hofer, R.; Rossi, A.; Feldman, K.; Ha¨hner, G.; Spencer, N. D. *Langmuir* **2000**, 16, 3257-3271.

(20) Foster, T. T.; Alexander, M. R.; Leggett, G. J.; McAlpnie, E. *Langmuir* **2006**, 22, 9254-9259.

(21) Gao, W.; Dickinson, L.; Grozinger, C.; Morin, F. G.; Reven, L. *Langmuir* **1996**, 12, 6429-6435.

(22) Pawsey, S.; Yach, K.; Reven, L. *Langmuir* **2002**, 18, 5205-5212.

(23) Helmy, R.; Fadeev, A. Y. *Langmuir* **2002**, 18, 8924-8928

(24) Spori, D. M.; Venkataraman, N. V.; Tosatti, S. G. P.; Durmaz, F.; Spencer, N. D. and Zu¨rcher, S. *Langmuir* **2007**, 23, 8053-8060 8053.

(25) Gnauck, M.; Jaehne, E.; Blaettler, T.; Tosatti, S.; Textor, M. and Adler, H. J. P. *Langmuir* **2007**, 23, 377-381.

(26) Bozzini, S.; Petrini, P.; Tanzi, M. C.; Z€urcher, S. and Tosatti, S. *Langmuir* **2010**, 26(9), 6529–6534

(27) Boczula, D.; Cały, A.; Dobrzyn´ ska, D.; Janczak, J.; Zon; J. *Journal of Molecular Structure* **2012**, 1007, 220–226.

(28) Podstawka, E.; Andrzejak, M.; Kafarski, P. and Proniewicz1, L. M. *J. Raman Spectrosc.* **2008**; 39: 1238–1249.

(29) Podstawka, E.; Kafarski, P. and Proniewicz1, L. M. *J. Raman Spectrosc.* **2008**, 39, 1396–1407.

(30) Pawsey, S.; McCormick, M.; De Paul, S.; Graf, R.; Lee, Y. S.; Reven, L.; Spiess, H. W. *J. Am. Chem. Soc.* **2003**, 125, 4174.

(31) Queffélec, C.; Petit, M.; Janvier, P.; Knight, D. A. and Bujoli, B. *Chem. Rev.* **2012,** April 24 (online).

(32) Luschtinetz, R.; Seifert, Gotthard; J., E.; Adler, H. J. P. *Macromol. Symp.* **2007**, 254, 248–253.

(33) Yee, C.; Kataby, G.; Ulman, A.; Prozorov, T.; White, H.; King, A.; Rafailovich, M.; Sokolov, J. and Gedanken, A. *Langmuir* **1999**, 15, 7111-7115.

(34) Hu, A.; Yee G. T., and Lin, W.B. *J. Am. Chem. Soc*. **2005**, 127 (36), 12486–12487.

(35) Chouhan, G.; Wang, D. S.; Alper, H. *Chem. Commun.* **2007**, 4809.

(36) Blackie, E. J.; Le Ru, E. C.; Etchegoin, P. G. *J. Am. Chem. Soc.* **2009**, 131(40), 14466–14472.

(37) Blackie, E. J.; Le Ru, E. C.; Matthias, M.; Etchegoin, P. G. *J. Phys. Chem. C* **2007**, 111(37), 13794–13803.

(38) Siirila, A. R. and Bohn, P. W. *Langmuir* **1991**, 7(10), 2193.

Chapter 6

SUMMARY

Depending on the simple experimental setup, low power dissipation, and controllable multi-electrodes, the bipolar electrochemical technique has attracted a great deal of scientific interest and been widely applied to many areas. By combining the bipolar electrochemical technique and other analytical techniques, four wireless sensing systems are reported in this dissertation.

A rechargeable miniaturized battery based on the Au microarray electrodes has been fabricated and characterized. Unlike the other methods of making microarray electrodes such as photolithography, a simple and speedy approach, without using sophisticated instruments, called toner transfer masking was used here. Because of the feature of wireless, the bipolar electrochemical technique allows us to modify electrodes with various sizes ranging from centimeters to micrometer, to even a nanometer scale that has been proved in our experiments via depositing conductive polymer, polyaniline, onto microarray Au electrodes. Raman spectroscopy was used to detect the changes in oxidation states of PANI. The experimental results reveal that the intensities of reduced PANI decrease with the increasing of applied potential due to the variation of electronic structure on the polymer backbone. The charge-discharge processes can be monitored visually based on the electrochromic property of PANI. The output voltages of the bipolar Au microarray electrodes were measured and the results show that the average value for one microelectrode is 0.2V. Interestingly, the voltage of a microarray battery

can be controlled by placing electrodes with different amounts and different array patterns on Au substrates which enables us to design batteries with a wide range of voltages.

Using ECL as a reporter, a novel wireless alcohol sensor has been successfully constructed through layer by layer self-assembly technique. The concentration of alcohol was detected by monitoring the ECL intensity. The experimental results indicate a linear relationship between the concentration of alcohol and ECL intensity in some concentration ranges and demonstrate the ECL annihilation reaction mechanism as well. The phenomenon of ECL enhancement was observed by enlightening the alcohol sensor in a bipolar electrochemical cell. An advantage of this sensor is that the expensive NAD^+ and $Ru(bpy)_3^{3+}$ can be regenerated automatically by simply changing the polarity of the driving electrodes after a measurement. The design reported here can be used as a detector element for use in microfluidic separations and in highly multiplexed multi-analyte detection platforms.

The antibody-antigen interaction has been implemented on a wireless magnetostrictive particles-based sensor. Two kinds of methods for chemically depositing Au were investigated. The approach via replacement reactions to deposit Au is simple with a short reaction period, but the Au film is not stable in aqueous solutions, so the electroless Au plating was therefore chosen to deposit Au onto the MSPs. To obtain a well-controlled and functional surface, a mixed $SH(CH_2)_{15}COOH$:$C_{18}H_{37}SH$=8:2 ethanol solution was chosen to form self-assembled monolayers. Contact angle measurement was

utilized to study the wettability of modified MSPs surfaces. The association constant Ka was calculated, and the value, $2.23\pm0.152\times10^{8}$ M^{-1}, indicates the high affinity of antibody-antigen binding reaction.

As a corrosion inhibitor, alkylphosphonic acid has been successfully assembled on the surface of Fe. The characterization was performed by using cyclic voltammetry and surface enhanced Raman spectroscopy. Three approaches used to pre-treat Fe surfaces were discussed. The results reveal that the passivated surface can facilitate the adsorption of phosphonate SAMs on Fe and the adsorption favors bidentate binding.

An application of phosphonate SAMs is reported here. By using the bipolar electrochemical technique, a multifunctional sensor platform has been fabricated in order to improve the efficiency of sensors. Two different functional groups from both ends of the bipolar electrodes were achieved. Using which, people can detect two different analytes on a sensor.

The experimental results also exhibit the features of bipolar electrodes. Namely, the bipolar electrodes are length dependent. The voltage applied on the different positions of bipolar electrodes varies. The closer to the ends of bipolar electrodes, the higher the applied voltage is. Consequently, the Raman intensities reduce with the increasing of distance from the detected spot to the end of cathode of the bipolar electrode.